DIVISION OF ENGINEERING
BROWN UNIVERSITY
PROVIDENCE, RHODE ISLAND

FINAL REPORT
[NSG - 3118]

EFFECT OF PROCESSING PARAMETERS ON
REACTION BONDING OF SILICON NITRIDE

SUBMITTED BY

M. H. RICHMAN

NSG - 3118
NASA LEWIS RESEARCH CENTER
CLEVELAND, OHIO

OCTOBER 1980
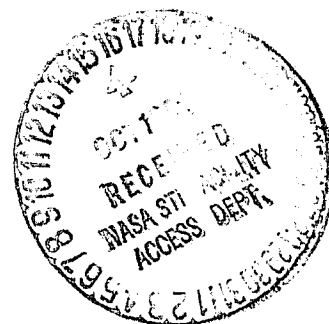
Final Report

[NSG - 3118]

Effect of Processing Parameters on
Reaction Bonding of Silicon Nitride

Submitted by

M. H. Richman[*]

Principal Investigator
Division of Engineering
Brown University
Providence, Rhode Island 02912

Summary

An investigation into the development of reaction bonded silicon
nitride has been conducted in which the relationship between the various
processing parameters and the resulting microstructures has been used
to design and synthesize reaction bonded materials with improved room
temperature mechanical properties.

----

* This Final Report was written by all present members of the research
group together. Alphabetically, they are Otto J. Gregory, Matthew B.
Magida and Marc H. Richman.

1. Introduction

During recent years, silicon nitride (especially reaction bonded silicon nitride) as well as other ceramics, has emerged as a viable substitute material for gas turbine applications. Due to the characteristics of materials presently used, the overall efficiency of the system is limited. The high temperature strength and resistance to thermal shock, ·orrosion and creep properties of silicon nitride would allow higher operating temperatures and thus increases in efficiency. Furthermore, the superalloys currently used are expensive and require many materials in strategically scarce supply. Thus research and development of silicon nitride has been quite active.

The investigation into the development of reaction bonded silicon nitride at Brown University has been concerned with the relationship between the processing parameters and the resulting microstructures. These results are then correlated to the bulk mechanical properties of the material. Through an understanding of these relationships, a program can be implemented to produce a superior ceramic material.

Work completed in the early stages of this investigation utilized a starting silicon powder (K series) of relatively high purity with iron being the major ($\sim$1 wt %) metallic impurity. It was confirmed that the purity and particle size distribution of the starting (green) silicon powder has a marked influence on the nitriding kinetics and resulting material. Since this investigation is concerned with the effects of various processing parameters on mechanical properties, a purer silicon powder ($\sim$.03 wt % Fe) was obtained in an attempt to remove the variances caused by impurity additions. Upon nitridation

of this new powder (E series), major differences were observed relative to the well-characterized K-series product.

The most striking difference between the two series was the color of the nitrided sample. The purer E-series powder nitrided to a dull goldish color in contrast to the normal gray color of the K series. The two series further differed in microstructure morphology and bulk mechanical properties. At this point, the investigation concentrated on the cause of these property variations and it was established that Fe as an impurity was directly responsible. With this information, the bulk of the later part of the investigation was concerned with producing, characterizing and testing silicon nitride produced from powder containing from .03 to 1 weight per cent iron. The per cent reacted, density, microstructure, strength and color of the nitrided product have been determined as a function of Fe concentration within the above range. The end results indicate that Fe must be present in the silicon powder in order to produce superior silicon nitride following conventional nitriding procedures.

2. Discussion of Results

The first silicon powder (K-series) used in this investigation was purchased from Kawecki Berylco Ind. Co. (Reading, Pa.) and specified as 99.4% pure (.35% Fe, .30% Aℓ, .03% Ca). The as-received powder purity was determined prior to subsequent processing by neutron activation analysis performed at the University of Rhode Island Nuclear Facility. These results are included in Table I. The impurity levels after powder processing were similarly determined and are presented in Table II.

TABLE I

Neutron activation analysis of K series Si in the as received condition in ppm. (percent where noted).

Element	Run 1	Run 2	Run 3
Aℓ	4.0% *	4.2% *	4.4% *
Mn	80	84	
V	326	336	343
Ti	304	292	418
Na	15	12	11
Sc	1.2	1.2	1.2
W	75	70	74
La	4.4	4.3	4.4
Fe	4822	5270	5117
Co	4.7	4.6	5.4
Cr	65	63	67

*   Not
Meaningful

TABLE II

Neutron activation analysis of the N, K, and E Series Si Powders as milled in ppm.

Element	N	K	E
Aℓ		4414 *	161.3 *
Mn		126	2
V	1	377	5.4
Ti		439	13.3
Th			4.9
Fe	5226	11187	
Co	205	306	6.7
Cr	956	1352	18.3
La	0.2	4.3	
W	1376	780	
Na	33		
Sc	0.07	1.08	0.11
Sb	0.2		
Ta	51		

*   Not Meaningful

The as-received powder contained particles with a mean size of 10-15 microns. It has been determined that smaller particle sizes are more easily nitrided to completion. Thus, processing to reduce the powder particle size was needed. It has also been established that nitrided strengths could be increased by increasing the green compact density. This relationship follows the classical fracture mechanics of brittle ceramic materials where the strength controlling flaws in this case are the pores. Thus, the powder was processed in such a way as to yield a higher green density.

White and Walton [1] have quantitatively shown that higher packing densities can be achieved using a mixture of different size particles. The smaller particles can pack, after thorough mixing, in the intersticial voids between the larger particles, leading to a more dense compact. They calculated that for optimum conditions, $r_2 = 0.414 \, r_1$ (r_2 and r_1 being the radii of the two-particle sizes). Using this particle packing theory, 100 grams of the as-received powder was ball milled in a Fritsch ball mill with 413 grams of WC balls and 100 ml. of acetone. After varying the ball milling time and determining the particle size distribution using a Fisher Sub Sieve Sizer, two particle size distributions were found in the ratio specified above. After driving off the acetone, the two powder lots were sized to -325 mesh and mixed together in a ratio of 1:1 by weight for 24 hours in a reaction bonded silicon nitride ball mill. The mill (Figure 1) was 3 in. (7.62 cm) in diameter and used five .75 in. (19 mm) reaction bonded silicon nitride cylinders as the grinding medium. It is interesting to note that particle size reduction using the silicon nitride ball mill resulted in a steeper and narrower particle size
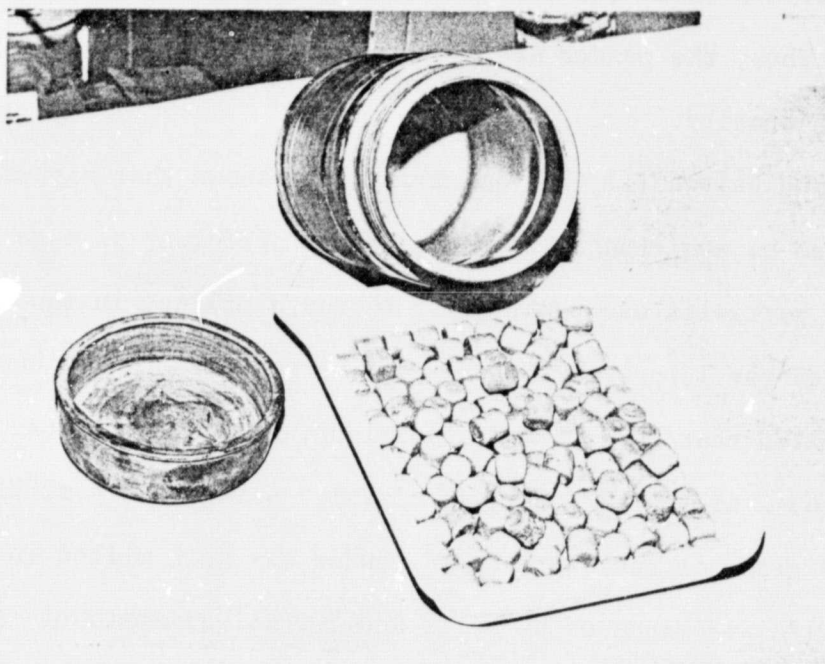
Figure 1

Si_3N_4-ball mill with

Si_3N_4 balls.

distribution (as shown in Figure 2) than had been found after milling with the WC balls. In this system, silicon nitride is not considered an impurity. The resulting powder had an average particle size of 2.9 microns with the largest particles less than 20 microns. The particle size distribution is shown in Figure 2. Figure 3 is a photomicrograph of the as-milled K series powder.

The K series powder was isostatically pressed at Norton Co.[*] in 6 in. (15.24 cm) diameter rubber bags approximately 8 in. (20.32 cm) long. Hard rubber plates were placed at the ends to insure a flat sur-face. These were then pressed at 35,000 psi (241 mn/m^2), yielding a green compact density of 1.46 g/cc. These cylinders were then processed and nitrided as described below.

The mechanically strongest material obtained from this powder exhibited a room temperature modulus of rupture of 42.0 Ksi in four point bending. This value compares very favorably with those values reported in the literature [2]. The particular nitriding schedule and material properties of this sample is given in Figure 4 and Table III.

Another powder (N series) nominally -325 mesh as-received was also used in conjunction with the K series powder during the first part of the investigation. This powder was purchased from Electronic Space Products, Inc., as nominally 99.99% Si. After processing, the purity was determined using neutron activation analysis and is given in Table II. This powder was sized to -325 mesh and then ball milled in a Fritsch mill. One hundred grams of powder was milled for 4 hours

----
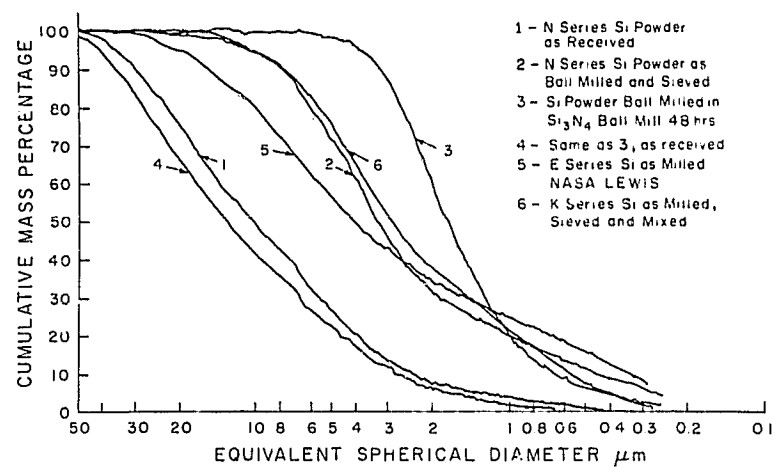
* Courtesy of Dr. M. Washburn.

Figure 2

Particle distribution for: the N series as
received, N, K, and E series powders as milled
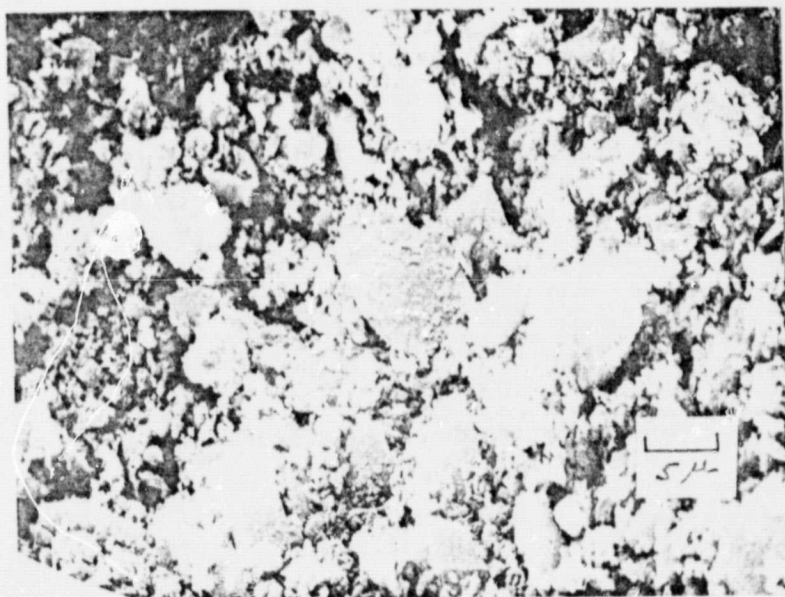and sieved; Si_3N_4 ball milled powder
before and after milling.

Figure 3

Scanning electron micrograph of the K series
Si powder as milled and sieved.
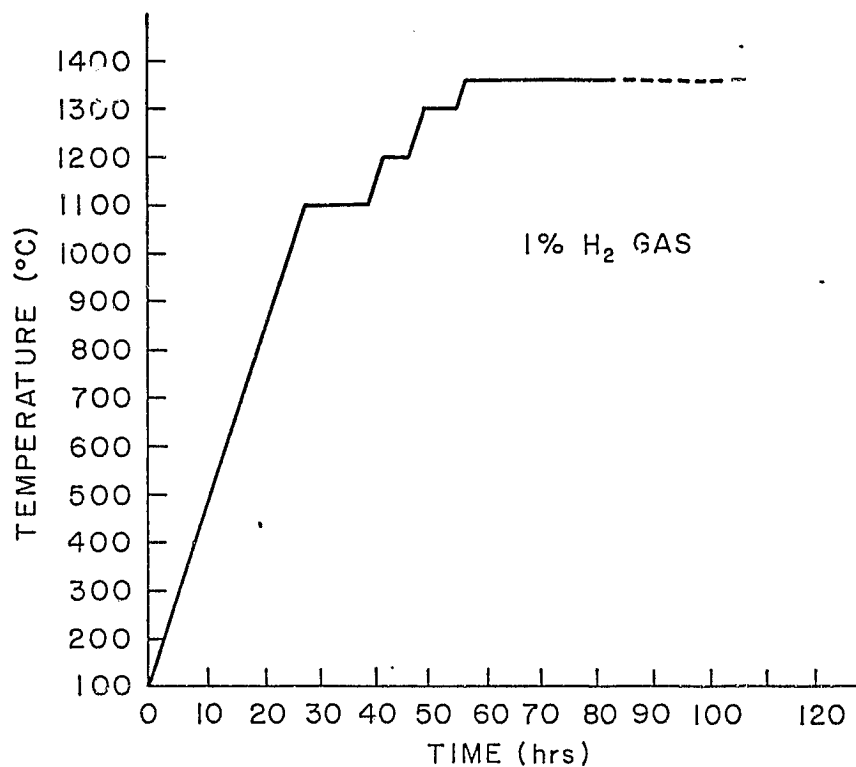
Figure 4

Time-Temperature Schedule for K-8 Run

TABLE III

Material Characteristics for Strongest RBSN to Date (Run K-8)

α/β	$\%\alpha$	α/Si	MOR(ksi)	K_{1c} MN/m$^{3/2}$	% Reacted
2.9	73	82	42.0	2.357	92

in a 4 inch (10 cm) diameter stainless steel jar using 320 grams of
0.25 inch (6 mm) WC balls as the grinding medium with 40 ml of acetone.
After milling and upon removal of the acetone, the agglomerated Si powder
was retu ed to the mill for 30 seconds. To further insure removal of
powder agglomerates, the powder was again sized to -325 mesh. The
resultant Si powder had a particle size distribution shown in Figure 2
with average and maximum particle sizes of 3.2 and 25 microns respectively.
The physical characteristics of the powder are shown in Figure 5. The
powder was then isostatically pressed at the Norton Co. in 1 inch (25.4
mm) diameter cylindrical polyethylene bags approximately 10 in (254 mm)
long at 40,000 psi (275 mn/m^2) without a binder. This yielded a green
compact with a density of 1.4 g/cc.

Using these two starting silicon powder compacts, experiments were
designed and performed in an effort to establish the effects various
processing parameters would have on the resulting reaction bonded silicon
nitride. Since increased strength is the main objective of this investi-
gation, it is important to establish the strength-controlling criterion.
It is widely agreed, that the strength of brittle materials like silicon
nitride is controlled, as described by the Griffith theory, by the stress
necessary to propagate the largest surface or internal flaws. Thus,
increased strengths could be achieved by controlling the size and shape
of these flaws. One of the major failure-initiating flaws has been the
porosity found in reaction bonded silicon nitride. It is therefore ex-
tremely important to understand the variations in the pore structure and
understand its development.

Four types of porosity have been observed and quantified during this
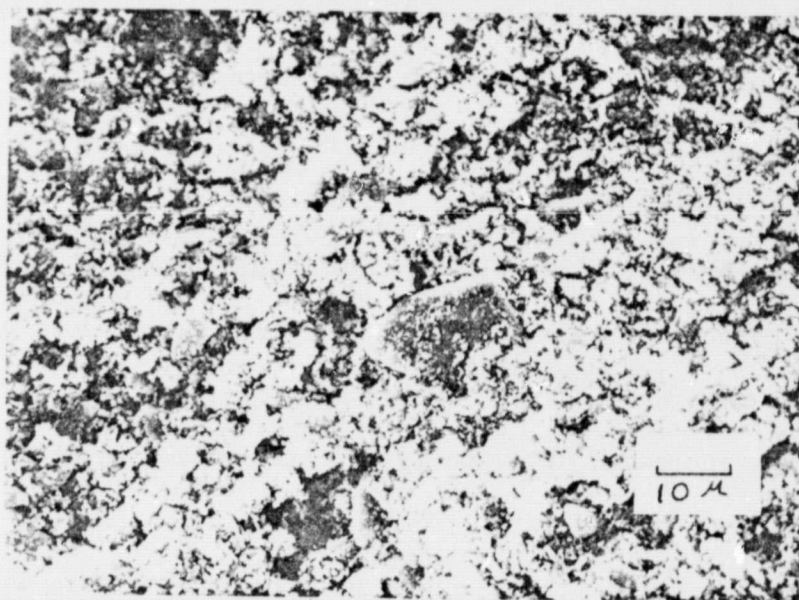investigation. The largest, macropores, are associated with the formation

Figure 5

Scanning electron micrograph of the N series

Si as milled and sieved.

of the green compact and are common to all ceramics (except those of theoretical density) formed by compacting powders. This post compaction porosity may vary in volume fraction from 0.27 to 0.44 porosity and in size from 10 to several hundred microns. Techniques for reducing the residual macro-porosity are well developed and include increased compacting pressures, decreased particle size and improved void filling processes (particle packing theory). Some densification aids such as MgO and CaO can be used, but they are detrimental at high temperatures due to their enhancement of creep.

The three other types of porosity have been labelled micro-pores, nano-pores and pico-pores in order of decreasing size (Figure 6). The micro-pores are associated with the melting of Si particles (either due to local impurity segregation or as a result of a large reaction exotherm) and may range in size (depending on original Si particle size) up to one hundred microns. The largest of the micro-pores are often found in materials formed from large starting Si powder particles and low α/β ratios. This is not to say that the β formation mechanisms require Si melting, but that this melting is associated with the formation of micro-pores.

The nano- and pico-pores result when silicon grains are reacted to form α-matte silicon nitride. The medium sized nano-pores are present in the unreacted silicon grain ahead of the Si - Si_3N_4 interface as shown in Figure 7. The finest pico-pores are found in the α-matte after the interface has passed through that portion of the silicon grain. Earlier mechanisms presented in the literature [3] for the growth of α-matte and those developed from this work jointly explain
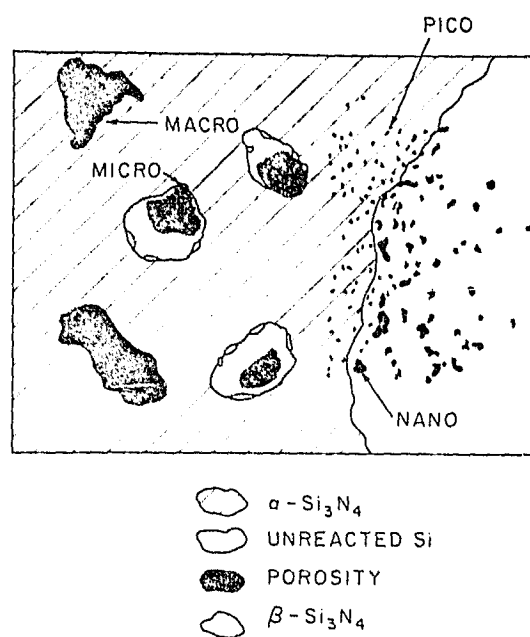
Figure 6

Schematic of the various pore sizes
associated with reaction bonded Si_3N_4.

Figure 7

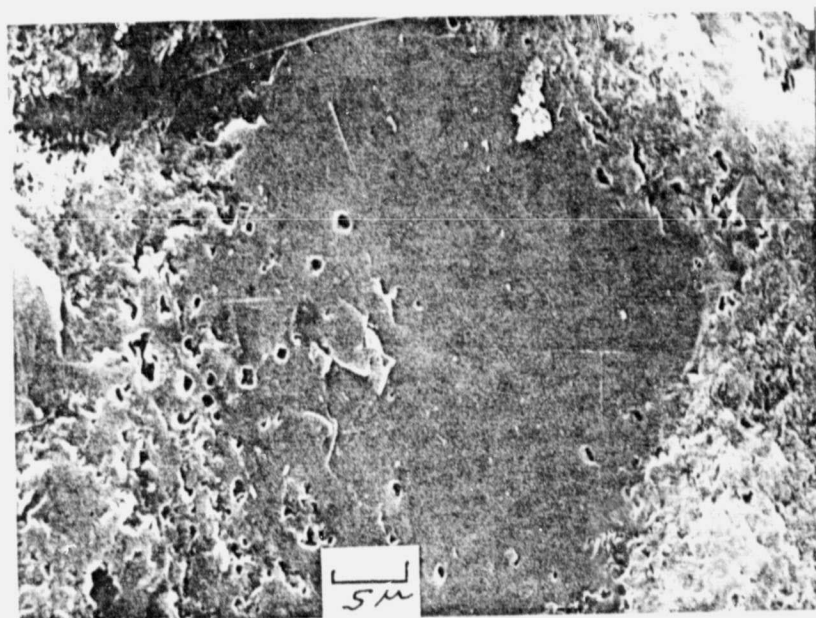Scanning Electron Micrograph of Pore Structure
Associated with α-Si_3N_4 Advancing into a Si Grain

the formation of these pores. Briefly, the nano-pores are the result of
the loss of silicon through either vaporization or diffusion (vacancy
condensation) of the silicon to the nitridation sites. These pores are
subsequently sealed off by the formation of the nitride. The pico-pores
form as a result of further nitridation inside the nano-pores by either
trapped or diffused nitrogen. The nano-pores are reduced to pico-pores
through the 22% volume increase upon nitridation. With a knowledge of
how these strength-reducing flaws are formed, it becomes important to
understand the effect of nitriding conditions on these mechanisms.

At this point it should be emphasized that extensive material
characterization was performed on the reaction bonded silicon nitride
products. Optical, scanning and transmission electron microscopy were
extensively used in the investigation and the experimental procedures
will be discussed later. The observed characteristics from this study
will be briefly reported below.

Silicon nitride exists in two crystallographic forms, α and β
which can form in distinct morphologies by several different reaction
mechanisms. The morphologies that will now be discussed include
α-needles, β-spikes and α-matte.

Alpha needles have a high aspect ratio (>10) and tend to form at
lower temperatures (<1300°C) primarily in the internal porosity or on the
external surface of the sample. Figures 8 and 9 show SEM and TEM images
of these needles. In Figure 9 the drop at the end of the needle marked A
indicates a vapor-liquid-solid (VLS) growth sequence. It has been shown
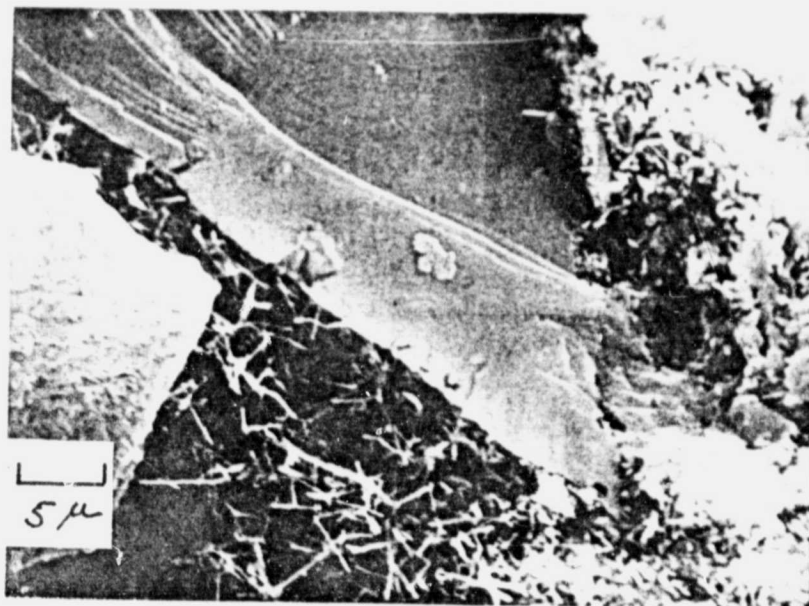that these beads contain high Fe concentrations which would facilitate

Figure 8

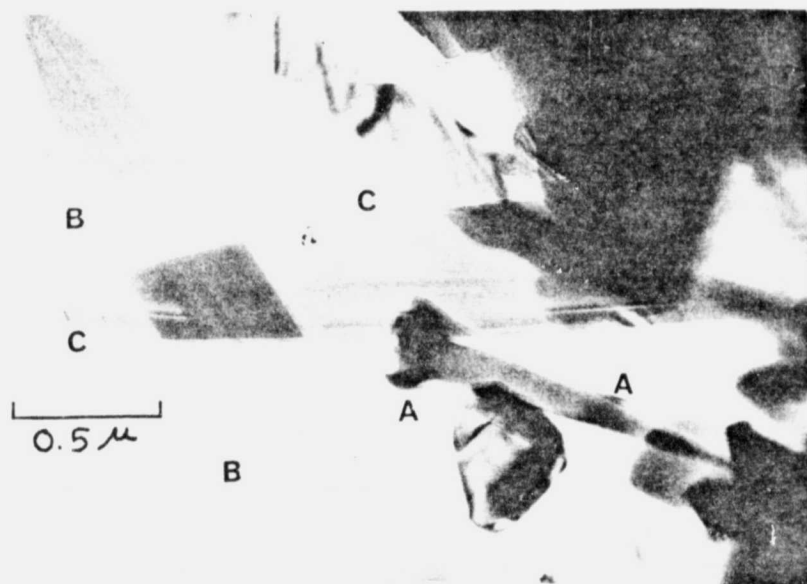Scanning electron micrograph of α-needles growing into a pore

Figure 9

Transmission electron micrograph of α-needles,
needle marked A has a bead at its terminus,
B and C have crystalline inner cores.

the VLS mechanism by lowering the temperature of fusion of the reacting Si. Needles B and C have crystalline inner cores with amorphous outer sheaths (determined by lack of tilt contrast). Figure 10 shows a helical banded structure comprised of impurity bands that segregate out of the liquid as the VLS interface progresses. These needle morphologies observed may contribute to the mechanical integrity of the nitride in much the same way as interlocking plates in cement.

Beta silicon nitride has a hexagonal unit cell with large hexagonal tunnels in the <0001> direction. The formation of β silicon nitride is proposed as being controlled by a solid state diffusion mechanism. These β grains can grow very rapidly into the silicon grains at higher temperatures due to the ease of diffusion of N_2 down the β tunnels. β grains that have grown into the silicon grains can be seen in Figure 11. As the β spikes grow, they converge on one another combining to form a uniform, dense $\beta\text{-}Si_3N_4$ matrix (Figures 12 & 13). It appears from optical microscopy that the size of the β grains is limited mainly by the Si particle size. Figure 14 shows a finer β-grain cluster as a result of nitriding a fine starting Si powder, under conditions aimed at yielding a high α/β ratio.

The β grains not only grow larger than α silicon nitride but also contain much higher dislocation densities. These dislocations (Figures 15 & 16) are thought to be the result of the solid state diffusion growth mechanisms and compounded by the 22% specific volume increase upon nitridation.

In an additional morphology, α silicon nitride can grow as a very fine grained (<1 micron) α-matte (Figure 17). Contrasting the directional

Figure 10

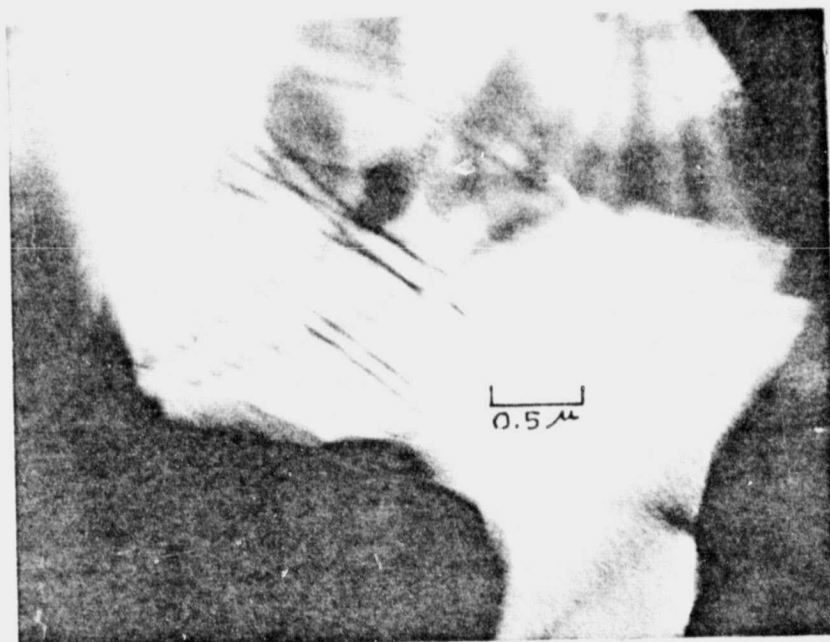Transmission electron micrograph of α-needles
with helical impurity bands (10°C tilt).
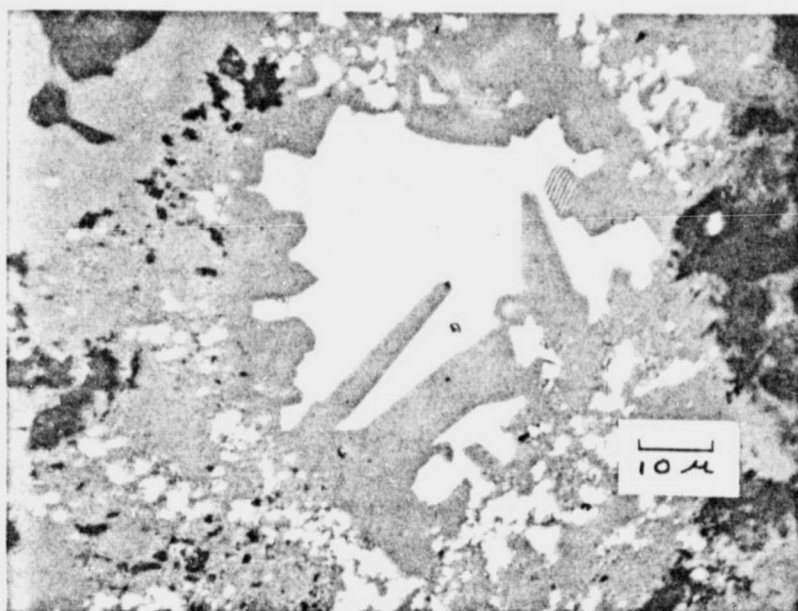
Figure 11

Optical photomicrograph of large β-grains
growing into a grain of unreacted Si
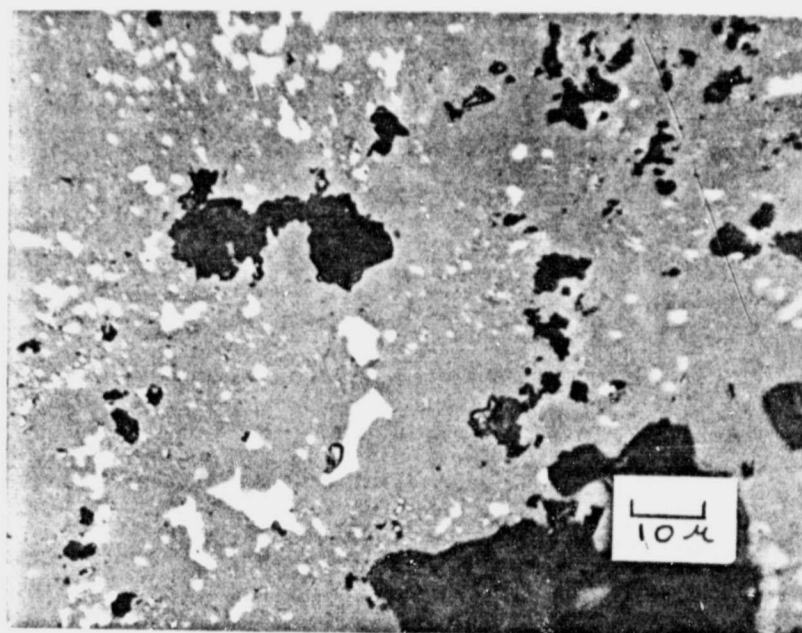(white is Si, gray is β-Si_3N_4,
and black is porosity).

Figure 12

Optical photomicrograph of β-grains (gray)
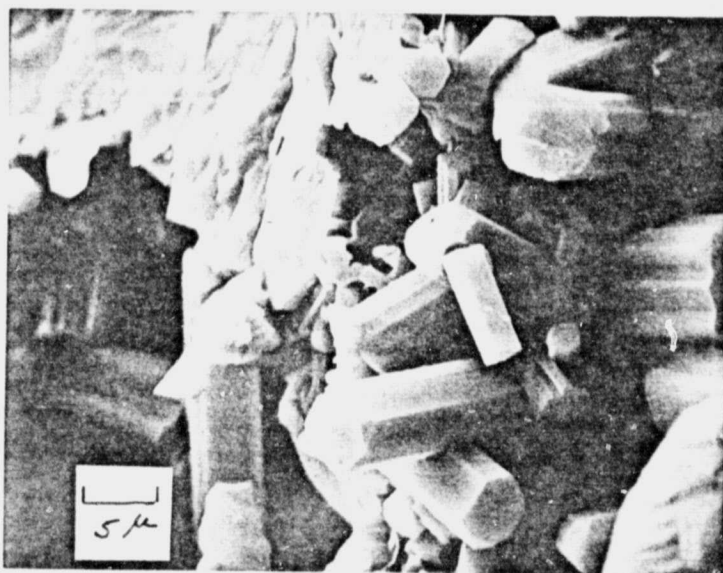forming a dense β-matrix
(Si is white, and porosity is black).

Figure 13

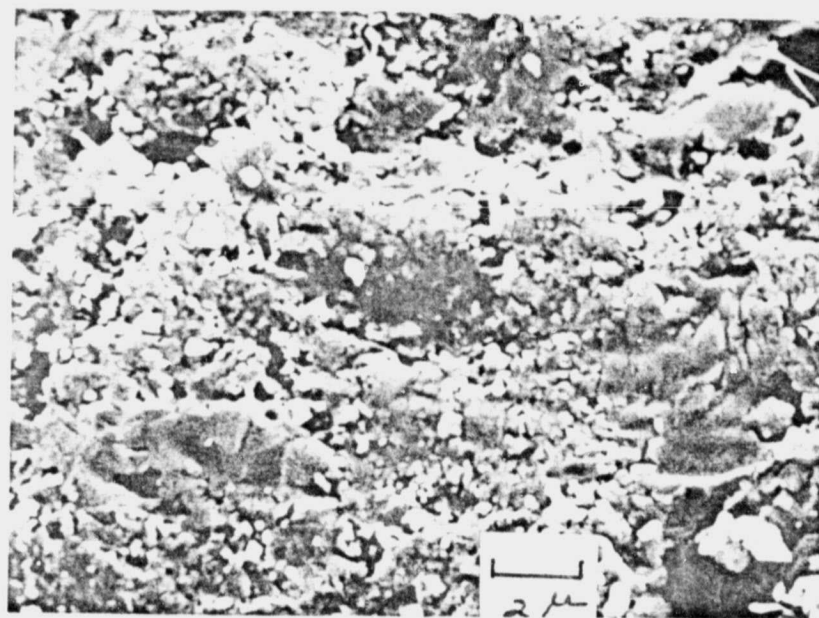Scanning electron micrograph of β-Si_3N_4
forming a dense β-matrix.

Figure 14

Scanning electron micrograph of finer ß-grain cluster
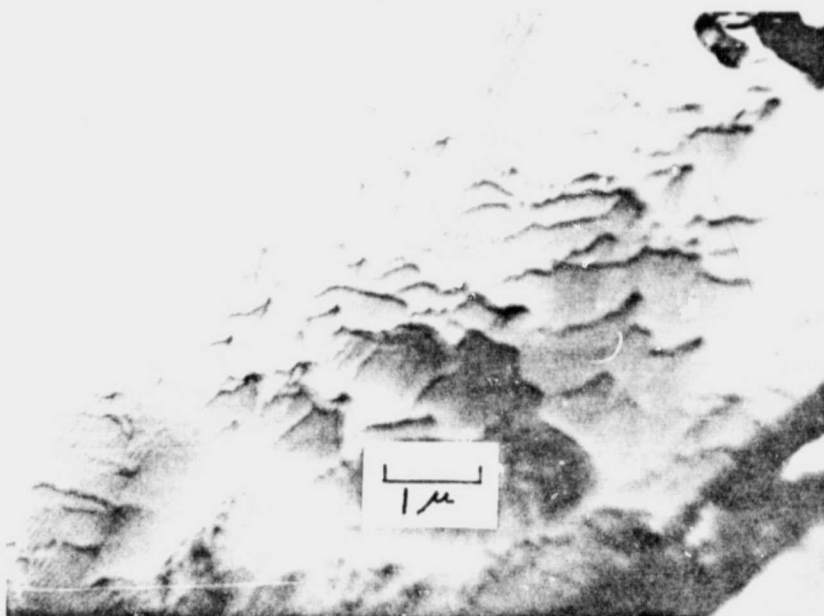size associated with reduced starting Si particle size.

Figure 15

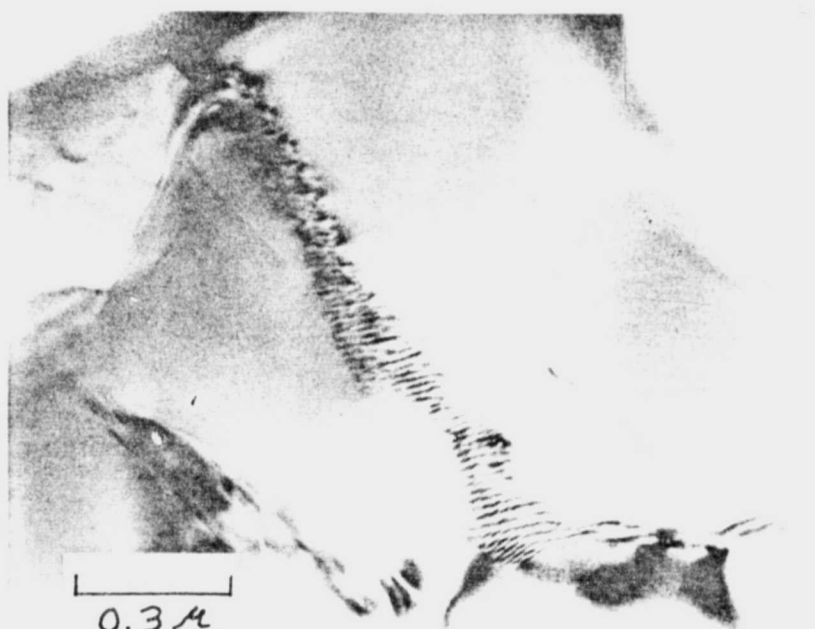Transmission electron micrograph of large β-grains
containing dislocations.

Figure 16

Transmission electron micrograph of large β-grains
containing dislocations.

Figure 17
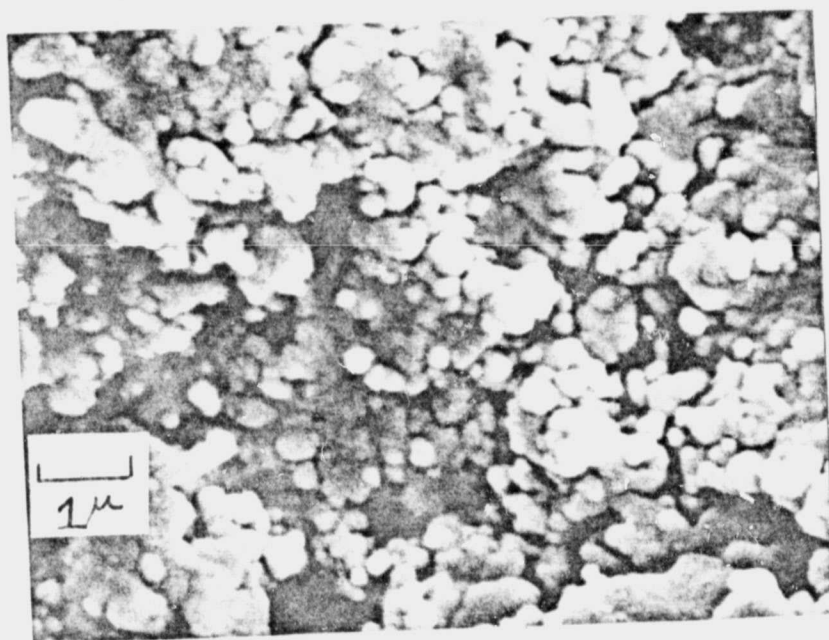
Scanning electron micrograph of fine grained α-matte Si_3N_4.

growth of β-Si_3N_4 into the unreacted silicon, α-matte forms an even bound-
ary on the silicon surface. This region then advances into the unreacted
grain as shown in Figure 18.

The fine grained structure of the α-matte is clearly seen in
Figures 19 and 20 . The fact that the grain size is substantially less
than the original silicon particles and the low dislocation density
observed, supports a mechanism involving a vapor phase reaction. Such
mechanisms have been proposed during this investigation and supported
elsewhere in the literature [3].

Since all these phases and morphologies are simultaneously formed,
knowledge of how to control the final microstructure would be advantageous.
It is the goal of this investigation to be able to form a microstructure
with the best resistance to crack propagation. In order to achieve this,
understanding of how the nitriding parameters effect the microstructure
is needed.

The nitriding variables of interest are the following: 1) Si particle
size and distribution, 2) Si powder purity, 3) temperature of nitridation,
4) gas flow rate, 5) O_2 content of the nitriding atmosphere, 6) utilization
of an argon pre-sinter, and 7) the N_2 content of the atmosphere. These
parameters affect such features as the green and nitrided density, the
percentage reaction, the phase ratios, the grain size and the resultant
pore size and distribution. All of these properties will affect the
final mechanical properties of the reaction bonded silicon nitride.

Large Si particle sizes hinder successful compacting (particle
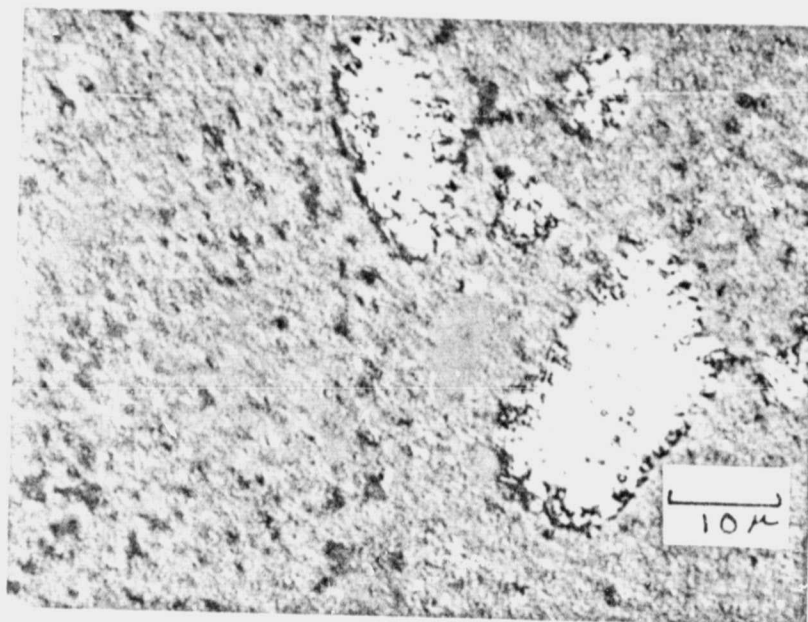packing) thus lowering the green density. Furthermore, complete

Figure 18

Optical photomicrograph of fine grained α-matte structure
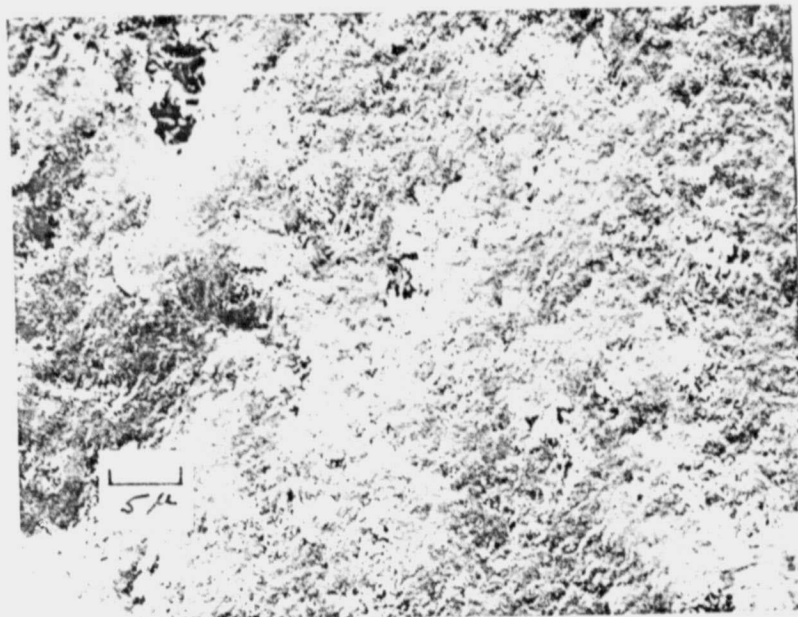advancing into an unreacted Si grain (white).
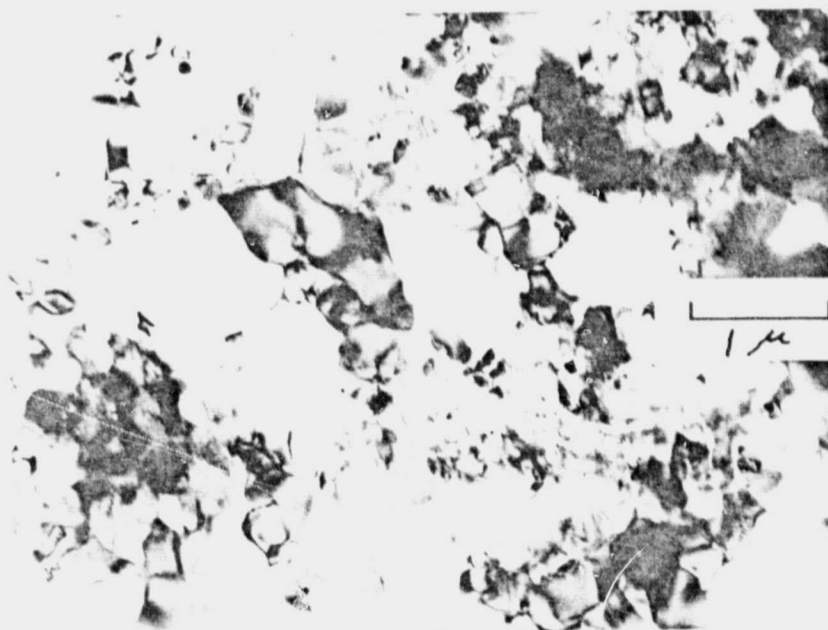
Figure 19

Scanning electron micrograph of K series Si_3N_4.

Figure 20

Transmission electron micrograph of fine
grained α-matte Si_3N_4.

nitridation of the silicon is impeded by the larger particles. The vapor phase and solid state diffusion reaction mechanisms involved are accelerated by reduced particle size due to increased vapor pressure and reduced diffusion paths. The effect Si particle size has on the microstructure can be seen in Figures 21 through 24 where the particle sizes used were <75, <45, and average particle sizes of 3.2 and 2.9 microns respectively. These pictures clearly show that reduced Si grain size leads to a more refined and uniform microstructure. The results indicate that reducing the Si particle size promotes the reaction mechanisms, reduces the nitriding time, increases nitrided density, refines grain size, reduces the general flaw size and hence promotes strength in reaction bonded silicon nitride.

The main concern in reducing the Si particle size is the maintenance of powder purity. Two main types of impurities were investigated. The first group, which are often added as densification aids, include MgO and CaO. These impurities are to be avoided as they tend to form a glassy grain boundary phase to the detriment of the material's ability to resist creep.

The second category includes impurities often present due to the processing techniques employed. These metallic impurities include Aℓ, Cr, Fe, Mn, Ca, Ni, Co, etc. Iron is the most important impurity due to its high concentration (a few ppm to several percent) and also due to its effect on the kinetics of the nitridation reaction. The role of iron as an impurity was studied in the later part of this investigation and will be discussed later. Briefly, iron tends to increase the

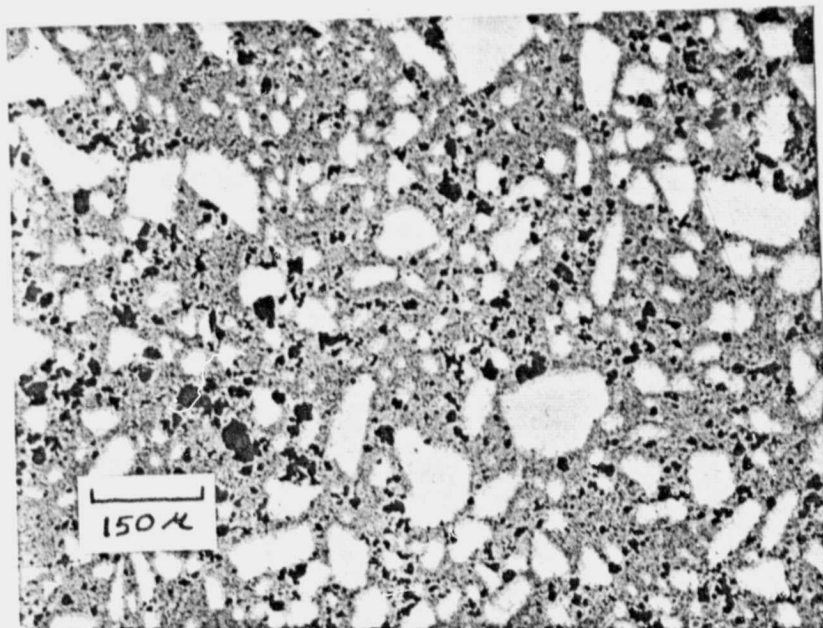Figure 21

Optical photomicrograph of reaction bonded Si_3N_4 made from
>75 micron starting Si powder, white is Si and black is porosity.

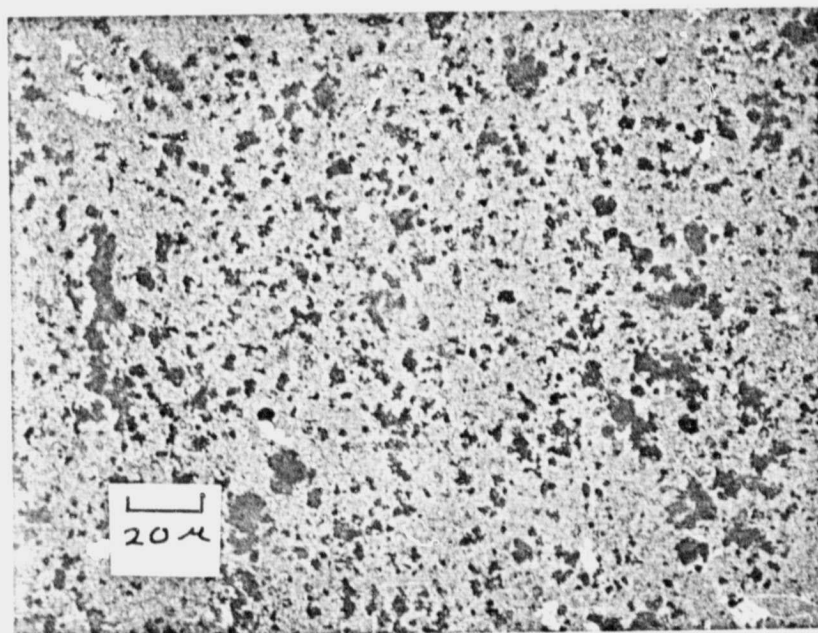Figure 22

Optical photomicrograph of reaction bonded Si_3N_4 made
from >45 micron starting Si powder.

Figure 23

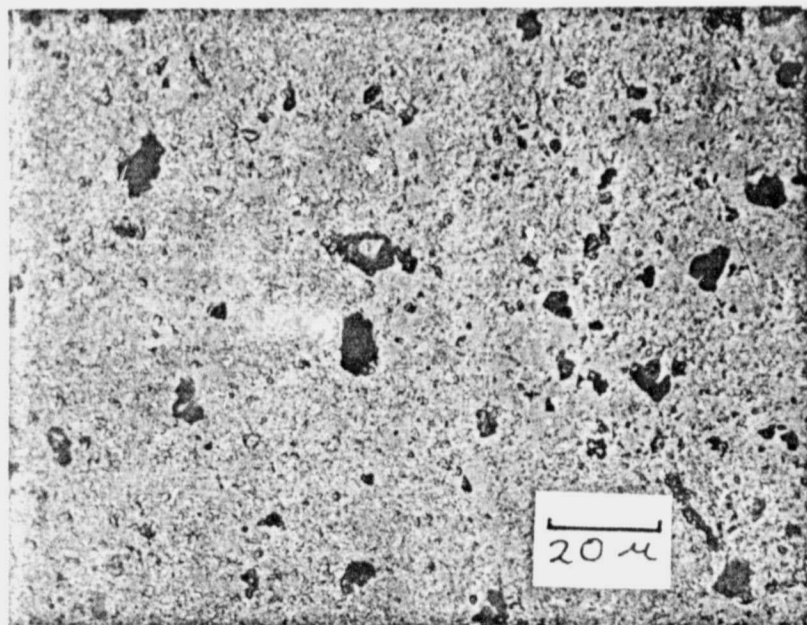Optical photomicrograph of reaction bonded Si_3N_4 made
from starting Si powder with an average size of 3.2 microns.
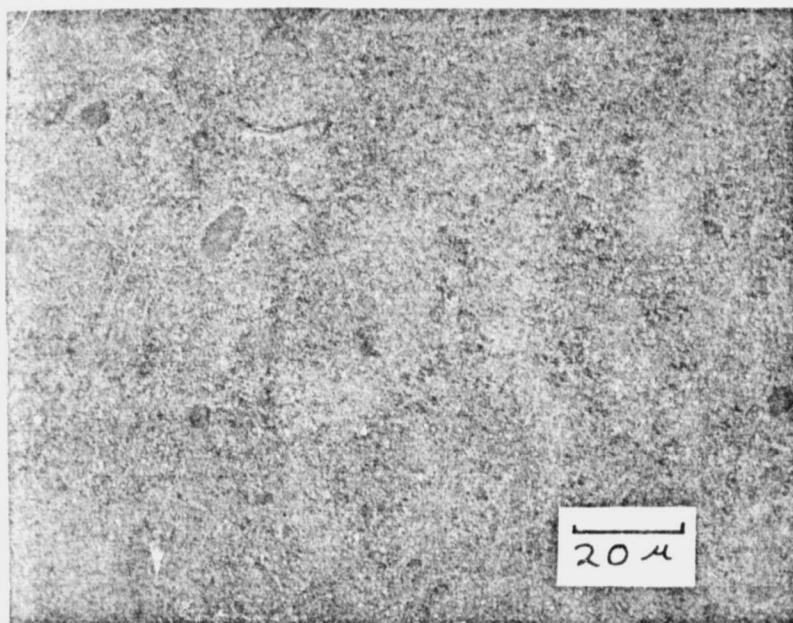

Figure 24

Optical photomicrograph of reaction bonded Si_3N_4 made
from starting Si powder with an average size of 2.9 microns.

reaction rates as well as the resultant α/β ratio (see Table IV).
Localized segregation of the iron can however be detrimental due to the
formation of low melting point SiFex compounds. However, as will be
shown later, Fe in the silicon powder is necessary in order to produce
superior reaction bonded silicon nitride.

The ultimate temperature and the heating rates used during nitridation
greatly affect the microstructure and resultant properties of the material.
Observed changes in the α/β ratio as a function of the ultimate nitriding
temperature is shown in Table V. The increase in β content with tempera-
ture can be related to existing reaction mechanisms. The high temperatures
associated with β formation also promote melting of the Si and the
formation of large strength reducing pores. If high temperatures are
reached too quickly, large β grains in an unreacted (melted) Si matrix
result (Figure 25). Since α is not present in this region, it would seem
that the β formed as the silicon was melting. It is thus observed that
high nitridation temperatures promote β growth and large pore sizes.
Unfortunately, it is often necessary to use such temperatures especially
when nitriding compacts with high green densities (>1.6 g/cc). A way to
minimize these high temperature effects is to hold the reaction at lower
temperatures in an effort to completely react the silicon prior to .
reaching the high temperature.

The heating rates used during nitridation seem to have an effect
similar to that of the ultimate temperature. High heating rates reduce
the α content while promoting rapid β growth. Large void formation is
associated with high heating rates thus opposing the increase in reaction
rates. Furthermore, a high heating rate in conjunction with the reaction

TABLE IV

Increase in the α/β Ratio Associated
with Nitridation in the Presence of Fe.
Pure Sample was Adjacent to Impure
Samples Within Furnace Chamber.

α/β Ratio of Sample Nitrided Alone	α/β Ratio of Sample Nitrided in Presence of Impure Si (Fe)
2.3	3.9
	4.2
	4.5

TABLE V

The Effect of Nitriding Temperature on the
α/β-Ratio for the N and K Series Si_3N_4 Samples

N Series Si_3N_4

Temperature $^\circ C$	α/β-Ratio
1300	4.4
1350	2.7
1350	2.2
1360	2.6
1410	1.0

K Series Si_3N_4

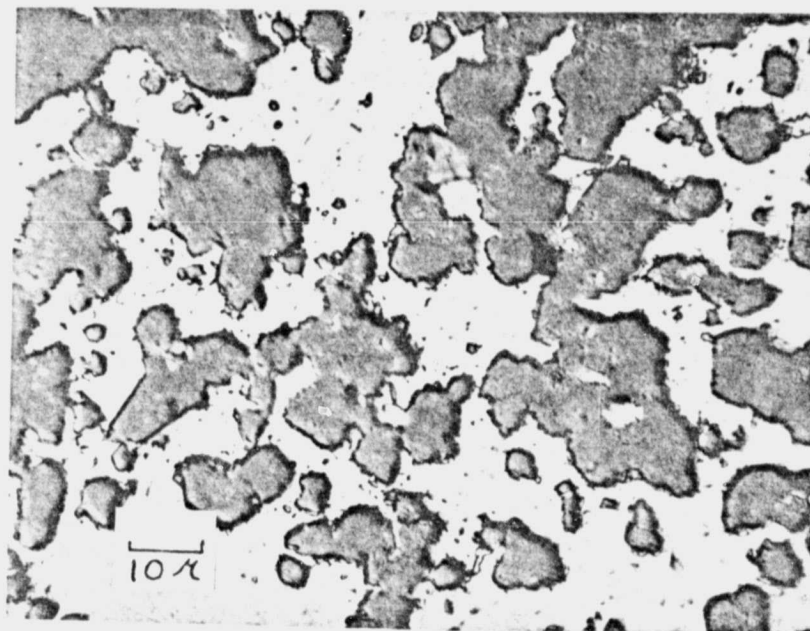| Temperature $^\circ C$	α/β-Ratio
1300	9
1300	9
1300	8.1
1360	2.9
1360	3.5
1400	3.5
1430	1.5

Figure 25

Optical photomicrograph of a sample heated too
quickly to $1420^{o}C$; note unreacted Si.

exotherm can lead to severe silicon melting and possible damage to the nitriding furnace. Thus slow heating rates are desired.

The effect of gas flow rate on the nitridation of Si has been well established. Since α formation mechanisms are enhanced by SiO vapor, under flow conditions this vapor is likely removed. This inhibits α formation, reduces the reaction rates, and lowers the resultant weight gain and density of the nitrided material. Reduction in the room temperature MOR is observed for material formed under flow conditions. This is explained by the effect gas flow has on the reaction kinetics which is to increase β formation with its accompanying increased flaw size. The more refined microstructure of reaction bonded silicon nitride formed with an effective gas flow rate of 0 is compared to that of a conventional cycle in Figures 26 and 27.

The role of O_2 in the nitriding system is not fully understood at this time. However, it is known to greatly affect the reaction rates and the resultant α/β ratio. Sources of O_2 in the system include: oxygen in the nitriding gas, the furnace liner (Al_2O_3 will liberate some O_2 at elevated temperatures), and the silicon powder in the green compact (in the form of SiO_2 or adsorbed onto the silicon particle surface). The major role that oxygen plays during the nitridation reaction seems to lie in its effect on the stability of the layer of SiO_2 on the silicon surface. If the O_2 concentration is maintained below the equilibrium vapor pressure of SiO_2, then the silicon will volatilize forming SiO vapor which aids in the formation of α. This will increase the α/β ratio while achieving complete nitridation to yield reduced flaw
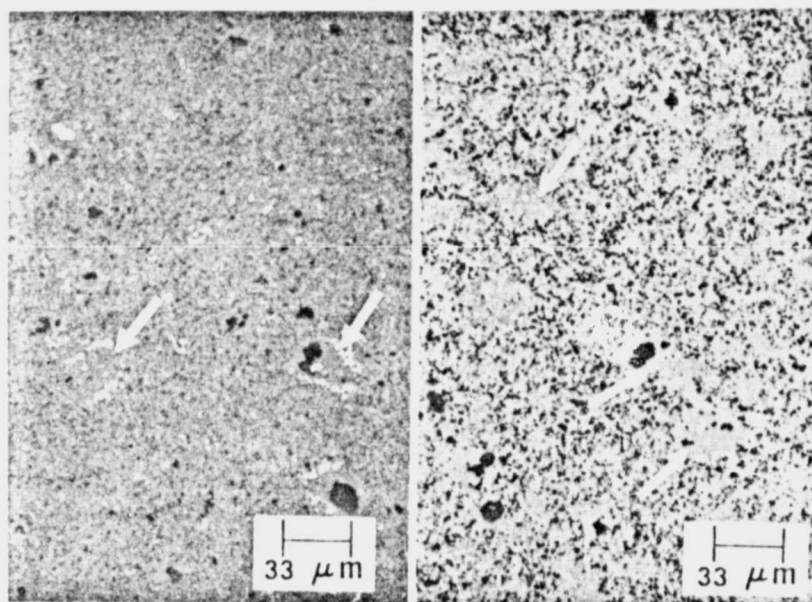
Figure 26

Optical Photomicrographs of Two Ford Motor Co.
Reaction Bonded Si_3N_4 Samples Nitrided
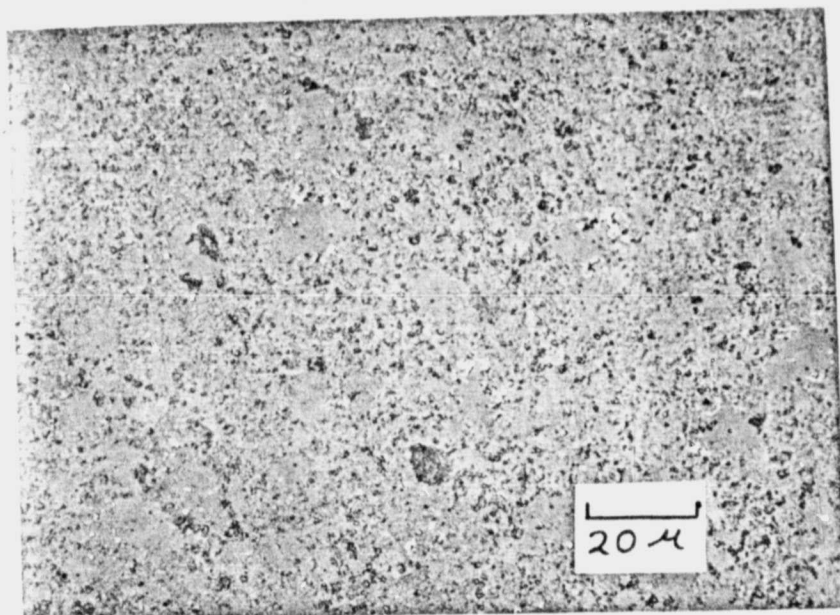Using a Conventional Cycle.

Figure 27

Optical Photomicrograph of Ford Motor Co. supplied
Green Si Compact After Nitridation in the K Series System;
Note the Relatively Small Pore Size Distribution
in Comparison to Figure 26.

sizes and refined microstructures. It should be noted that this is an upper limit on O_2 concentration and that much less O_2 in the system reduces the α/β ratio. The results from the investigation show the maximum α/β ratio for the N series (1.5 wt % O_2) was 4, while the K series (2.4 wt % O_2) was 9. Although the higher α/β ratio reduces the pore size distribution, large amounts of unreacted Si are also found and this is detrimental to the strength of the finer material. Thus, O_2 can be both beneficial and detrimental to the formation of quality reaction bonded silicon nitride.

Often, in an effort to impart greater strength to the green silicon compact for machining, a presinter in argon is performed. Table VI summarizes the results of an argon presinter of the N series material and shows a decrease in the α content as a result. Argon sintering will reduce the surface area of the silicon particles which in effect lowers the vapor pressure (larger radii of curvature) thus reducing the formation of α. The formation of α can be further reduced if argon acts to effectively "clean" the silicon surface resulting in the loss of SiO_2 and leaving virgin silicon, a condition that will encourage β formation. The sintering of the silicon particles is shown in Figures 28 and 29 as indicated by the inter-particle neck formations. These are the result of a 48-hour $1200^{\circ}C$ argon presinter of the K series Si compact.

The addition of H_2 to the nitriding atmosphere has been known to be beneficial to both the room and high temperature properties of reaction bonded silicon nitride. This has been attributed to a finer more uniform grain structure and reduced grain boundary impurity

TABLE VI

The Effect of an Argon Pre-Sintering Treatment
On the α/β-Ratio for N Series Si Compacts.

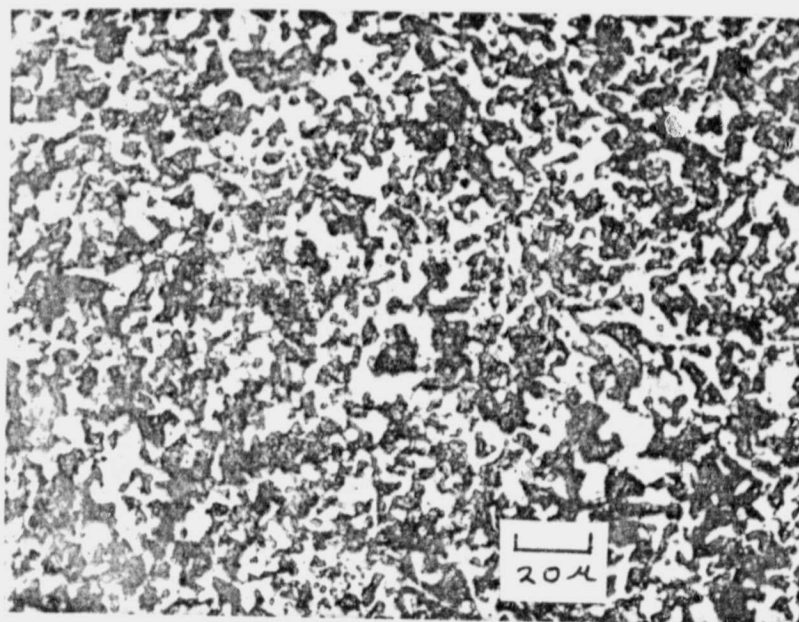| Pre-Sinter	N_2 Flow Rate cc/min	Temperature $^\circ$C	α/β-Ratio
None	0	1390	2.3
None	130	1470	3.5
1100°C	0	1400	1
1100°C	0	1460	1
1200°C	44	1415	2

Figure 28

Optical Photomicrograph of Polished K Series Si Compact
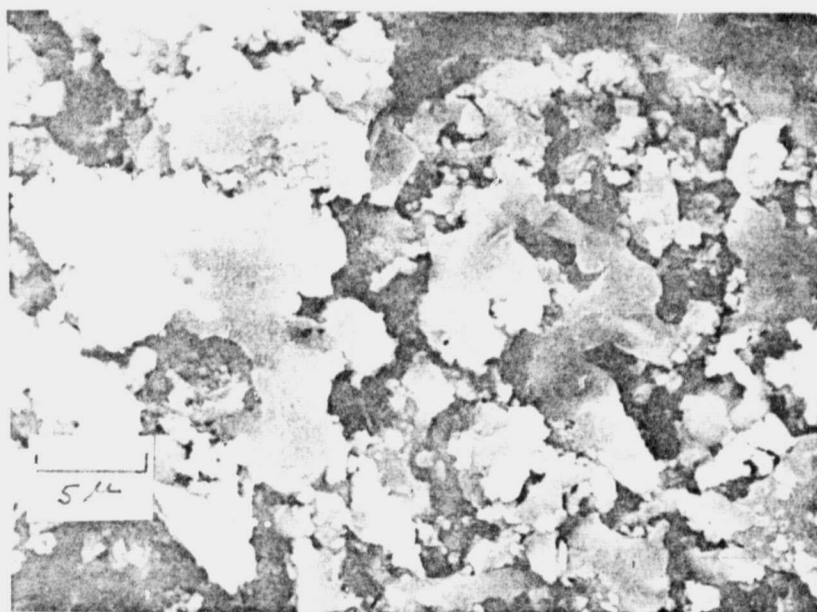After an Argon Pre-Sinter; Note the Neck Formation

Figure 29

Scanning Electron Micrograph of K Series Si Compact After
an Argon Pre-Sinter; Note the Neck Formation
and the Effectively Large Grain Size.

segregation. It is believed that the H_2 can readily promote increased SiO vapor concentration (through reaction with impurities and oxides which liberate H_2O and other lower more volatile oxides) accounting for the more refined microstructure (Figures 30 and 31). Table VII shows that under those nitriding conditions favoring β formation, the addition of H_2 lowered the α/β ratio. Furthermore, under those conditions favoring the formation of α, the H_2 addition accelerated the rate of α silicon nitride formation.

The results of the K series experiments reveal that there was no significant variation in α/β or α/Si ratio with or without H_2 in the nitriding atmosphere. It appears that these ratios are largely determined by the Si particle size, temperature and oxygen content of the silicon powder. Indications are that the role of H_2 is the refinement of the microstructure, flaw size and grain size through the increased nucleation of silicon nitride by vapor phase transport.

The results presented below are from experiments designed to correlate the reaction mechanisms with the resultant microstructures. The representative curves in Figure 32 show the possible variations in pore size distribution as a function of α/β ratio at constant density. In Figure 33, it may be seen that C (defined as the pore size where there was an average of 1 pore per 0.018 mm^2) is independent of density. This further shows the importance of pore size and distribution on the strength of reaction bonded silicon nitride. In Figure 34, C is plotted against α/β ratio for two silicon particle sizes and constant density. It is observed that as the α/β ratio increases, C decreases and that for constant α/β, the pore size
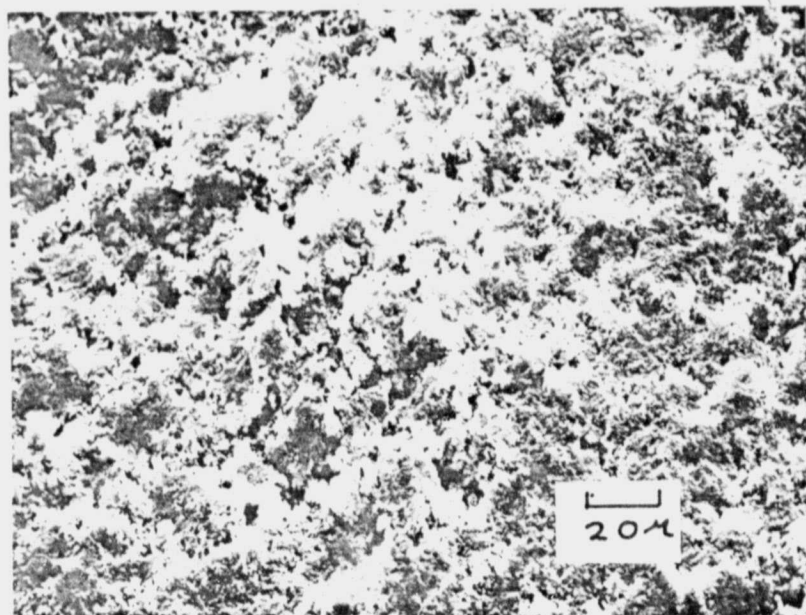
Figure 30

Scanning Electron Micrograph of K Series Si_3N_4 Nitrided Without
H_2; Note the Coarse Structure in Comparison to Figure 31.
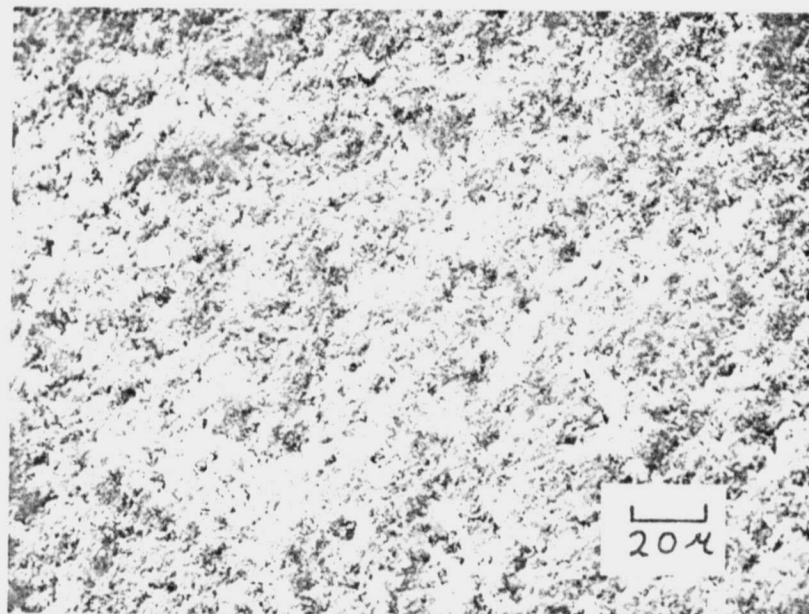
Figure 31

Scanning Electron Micrograph of K Series Si_3N_4 Nitrided With
1% H_2 Added to the Atmosphere;
Note the Fine Structure in Comparison to Figure 30.

TABLE VII

The Effects of H_2 Additions to the Atmosphere on the
α/β-Ratio for the N Series Si_3N_4 Material.

Gas	Flow Rate cc/min	Temperature ^oC	α/β-Ratio
N_2	0	1360	4
N_2	0	1400	4
N_2	10	1400	10
N_2-1%H_2	0	1450	3.2
N_2-1%H_2	2	1450	2.0

Figure 32

Pore Size Distribution Curves vs.
α/β-Ratio for the N Series Si_3N_4.

Figure 33

Pore Size Parameter C vs. Density
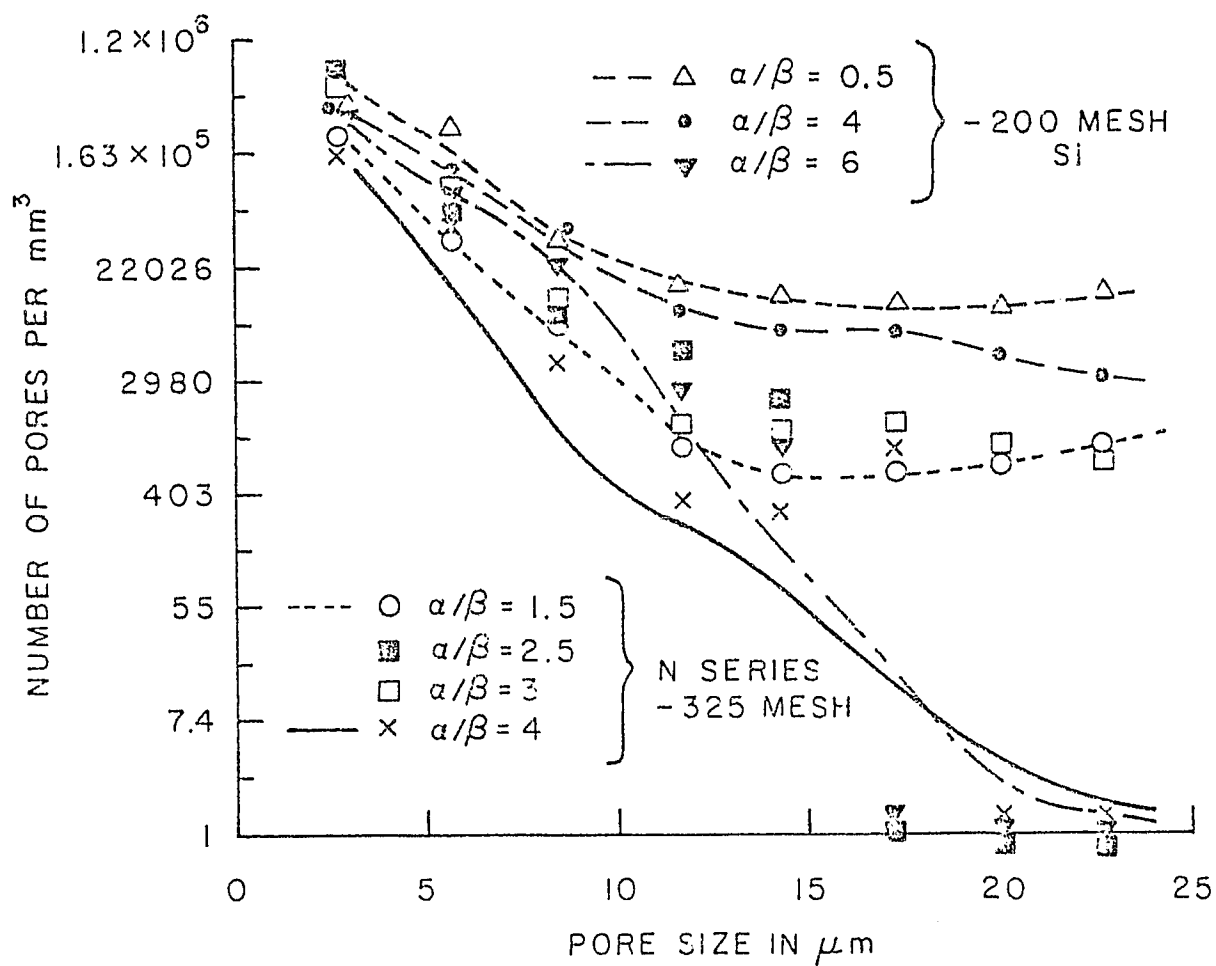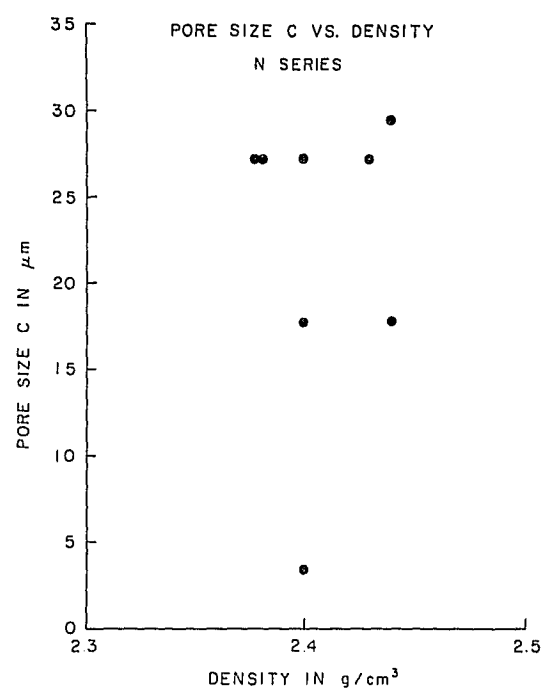for the N Series Si_3N_4.

Figure 34

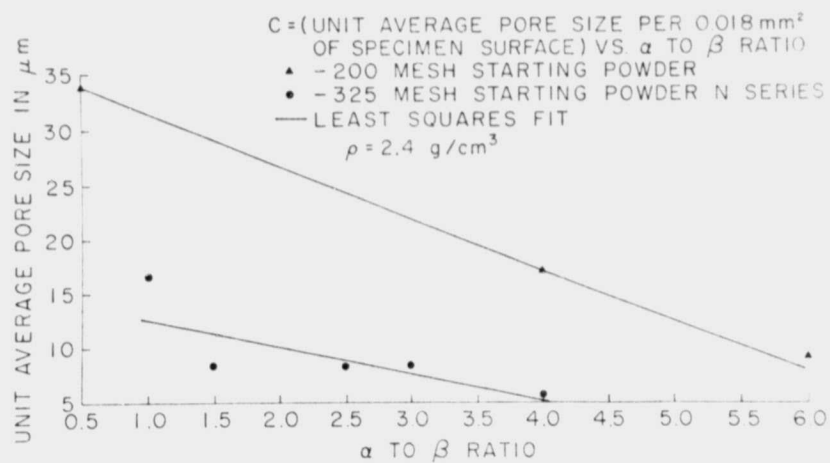Pore Size Parameter C vs. α/β-Ratio for
the N Series Si$_3$N$_4$ at Constant Density.

Figure 35

Optical Photomicrograph of the Pore Size Distribution
of N Series Si$_3$N$_4$ with an α/β-Ratio of 1.

distribution decreases as the silicon particle size decreases. Typical microstructures and pore distributions for the N series material is shown in Figures 35 and 36 with α/β ratios of 1 and 4 respectively. Similar results were observed for the K series material and these in turn were related to the reaction mechanisms involved.

A thorough understanding of the relationships between the processing parameters, reaction mechanisms and microstructures indicated that microstructural control could be employed here. The results have been the production of an N series material with a density of 2.4 g/cc and a room temperature MOR of 42 ksi (275 MN/m^2) in three point bending. With a density of 2.46 g/cc, K series material exhibited an MOR of 50 ksi (344 MN/m^2) in three point bending. Following is a more detailed presentation of the effects previously mentioned with respect to mechanical properties.

The N series modulus of rupture was determined using a three point bend rig (Figure 37) while the K series was tested using a four point bend rig designed through the courtesy of the NASA Lewis Research Center (Figure 38). Figure 37 also reveals the specimen geometry and the test parameters used. It is important to note that while any particular MOR test may be used to compare silicon nitride materials, only carefully standardized tests can be used to quantitatively compare results from different investigations.

The K series bend bars were diamond ground to final dimensions of 1.250 x 0.250 x .1250 ± 0.001 in. (31.75 x 6.35 x 3.17 ± 0.0254 mm) with a 0.005 in (0.127 mm) 45° edge chamfer to reduce edge failure. An Instron testing machine with a cross head speed of 0.02 in/min
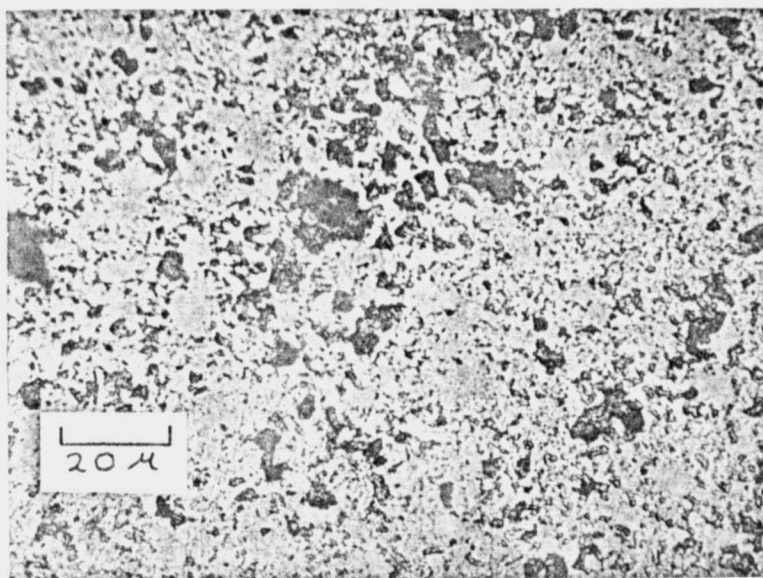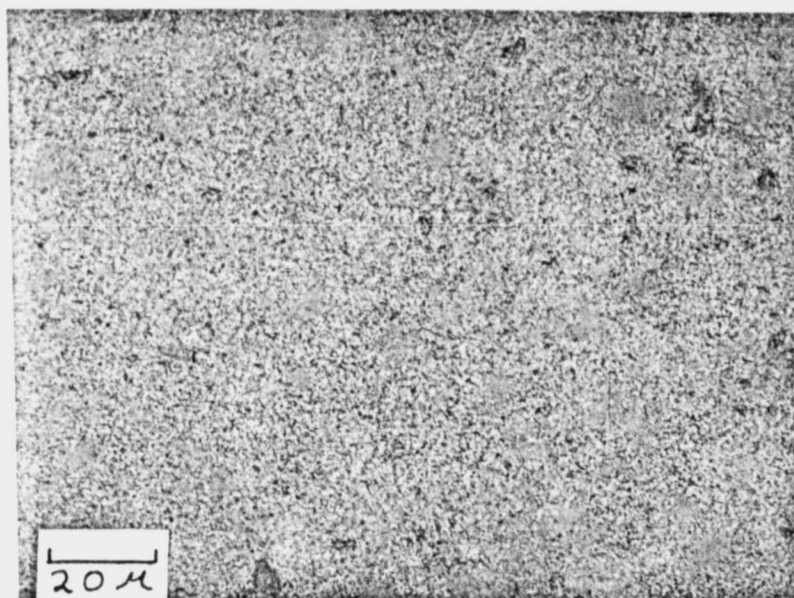
Figure 36

Optical Photomicrograph of the Pore Size Distribution
of N Series Si_3N_4 with an α/β-Ratio of 4.

CROSS HEAD SPEED
0.02"/min
(0.508 mm/min)

P

0.3"
(7.6 mm)

0.2"
(5.08 mm)

A

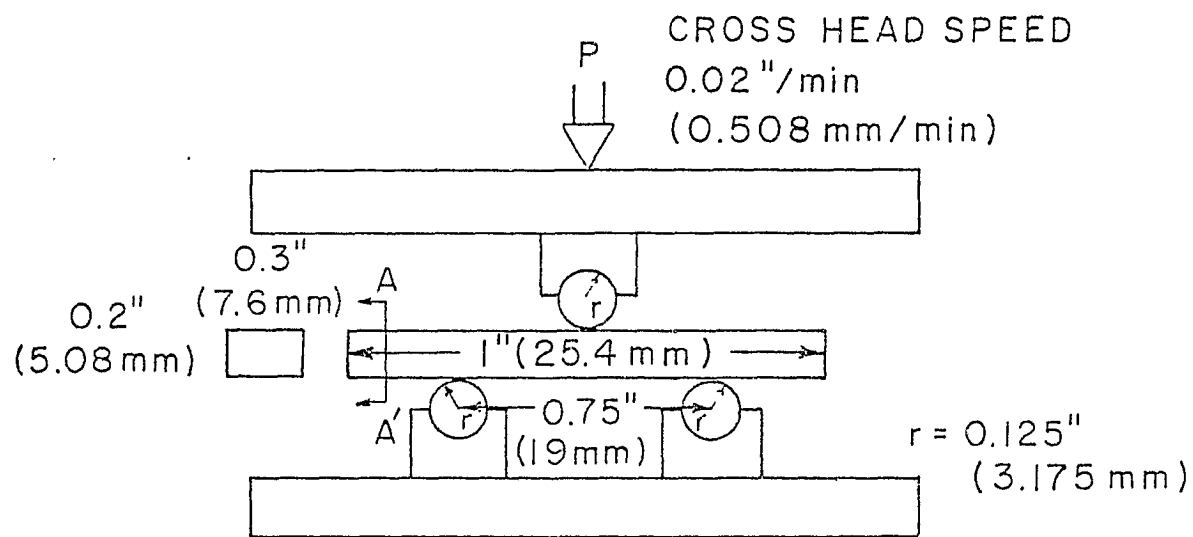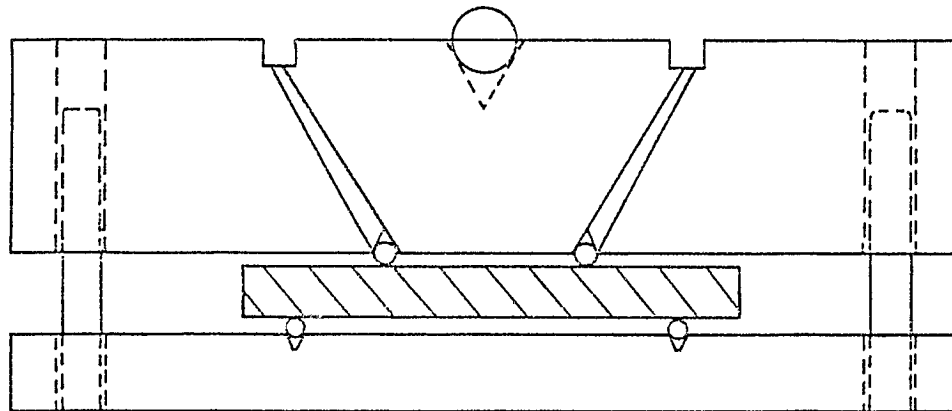1"(25.4 mm)

A'

0.75"
(19 mm)

r = 0.125"
(3.175 mm)

Figure 37

Schematic of N Series Three Point Bend Fixture.

FOUR POINT BEND TEST RIG

Figure 38

Schematic of Four Point Bend Fixture.

(0.5 mm/min) was used for both the three and four point testing.

When testing a brittle material such as silicon nitride, the surface finish of the test bar is of major concern. Damage caused by grinding will often be the failure initiating flaw. The bars tested during this investigation were prepared following the grinding specifications shown in Table VIII. Figures 39 and 40 show failure initiating from a surface defect while Figure 41 shows an internal failure initiation site.

As previously noted, the pore size C for the N series decreased with increasing α/β ratio. Thus, it would be expected that the N series MOR would increase with decreasing pore size and increasing α content. Figures 42 and 43 confirm this observation.

The results for the K series material, however, do not yield such a direct relationship. The K series MOR varied from 30 to 42 ksi (in four point bending) but did not show a continuing increase with increasing α/β ratios. Samples with high α/β ratios (8 to 9) had MOR values of 30.3-33.6 ksi (209-231 MN/m^2). Those samples with maximum MOR had α/β ratios from 3 to 5 while those with ratios below 3 had reduced MOR values. This data is shown in Figure 44.

One possible explanation of the K series results is the amount and role of the unreacted silicon. The K series material with high α-content are also found to contain larger amounts of unreacted Si. Figure 45 is a photomicrograph of such a material and Figure 46 shows an unreacted Si particle as the failure initiating flaw. Samples of silicon nitride with low α/β ratios (<3) are well reacted but exhibit reduced strength

TABLE VIII

Grinding Specifications for K Series
Four Point Bend Bars.

Rough Grind

Wheel Spec.	100 grit	
Wheel Speed	5000-6000 sfpm	
Downfeed	0.002-0.003 in	inches/pass
Crossfeed	1/8-1/4 in	inches/pass
Table Speed	300-400	inches/min

Intermediate Grind

Wheel Spec.	150 grit	
Wheel Speed	5000-6000 sfpm	
Downfeed	0.001 in	inches/pass
Crossfeed	1/8-1/4 in	inches/pass
Table Speed	200	inches/min

Finish Grind

Wheel Spec	320 grit	
Wheel Speed	5000-6000 sfpm	
Downfeed	0.0005 in	inches/pass
Crossfeed	1/64 in	inches/pass
Table Speed	100-140	inches/min
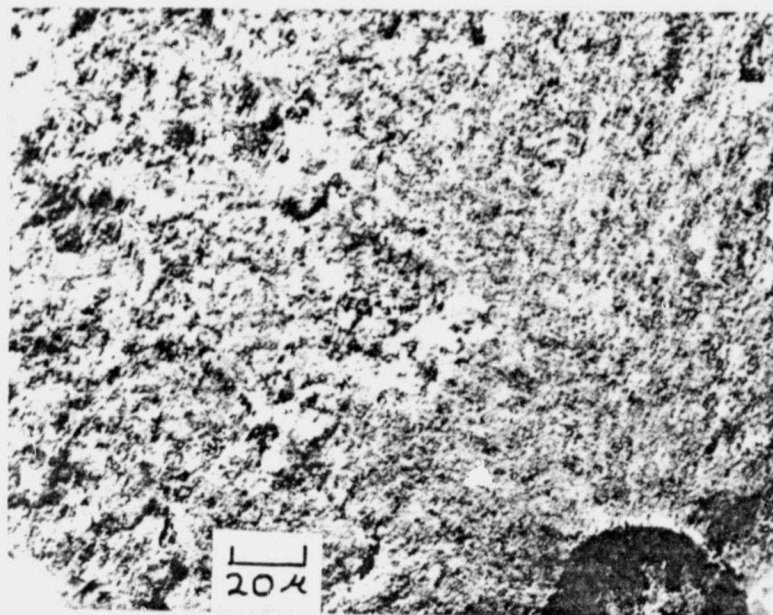
Figure 39
Scanning Electron Micrograph of Failure Initiating
Flaw at Corner for K Series Sample.
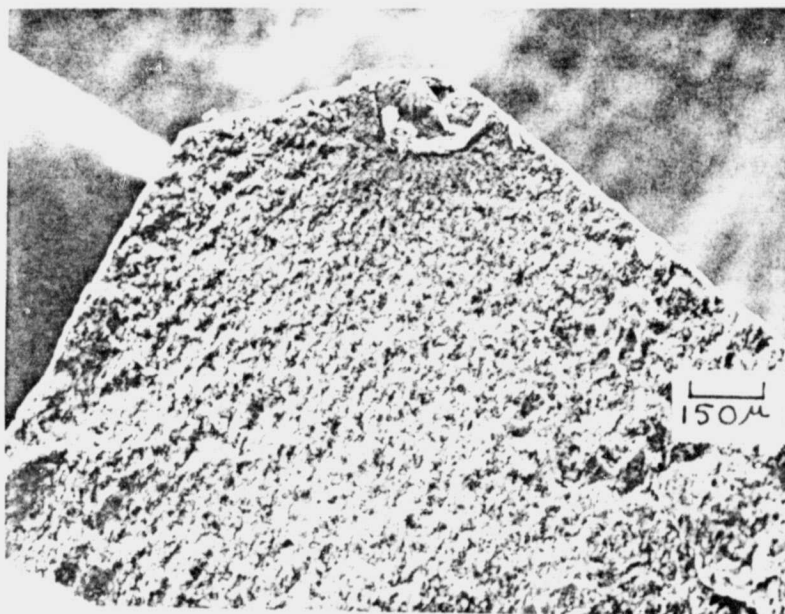
Figure 40
Scanning Electron Micrograph of Failure Initiating
Flaw at Corner for K Series Sample.
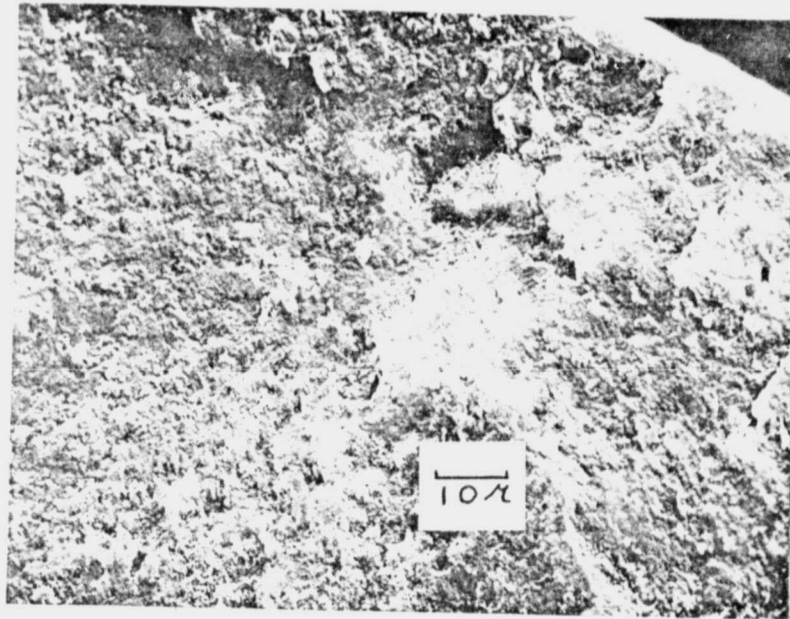
Figure 41

Scanning Electron Micrograph of Internal Failure
Initiating Flaw for K Series Sample.
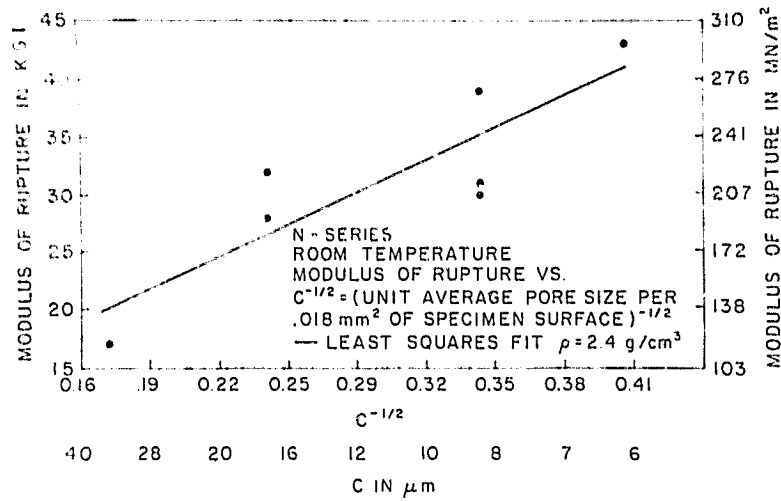
Figure 42

MOR vs. Pore Size Parameter $C^{-0.5}$

for the N Series Reaction Bonded Si_3N_4
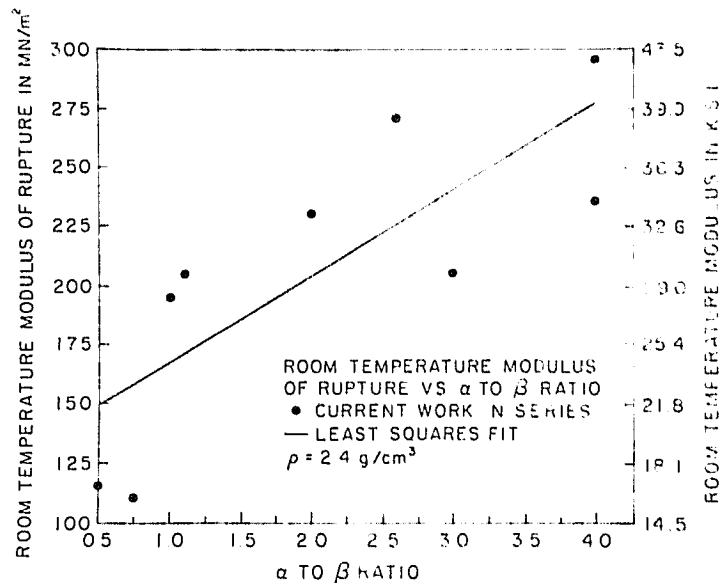
Figure 43

MOR vs. α/β-Ratio for the N Series Si_3N_4
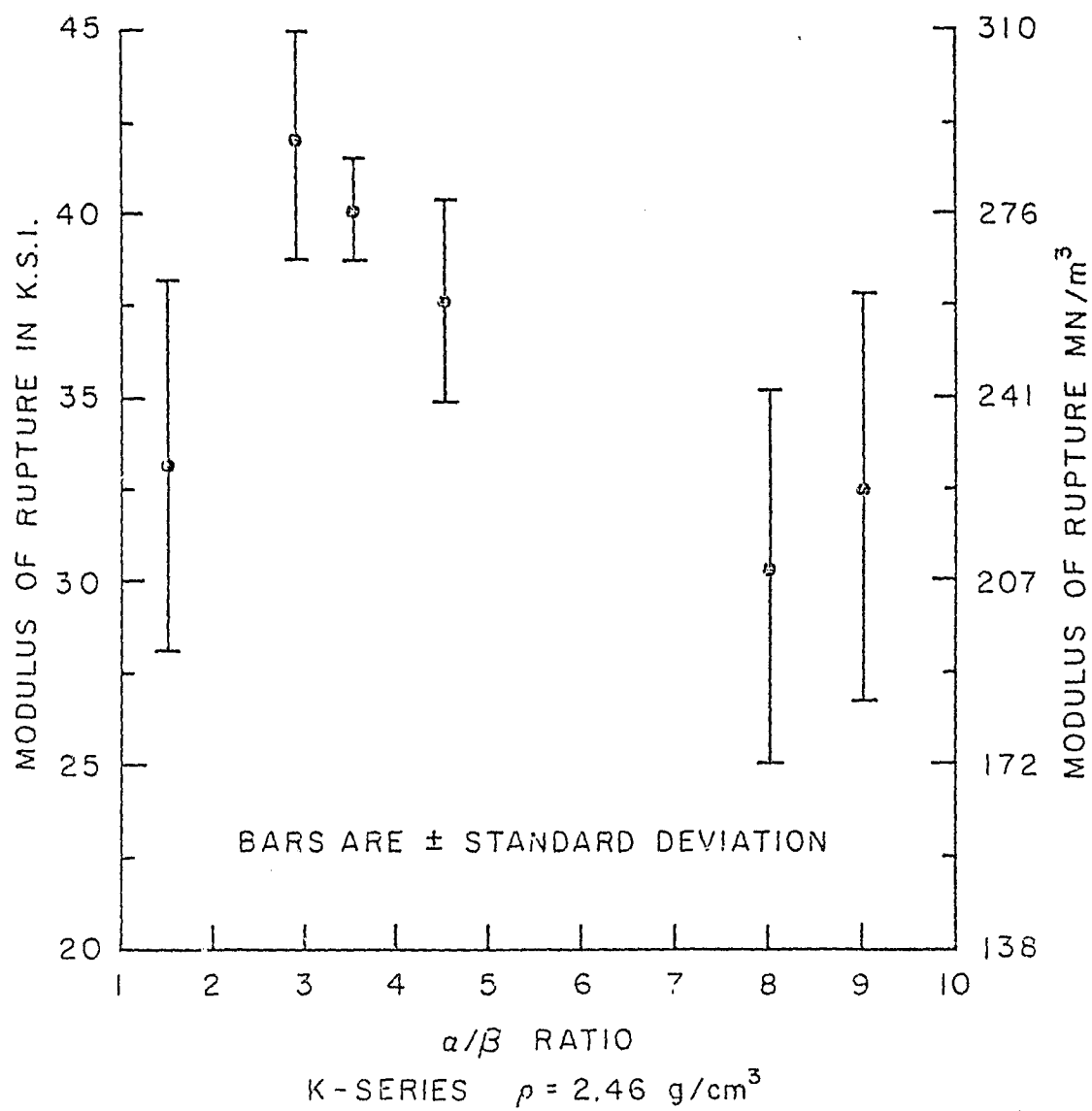
Figure 44

MOR vs. α/β-Ratio for K Series Si_3N_4 Samples;
Note Maximum MOR Does Not Coincide
With Maximum α/β-Ratio.
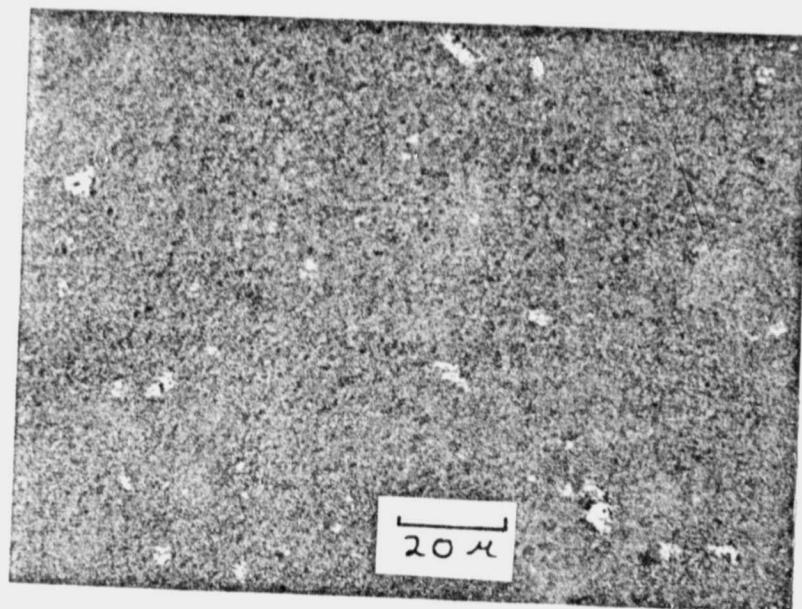
Figure 45

Optical Photomicrograph of a High α-Si_3N_4
K Series Material; Note the Unreacted Si (white)
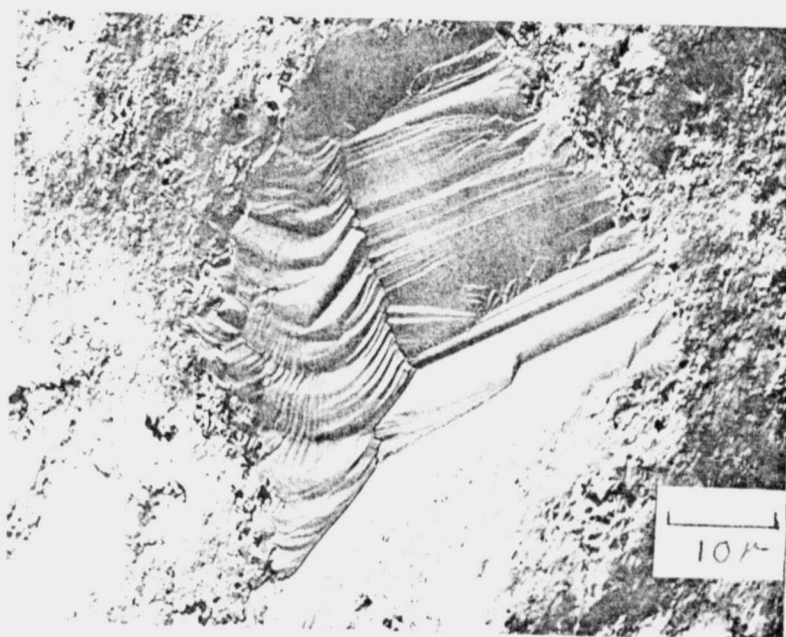
Figure 46

Scanning Electron Micrograph of Large Si Grain
as the Failure Initiating Flaw in the K Series.

as a result of large pore size distributions. Thus, for maximum MOR, one must insure both minimum flaw size and complete reaction.

Efforts at determining the elastic modulus from the four point bend load-elongation curves were unsuccessful. This was mainly due to the large compliance of the test fixture with respect to the material being tested. The elastic constant E was successfully measured using elastic wave propagation. E was measured for the K-series material as 24.2×10^6 psi (166 GN/m^2).

When considering the use of ceramics in structural applications, component design and fabrication as well as failure prediction and analysis become quite important. To aid these analyses, the evaluation of the plane strain fracture toughness (K_{1c}) is required. K_{1c} is a measure of the material's inherent resistance to the propagation of a crack. Once K_{1c} is determined, the critical flaw size, 2a, can be calculated in conjunction with the material's strength. Furthermore, if the elastic modulus, E, is known, the effective surface energy for failure initiation can be determined.

In order to measure K_{1c}, a 0.078 in (1.988 mm) notch was cut in the center of the K series bend specimens using a .006 in (0.15 mm) thick diamond wafering blade (Figure 47). The resulting notch root is shown in Figure 48. As can be seen, the region just ahead of the notch root contains small natural cracks. The K_{1c} tests were performed using the four point fixture with a cross head speed of 0.02 in (0.5 mm) per minute. The test bar had a width of 0.125 in (3.175 mm) and a thickness of 0.250 in (6.35 mm).

Figure 47

Specimen Configuration for K_{lc} Test
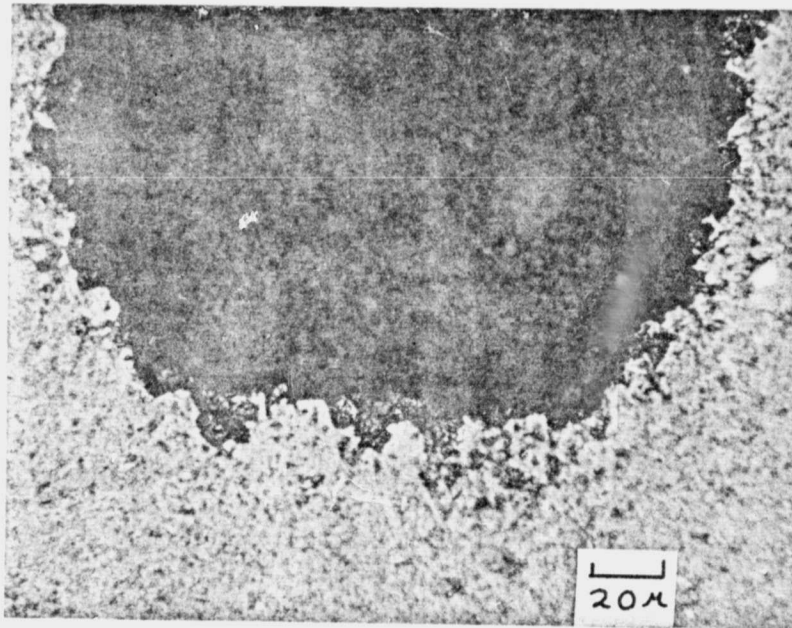
Figure 48

Optical Photomicrograph of Damage at Notch Root

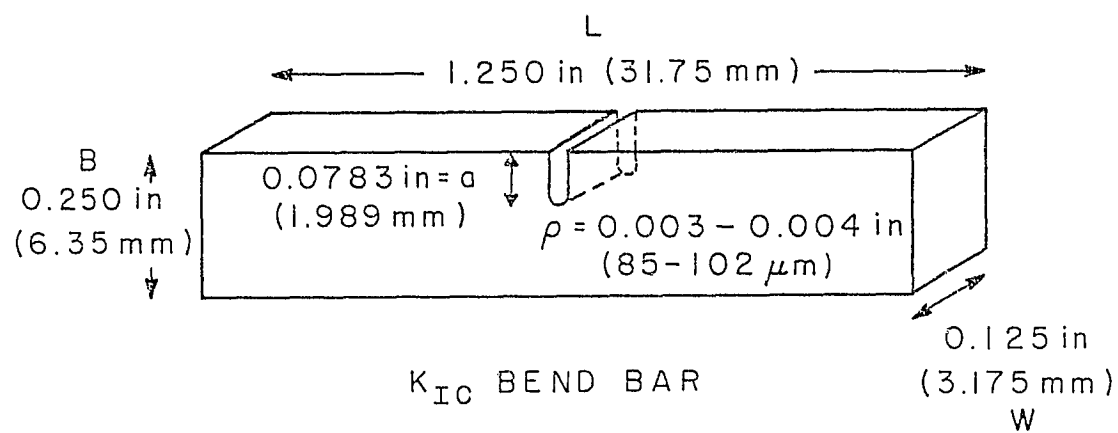It is seen in Figure 49 that the fracture toughness is constant with respect to the α/β ratio of the material tested. The average K_{1c} value is 2107.4 ± 160 lbs/in$^{1.5}$ (2.316 ± 0.175 MN/m$^{1.5}$). The variations found for the MOR results with pore size and α/β ratio are not present for the fracture toughness. The main variation in K_{1c} observed was for those samples which were argon sintered prior to nitridation. These samples had an average K_{1c} value of $2,318 \pm 232$ lbs/in$^{1.5}$ (2.55 ± 0.3 MN/m$^{1.5}$). The exact role argon has in this increase is presently unknown. It is thought that the argon may yield increases in grain boundary energy and through its grain coarsening effect, increase the frictional energy term.

The fracture surface energy γ_i for the materials tested was determined yielding an average value of $9.08 \times 10^{-2} \pm 1.8 \times 10^{-2}$ in-lbs/in^2 (15.9 ± 3.25 J/m^2). This value is in good agreement with results found elsewhere for other Si_3N_4 materials. The argon sintered material exhibited an increase in γ_i to $1.12 \times 10^{-1} \pm 2.2 \times 10^{-2}$ in-lbs/in^2 (19.6 ± 3.9 J/m^2) as would be expected from the K_{1c} data.

Using these values, the critical flaw sizes were evaluated and found to range from 106 microns for an MOR of 30.3 ksi (209 MN/m^2 with $\alpha/\beta = 9$) to 52 microns for an MOR of 42 ksi (290 MN/m^2 with $\alpha/\beta = 3.5$). The size of these critical flaws are comparable to the largest microstructural features observed.

This data indicates that through control of the various processing parameters and an understanding of their effect on the reaction mechanisms, one can design and produce an improved microstructure that will encourage superior mechanical properties.
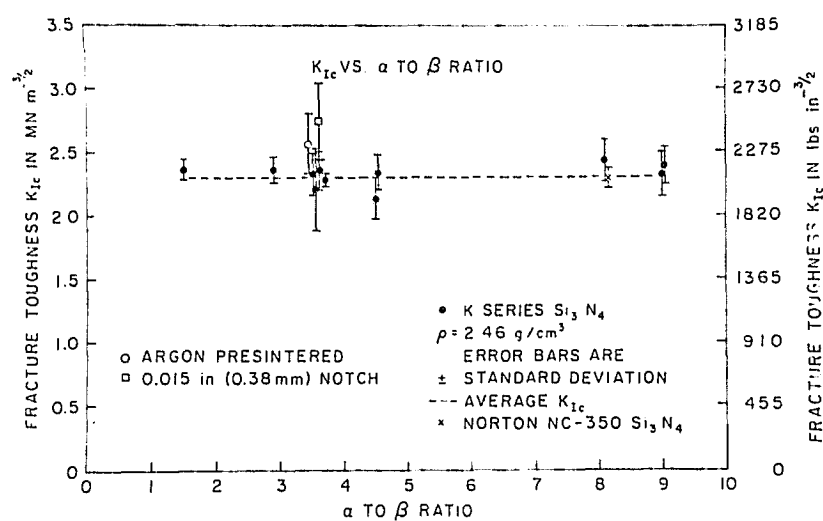
Figure 49

Fracture Toughness K_{1c} vs. α/β Ratio for K Series Si_3N_4

The next stage of this research effort concerns the effect of impurities in the starting silicon powder on the reaction mechanisms (of nitride formation) and the properties of the resultant material. In an effort to remove the variances caused by impurity additions, 99.999% pure silicon powder was purchased from Electronic Space Products, Inc., Los Angeles, California. The as received powder purity was determined by neutron activation analysis and is given in Table IX. The powder (E series) was nominally -325 mesh (<44μ) but further reduction in particle size was required for optimum nitridation. The powder was, therefore, further processed at NASA Lewis Research Center * by a method developed there [4]. Using an attritor mill (similar to a ball mill, but one in which the action of the balls and additional force is accomplished by an internal rotating oar or paddle) modified to maintain a nitrogen atmosphere, it was found that the steel balls used became intimately coated with a continuous layer of silicon. This protective coating was also established on the walls of the mill. Thus, a situation developed such that silicon was grinding silicon, maintaining the purity of the powder. Table II gives the purity levels after milling.

During the milling process, air cannot be allowed to enter the system or the silicon will be rapidly oxidized and the protective layer will spall off. This oxidation phenomenon represents a problem of major concern with this method of comminution. After milling, the silicon powder is extremely pyroforic. The oxidation process is

----

* This work was performed by Drs. T. H. bell and T. Glasgow.

TABLE IX

Neutron Activation Analysis of the E Series
Si Powder Before and After Milling at NASA LEWIS in ppm.

Element	Before	After
Aℓ	95 *	161.3 *
Mn		2
V		2.7
Ti		13.3
Th	5.4	4.9
Fe		
Co		6.7
Cr		18.3
Sc	0.39	0.11

*   Not
         meaningful

strongly exothermic and the powder can glow white hot if introduced to air in an uncontrolled manner. Hence, the powder was removed in a sealed nitrogen atmosphere, evacuated and then introduced to air slowly. The temperature and pressure of the sealed container was carefully monitored during this step so as to allow the reaction to go to completion to avoid runaway oxidation. This process resulted in a higher O_2 content (in the form of SiO_2) of the powder than the 1.6 or 2.2% O_2 contained in those other powders used previously in the investigation.

Another problem associated with this process is that the mean particle size is not reduced with more grinding time below the low micron range. This has been attributed to the fact that since the powder is milled dry, agglomerates or weak welds between particles develop and are not broken up as shown in Figure 50. Nevertheless, this process was successful in maintaining the basic purity of the powder. Since purity was of major concern, and the powder exhibited excellent compaction properties, no further refining was performed prior to compaction.

The processed powder had an average particle size of 4 microns and a maximum particle size of 30 microns with a size distribution shown in Figure 2. This powder was then compacted using isostatic pressing at the NASA Lewis Center. Two cylinders 3 1/4 inches in diameter and approximately 8 inches long were pressed at 40,000 psi (275 MN/m^2) and 60,000 psi (355 MN/m^2). This led to a green density of 1.33 and 1.38 g/cm^3 respectively. These cylinders were then cut into wafers using a clean hacksaw blade. These wafers were cut using the same blade and shaped into blocks 1.3 x 1.3 x 0.6 in (3.3 x 3.3 x
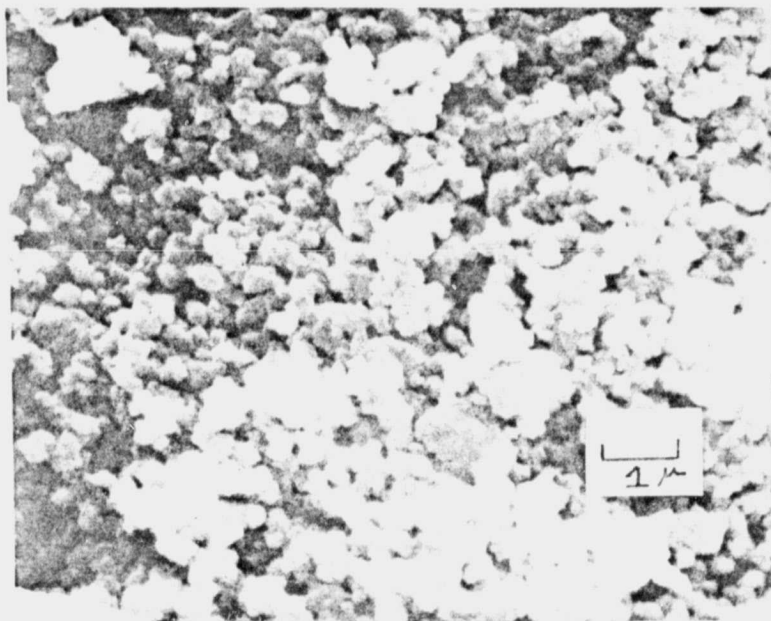
Figure 50

Scanning Electron Micrograph of the E Series
Si Powder as Milled at NASA Lewis

1.5 mm) by hand grinding on 60 grit SiC papers. These blocks were then
nitrided to form reaction bonded silicon nitride.

Upon removal from the furnace, the nitrided E series silicon compact
was covered with the normal layer of light blue gray silicon oxide fur.
After light polishing removed this coating, the reaction product ex-
hibited a dull gold color. All of the reaction bonded silicon nitride
made during this investigation and those reported throughout the litera-
ture were gray in color. After x-ray diffraction determined that the
compact was indeed silicon nitride, an investigation into what was
different about the E series began.

The material characteristics and properties of the E series product
will be reported first, and then the results of the investigation into
the gold silicon nitride will be presented. On a macroscopic level,
there often appeared small circular areas of dark gray color
(characteristic of the K series nitride) within the gold material.
These gray freckles may be associated with localized impurity segrega-
tion. Magnetic susceptibility and emission spectroscopy (performed at
Texas Instruments, Inc., Attleboro, Massachusetts) were performed on
three darker areas and the results are listed in Table X. Upon micro-
scopic examination, no change in microstructure across the freckle-
matrix interface could be discerned.

The microstructure of the E series reaction bonded silicon nitride
exhibited three main morphologies. Most striking was the observation
of large interconnected pore channels. This type of pore structure is
shown in Figure 51 and was not apparent in the K-series material. In
another morphology, large pores are present but are not as interconnected

TABLE X

Analyses of Impurities in Gray Freckles
Associated with E Series Silicon Nitride.

Magnetic Susceptibility

Gold Si_3N_4 (E series) 3.5×10^{-4} % Fe[*]

Gray in Gold Si_3N_4 (E series)   0.02% Fe[*]

Gray Si_3N_4 (K series)   0.24% Fe[*]

[*] It was assumed that the mass of ferromagnetic impurity as reflected
by susceptibility was due to Fe.

Emission Spectroscopy

	Major	Minor	Trace	
Gold Si_3N_4 (E series)	Si	Fe, Aℓ, Ni, Ti, Co	Mg, Cr	
Gray in Gold Si_3N_4 (E series)	Si		Mg	Ni, Aℓ, Fe, Ti, Co
Gray Si_3N_4 (K series)	Si		Mg	Ni, Aℓ, Fe, Ti, Co

	NA
Gold Si_3N_4 (E series)	Low
Gray in Gold Si_3N_4 (E series)	High
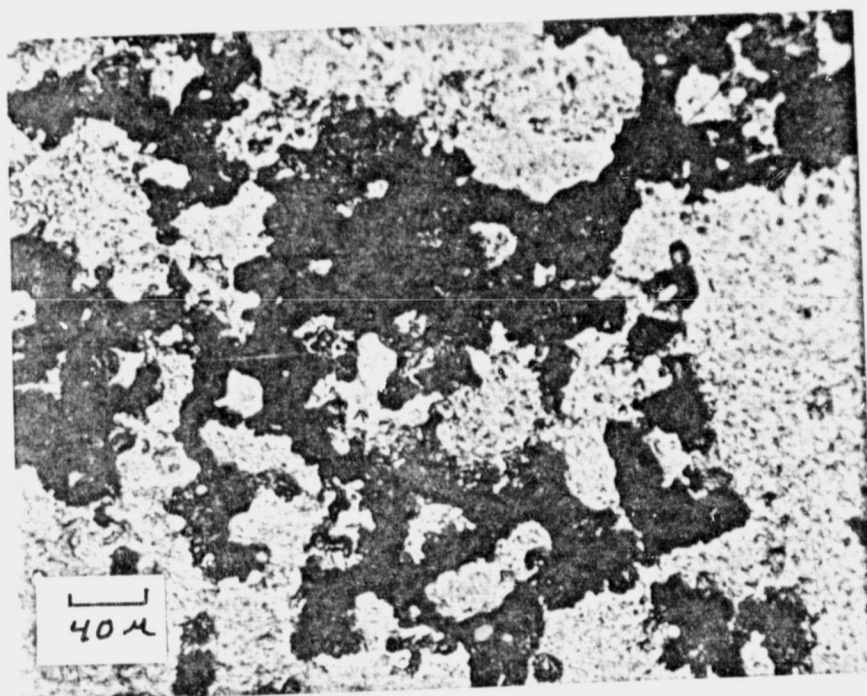
Figure 51

I terconnected Pore Channel Structure in
E Series Si_3N_4 Compacted at 40 Ksi.

as the channels mentioned above. This structure (Figure 52) and the

pore channels could have been caused by poor compaction. However, other

evidence including the green density achieved indicates that these mor-

phologies are due to reaction mechanisms peculiar to the purer E series

compacts. Figure 53 shows the pore structure associated with the

E-series compact that was pressed at 60 ksi (355 MN/m^2) was similar to

that of Figure 52. The third morphological feature observed was more

comparable to the K-series material. This more refined and smaller

pore structure is shown in Figure 54 along with an unreacted silicon

grain into which the nitride was advancing.

The nitridation reaction was generally not as complete for the

E-series material as it was for the K series. Following the nitriding

schedule that yielded the best K-series material (Figure 4) resulted

in an E series compact that was 86% reacted. The mechanisms mentioned

earlier could explain this as being caused by the increased O_2 content

of the E series powder. The oxide layer on the silicon particles could

remain stable longer due to the increased amount of O_2 and hence inhibit

the extent of the reaction. It was observed that just prior to the

$1200^{o}C$ nitriding hold, a large amount of fur formed in the hot zone of

the furnace surrounding the sample (as observed through an optical

pyrometer). This phenomenon coincided with a surge in the nitrogen

demanded by the reaction. It is proposed that these occurrences are

related to the higher O_2 content and the absence of volatilizing (and

cleaning of SiO_2) aids such as Fe. It is interesting to note that one

sample was nitrided at high temperature to 78% completion and then

renitrided to 89% reacted following a more conventional nitriding schedule.
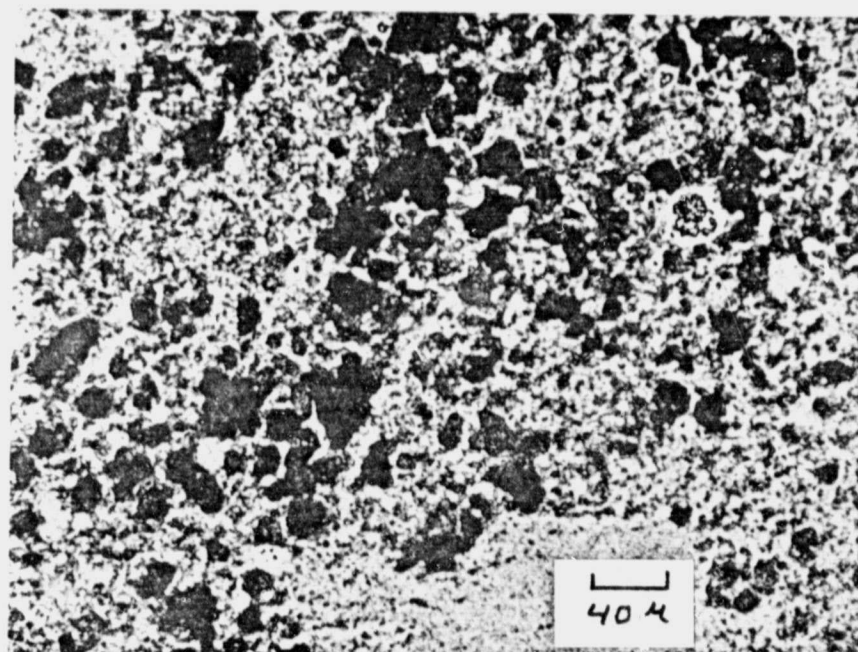
Figure 52

Large Pores Associated With E Series Nitrided From 40 Ksi Compact
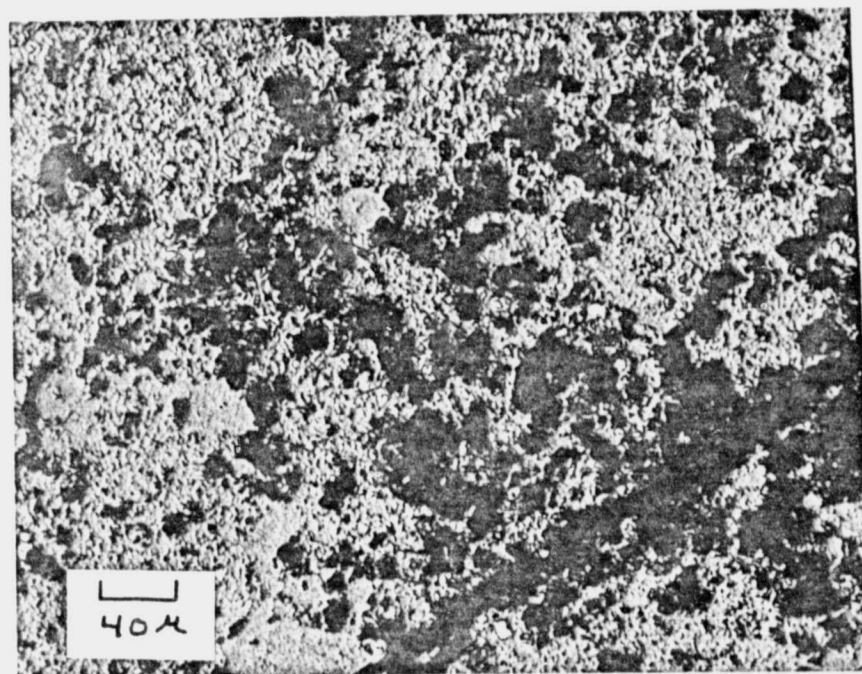

Figure 53

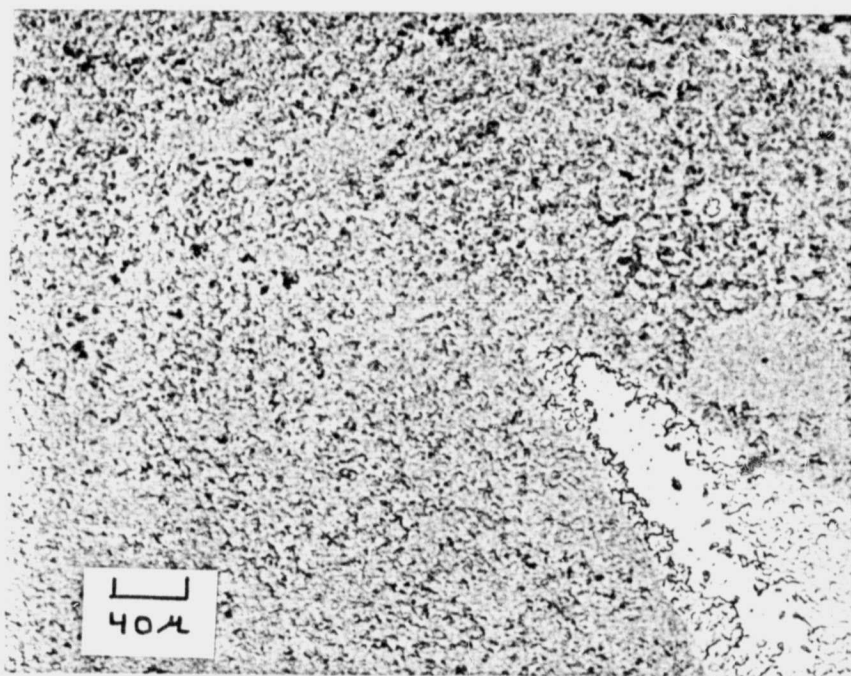Large Pores Associated With E Series Nitrided From 60 Ksi Compact

Figure 54

Photomicrograph of E Series Si_3N_4 With
A Morphology Similar to K Series

The ratio of the two phases (α/β) present in reaction bonded silicon nitride ranged from 1.96 to 5.53 for the E series material. As was the case for the K series, the role H_2 had was to promote formation of the phase which was favored by the nitriding schedule. For example, two nitriding runs made using the 4%H_2 gas resulted in α/β ratios of 3.79 and 1.96: the former following the standard schedule (Figure 4) and the latter modified towards longer times at the higher temperatures.

When the E series compact was subjected to an argon pre-sinter, the α/β ratio increased (>5). This is contrary to earlier results and is not fully understood at this time. Furthermore, the argon pre-sinter seemed to refine the E series microstructure (Figure 55) although Figure 56 shows a microstructure more consistent with the mechanisms proposed earlier.

Since the E series reaction bonded silicon nitride exhibited a complicated and overwhelming pore structure, it was not possible to determine the pore size distributions as was done for the K series. However, as would be expected, the enlarged pore structure had an adverse effect on the room temperature mechanical properties. The average modulus of rupture for the E-series material was 15.85 ksi (109 MN/m^2) and the fracture toughness was measured as 1640.6 $lbs/in^{1.5}$ (1.803 $MN/m^{1.5}$). The strongest E series product exhibited a MOR of 17.6 ksi (121 MN/m^2) and corresponded to an argon pre-sinter.

As was the case with the N series, the MOR of the E-series material increased with increasing α content (strongest MOR at α/β = 5.12). The
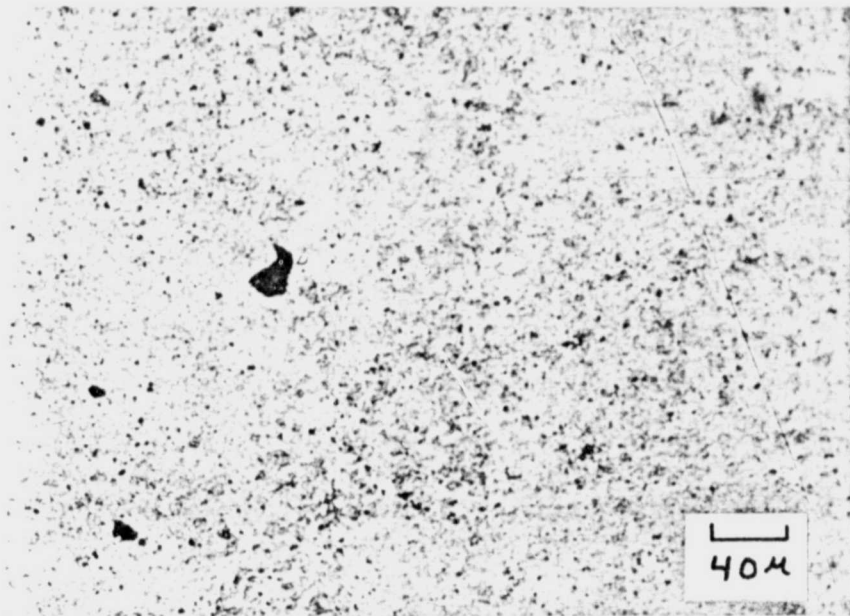
Figure 55

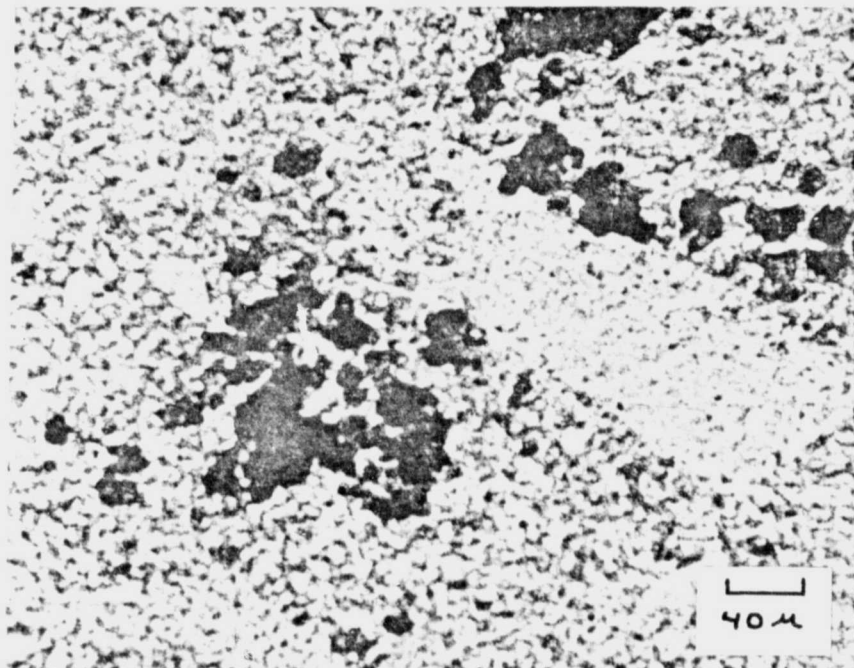Nitrided E Series Microstructure as Refined by
Argon Presinter (9 hrs. at 1000°C)

Figure 56

Nitrided E Series Microstructure Showing β and Large
Pores Associated with Argon Presinter

results may also be comparable to the K series but no tests were con-
ducted on E-series material with larger α/β ratios. The density of the
nitrided E-series material was fairly constant, despite various nitrid-
ing schedules, with the average being 2.14 g/cm^3. The two densest
nitrides, 2.166 and 2.165 g/cm^3, were from E-series material that was
argon presintered and made from the compact pressed at 60 ksi, respect-
ively.

These results indicate that the purer E-series silicon compacts
nitrided to form reaction bonded silicon nitride containing a large
pore structure with reduced room temperature mechanical properties.

When the furnace was first opened after the initial E series run,
a strong smell of rotten eggs was observed. This, with the goldish
color, pointed to the possibility that sulfur had been introduced into
the system. As a test, the nitriding gas used was bubbled through lead
acetate in order to precipitate sulfides. No positive results were
obtained. Due to the background nitrogen would produce, mass spectrometry
of the nitriding gas used was not performed. Eventually, a second E
series compact was nitrided using a new supply of gas and produced gold
silicon nitride.

This gas had previously been used to nitride a K series compact
resulting in the typical gray color. Thus, the nitriding gas used was
no longer considered to be the cause of the color change.

A comparison of x-ray diffraction patterns of the K and E series
starting silicon powders was made. The E series pattern was unusual
in that the silicon peaks were very broad especially at their base.
This typ. of peak broadening could be caused by reduced particle size,

residual stresses and strains or an amorphous component in the powder. Another set of x-ray patterns was obtained after a 16 hour 800°C argon sintering of the K and E series powders. The amorphous nature of the E series powder was no longer present. The sintering process would have relieved residual stresses and could have crystallized any amorphous material. It is possible that the two powder lots contained different oxides of silicon, which could effect the reaction kinetics, but no evidence of this was found.

A piece of each nitrided series was metallographically polished for reflectivity measurements. This test revealed that both reaction bonded silicon nitride materials absorbed the same part of the spectrum. However, it was observed that the two patterns differed in amplitude with the K series nitride being approximately one percent more reflective.

The x-ray anomaly mentioned above indicated a need to measure the crystallization temperature of the two powders. A Vacuum Technology Assoc. RF diode sputtering unit was used and operated at a frequency of 13.56 MHz to sputter an amorphous silicon film. The targets made from the E and K series silicon compacts were 2 x 2 x 0.25 in (5.08 x 5.08 x 0.635 cm) and were cleaned by sputtering onto dummy substrates. Two (per series) sapphire single crystal (Al_2O_3) substrates were attached to the vertical plate anode using Dow Corning 340, a silicone heat sink paste. With a plate current of 110 ma, RF voltage of 800v and pressure maintained at 4.0 x 10^{-2} torr (argon flow), a sputtering rate of ~3μm/hr. was achieved. The final film thickness measured optically and by using a Tallysurf surface profilometer was between 10 and 15 μm.

X-ray diffraction analysis confirmed that both the K and E series films were initially amorphous. Two films (one from each series) were then heated in a flowing argon atmosphere to 700°C and held there for three hours. After slow cooling, the samples were analyzed by x-ray diffraction. The films appeared to be deteriorating and spalling off. This could have been due to some crystallization but was not supported by the x-ray data.

Several other attempts were made in a similar fashion but no difference was detected between the two films. Due to time limitations, however, no further work was conducted along this line. The ability to sputter both silicon powders successfully was established and it is recognized that this could be important for future silicon nitride development.

Throughout these experiments investigating the E series reaction bonded silicon nitride, work was being done to establish the actual purity of the silicon powder (Table XI). The purity of the powder was measured through the various processing steps and is shown for both the K and E series starting silicon powder.

As already noted, both magnetic susceptibility and emission spectroscopy analyses were made on the E and K series silicon nitride. These tests were in close agreement with the results obtained from the neutron activation analyses. Two other tests[*] to determine purity were attempted without success. By using an Auger analysis[*] in conjunction with an ion mill, it would have been possible to obtain an elemental profile of the nitrided sample. Unfortunately, the reaction bonded silicon nitride was not conductive enough. The attempt to use plasma emission spectroscopy[*]

---

* Performed at Texas Instruments, Inc., Attleboro, Mass. - Dr. S. S. White

Table XI

Neutron Activation Analysis of the K and E Series
Through the Processing and Nitriding Steps

Element	K series green powder	K series argon sintered only	K series Nitrided only	K series argon sintered & nitrided	E series as received	E series after ball milling	E series argon sintered	E series nitrided only
Fe	10,570	10,037	7,775	7,083	→ 0	320	450	603
Na	–	–	–	83	53	80	97	33
Mn	143	146	93	90	–	8	9	9
Mg	1,330	2,820	1,000	1,592	–	50	20	354
V	547	561	388	387	–	101	101	67
Ti	422	430	340	342	–	–	–	–
Cr	1,498	1,482	1,149	1,036	8	23	27	30
W	1,055	1,044	953	880	–	5	–	280
Co	300	293	260	242	–	9	6	47
Ni	985	1,053	706	650	–	101	44	–
Th*								
Sc*	34	31	23	21	–	1	–	–

*Concentration in PPM

failed as the silicon nitride could not be made to go into solution.

Based on the results that were obtained, it became apparent that Fe as an impurity was most important. The results from the magnetic susceptibility test (Table X) strongly substantiates this fact. The gray in the gold E series nitride exhibited a susceptibility, attributed to Fe, between the values attained for the K and E series nitrides. Thus, a series of experiments were designed to try to verify the role of iron as an impurity.

The E-60-Fe experiment was designed to try to introduce electrolytic grade iron into the E series silicon compact pressed at 60,000 psi. Three silicon samples were prepared according to Table XII. These samples were dried in an oven at $90^{\circ}C$ prior to nitriding using the 1% H_2 gas according to the following schedule: $1000^{\circ}C$, 2 hrs.; $1100^{\circ}C$, 24 hrs.; $1190^{\circ}C$, 18 hrs.; $1360^{\circ}C$, 3 hrs.

Macroscopically, samples A and B appeared light gray around the edge and the bulk was brownish gold. Sample C was basically light gray with many small dark dots and some isolated golden areas. Samples A, B and C did not react to completion and were 59%, 46% and 38% reacted respectively. Their respective α/β ratios were 12.5, 7.7 and 13.1.

Microscopic observation of the microstructures revealed a morphology of disjointed material (Figure 57) that was later seen to be connected by an underlying matrix. Figures 58 and 59 represent the microstructures of samples B and C respectively. The open, interconnected pore channels associated with the E series silicon nitride were not as prevalent in these samples.

Table XII

E-60-Fe Sample Preparation

Sample A. 1 small silicon wafer soaked in 125 mℓ HCℓ + 375 mℓ
distilled water + 5 g. electrolytic grade iron for
64 hours

Sample B. 1 large silicon wafer soaked in above solution plus
methanol (1 : 1) to break surface tension for 64 hours

Sample C. E-60 forming powder soaked in solution for 40 hours.
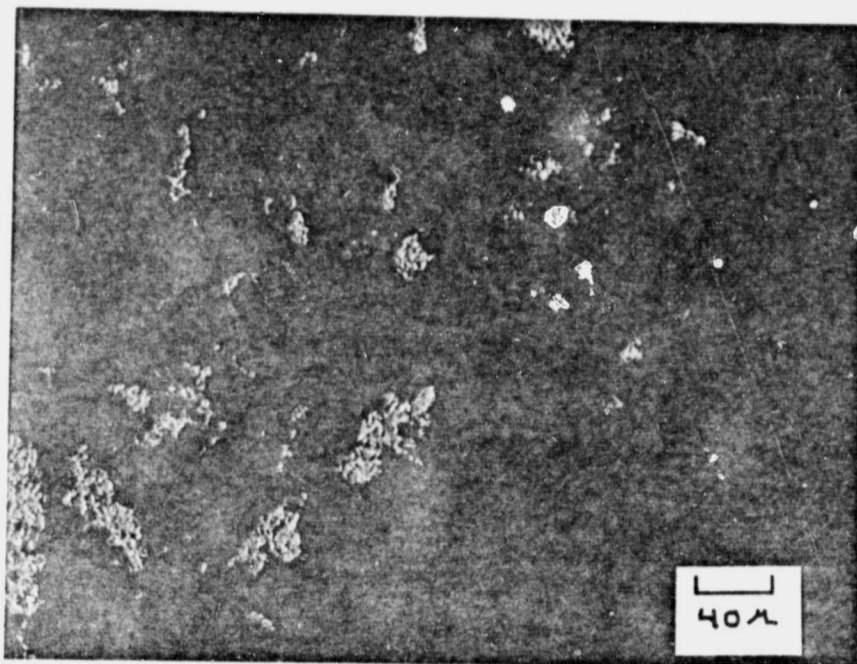Repressed using die at 6,000 psi.

Figure 57
Photomicrograph of E-60-Fe Sample C Showing Disjointed Material Appearance

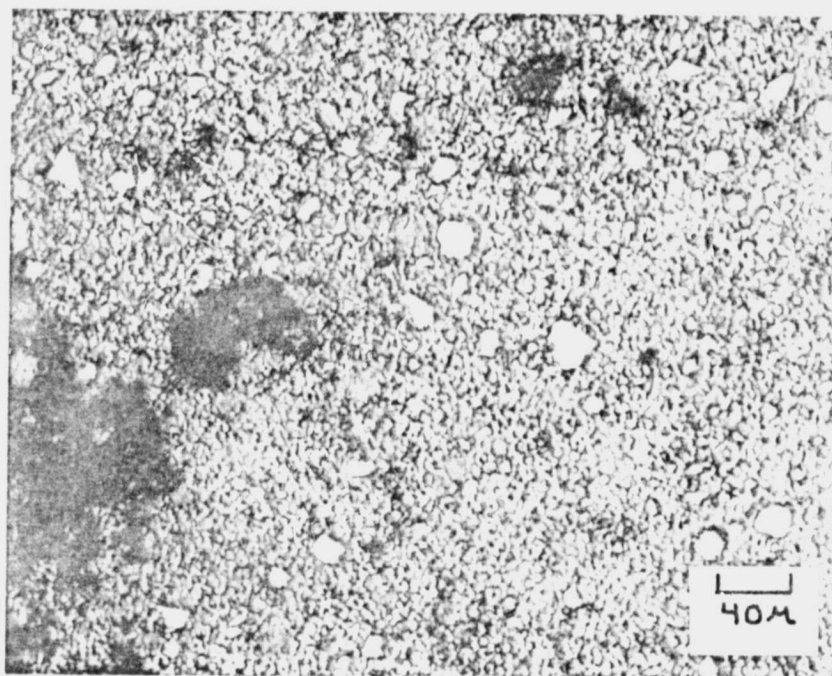ORIGINAL PAGE IS
OF POOR QUALITY

Figure 58
Photomicrograph of E-60-Fe Sample B Showing More Refined Microstructure as
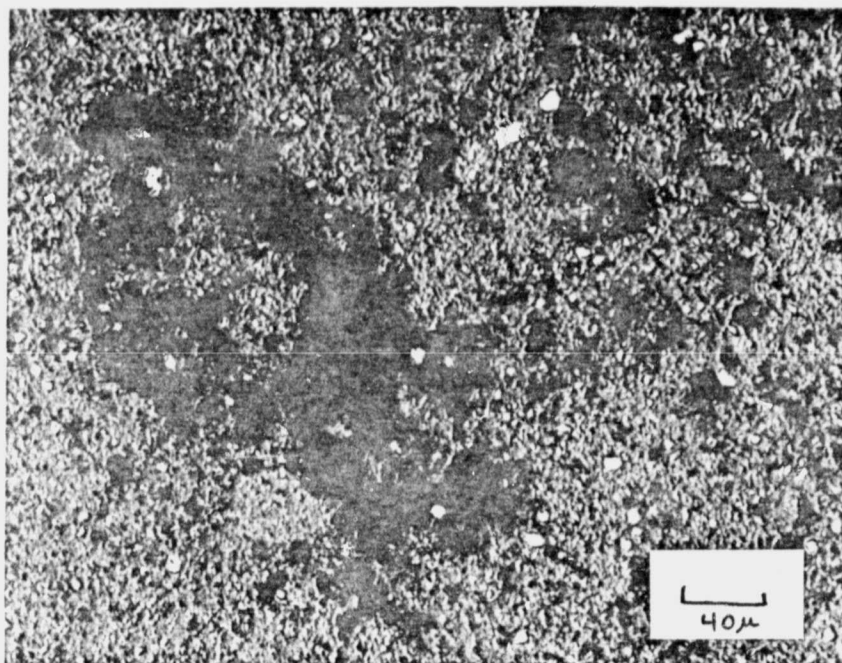Compared to E Series Material. Note Unreacted Silicon (white)

Figure 59

Photomicrograph of E-60-Fe Sample C
Note Large Pores But Absence of Pore Channels

The results from the E-60-Fe experiment offer positive proof that Fe as an impurity in the starting silicon powder is responsible for the observed color changes in reaction bonded silicon nitride. The next group of experiments was designed to repeat the E-60-Fe program in a more controlled manner. The sample preparation for this GTG series is listed in Table XIII. These samples were nitrided using the 1% H_2 gas following a schedule of: $110^{\circ}C$, 21 hrs.; $1200^{\circ}C$, 10 hrs.; $1300^{\circ}C$, 10 hrs.; and $1390^{\circ}C$, 48 hrs.

GTG-1 reacted to the typical gold color associated with the E series silicon nitride. On the top edge of the sample, a layer of gray silicon nitride had formed. It is believed that since all of the GTG samples were nitrided together, the vapors associated with each sample may have mixed. Thus, it becomes apparent that some Fe transported to the sample in the vapor state causing the shallow layer of gray silicon nitride. The microstructure of this sample was characteristic of the E series but the pore structure was more refined (Figure 60). This could also be a result of increased vapor activity. The sample was 82.4% reacted with an α/β ratio of 7.2.

The macroscopic appearance of GTG-2 was typical of the K series silicon nitride. The microstructure, however, exhibited the disjointed morphology shown in Figure 61. Observations made using the SEM revealed that a typical matrix of silicon nitride lay below and in between the isolated islands of material (Figure 62). This sample was 89.4% reacted with an α/β ratio of 3.7.

Sample GTG-3 was light gray in color with a slightly pitted surface. The color of this silicon nitride indicates again that Fe as an impurity

TABLE XIII

Sample Preparation for GTG Experiment

Sample	Purpose	Processing
1	E series control brick	10 g. brick
2	K series control brick	11 g. brick
3	To introduce Fe impurity to E series powder	10 g. of E powder for 23 hours in solution* plus 3.00 grams of Fe** powder, repressed at 6000 psi
4	To remove metallic impurities from K series powder	10 g. K series powder soaked in 1:1 HF:H_2O (distilled) for 22 hrs. Powder repressed at 6000 psi
5	To chemically etch metallic impurities	10 g. K series powder soaked for 41.5 hrs. in solution*
6	To introduce Fe into E series compact	9 g. brick soaked in 100 ml of solution + 50 ml ethyl alcohol + 3 g. Fe** for 20 hrs.
7	To remove metallic impurities from K series brick	10.5 g. brick soaked in 100 ml of solution* for 20 hrs.

* Solution: 250 ml reagent grade HCl + 750 ml distilled H_2O

** Fe: Electrolytic grade iron

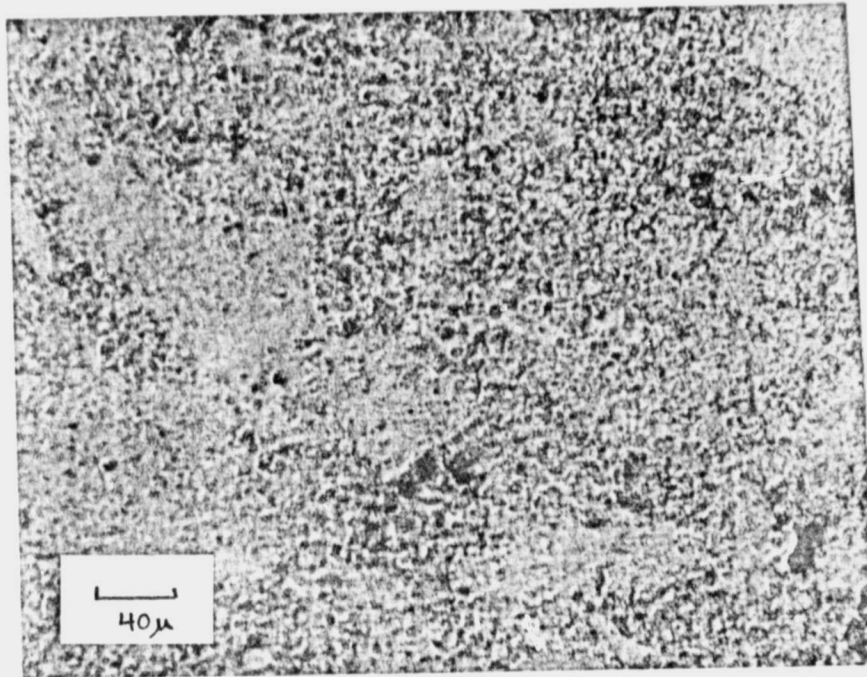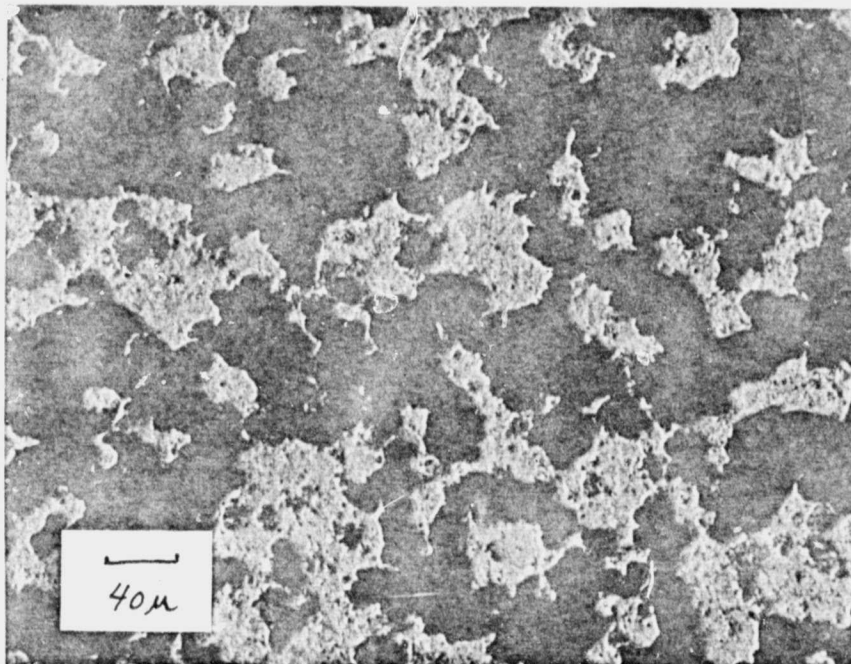Figure 60

Photomicrograph of GTG-1 Microstructure
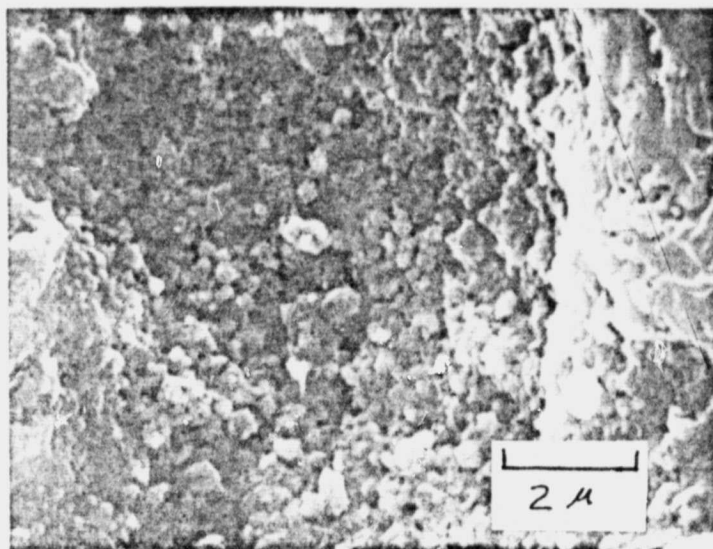
Figure 61

Photomicrograph of GTG-2 Microstructure

Figure 62

Scanning Electron Photomicrograph of GTG-2
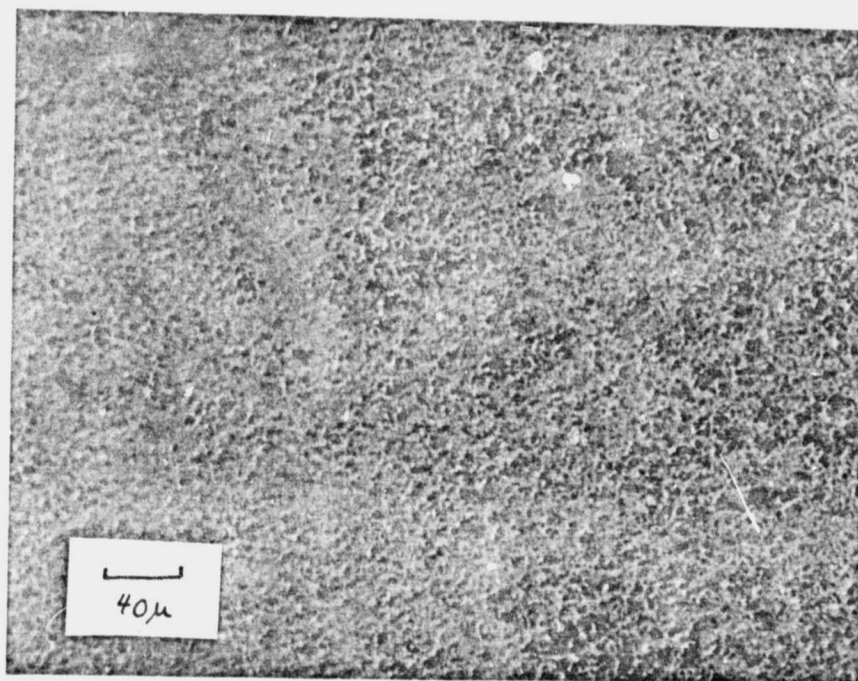
Revealing Underlying Si_3N_4 Matrix

Figure 63

Photomicrograph of GTG-4 Microstructure

was present. The microstructure observed was similar to that of GTG-2 except that the isolated islands of material were larger. GTG-3 was 76.6% reacted with α/β = 4.21.

GTG-4 exhibited a gold color with a shallow gray area on the top face (similar to GTG-1). A small internal gray area was also present and indicates a local concentration of Fe. The microstructure of the sample is shown in Figure 63 as being porous but very tight. The porosity may be due to the low compacting pressure used. This material was 87.6% reacted and had a high α/β ratio of 11.1.

Although GTG-5 was prepared to remove metallic impurities, it was macroscopically similar to K-series silicon nitride. The powder used here was washed in a HCℓ solution. The results, however, indicate that the HCℓ was never able to "clean" the silicon particles due to its inability to penetrate the native SiO_2 layer on the particle surface. The microstructure of GTG-5 was similar to that of GTG-2 as previously reported. This sample reacted to 79% completion with an α/β ratio of 3.0.

The center of GTG-6 was a light gold color that darkens progressively to gray at the edges. This indicates that the Fe transporting solution did not thoroughly penetrate the compact. The microstructure exhibited porosity and isolated material morphologies. The sample was 88.1% reacted and had an α/β equal to 2.38.

The GTG-7 sample was gray throughout indicating the lack of HCℓ penetration mentioned for GTG-5. The bulk of the material was very porous and exhibited the island morphology. This material was 88.1% reacted with a resultant α/β ratio of 3.9.

In order to use plasma emission analysis to determine the impurity content of the GTG reaction bonded silicon nitrides, The material first had to be put into solution. Attempts were made to fuse the silicon nitride powders by mixing with sodium carbonate ($NaCO_3$) and heating in a platinum crucible. Solution was not achieved by this or several other methods, and a more indirect method had to be used.

To determine if the GTG sample preparations did indeed accomplish the objectives, plasma emission analysis was conducted on the original solutions used in the sample preparation (see Table XIV) and these results were compared to the plasma emission results on the filtrates. This comparison indicated clearly that the goals of the sample preparations were achieved (except as noted above for GTG-5 and 7). Further confirmation of this was attained by microprobe elemental analysis of the GTG nitrided samples using an ARL microprobe unit.

The results of the GTG experiment shows that when Fe is removed from the K series silicon powder (which normally nitrides to a gray color), gold reaction bonded silicon nitride results. Furthermore, the gold silicon nitride produced from the E series silicon powder becomes gray when Fe is added. Thus, Fe as an impurity in the starting silicon powder has a major effect on the production of reaction bonded silicon nitride. These effects were further investigated and will be reported later.

Since various impurities greatly affect the nitridation of silicon, an investigation concerning the nitridation of single crystal silicon was initiated. To better understand the nitridation mechanisms responsible for the densification of silicon compacts during the reaction

TABLE XIV

Plasma Emission Analysis*

Values in μg/mℓ

Sample	Description
1	Solution (250 mℓ HCℓ + 750 mℓ H_2O) + 3 g. iron
2	GTG-3 Filtrate
3	GTG-4 Filtrate
4	GTG-6 Filtrate
5	GTG-7 Filtrate

Sample	Cr	Fe	Mg	Ni	Aℓ	Si
1	23	25,500	1.9	24.1	2.6	9.0
2	-	1,025	2.4	166	240	31.1
3	41	285	2.1	41	80	2355
4	-	915	2.3	152	219	30.3
5	149	905	2.4	143	241	30.3

* Performed at Texas Instruments, Attleboro, Massachusetts: Dr. A. Savolainen.

bonding process. A series of nitriding experiments were carried out on Czochralski grown single crystals of Si (semiconductor grade). Wafers were metallographically polished and then nitrided using a heating rate of 50°C per hour in each of the following schedules: 1) 1100°C, 20 hrs.; 1360°C, 90 hrs. or 2) 1100°C, 24 hrs.; 1200°C, 40 hrs.; 1330°C, 24 hrs. The nitriding gas used throughout these experiments was N_2 - 1% H_2 which had been dried over P_2O_5 and gettered for O_2 over pure Si metal.

In addition to the usual characterization of the nitride by x-ray diffraction and SEM, Laue (back-reflection) x-ray diffraction patterns of the polished silicon wafer faces were taken to determine the orientation of each face and thus the nitriding direction. The wafers had been cut such that the (111) planes of the silicon crystal were parallel to the faces of the wafer and this established the nitride growth direction as being parallel to the [111] silicon direction.

The silicon nitride formed on single crystal silicon was quite different from the nitride developed from Si pr der compacts, especially with respect to phase content and microstructure. Due to the different crystal structures of silicon nitride and silicon, there was no evidence of epitaxial growth of the silicon ni   from the silicon surface [5]. The thickness of the silicon nitride   yers varied from about 10 to 16 μm depending on the schedule used, with thicker layers being developed at higher temperatures. The extent of nitridation depends primarily on the solid state diffusion of nitrogen through the silicon nitride already formed as also indicated by the kinetics of nitridation.

X-ray diffraction analysis of the Si_3N_4 layers revealed a pre-
dominantly β-Si_3N_4 product. The presence of a large amount of β-Si_3N_4
in the reacted layer was verified by examining fracture and nitrided
surfaces using SEM. A typical SEM micrograph of a fracture surface of
the wafer is shown in Figure 64. The morphology of this Si_3N_4 layer is
characteristic of these products on single crystals, in that they are
composed of a dense, continuous glassy like phase (β-Si_3N_4) which
appears smooth and with very small pores. Associated with these pores at
the free surface is a small amount of α-Si_3N_4 (needles), as seen from
the SEM micrograph of the free nitride surface shown in Figure 65.
X-ray diffraction revealed only small amounts of α-Si_3N_4 and thus small
α/β ratios. This result is consistent with the α-Si_3N_4 formation
mechanisms proposed by Jennings [6] and Danforth [7]. Only when
elemental Si is volatilized from the bulk crystal through the vapor
phase to beads surrounded by nitrogen gas can the α phase develop. The
amount of α formed is limited by the nitride product already formed on
the crystal. Silicon must diffuse through this layer, most likely
through any porosity or breaks in the film to a free surface where there
is a supply of N_2 gas, and volatilize at the exterior of the product.
Since there is only a single flat grain, there is little opportunity for
further surface reaction and thus minimal α formation. The largest of
these pores is on the order of 5 µm. A high magnification SEM micro-
graph of one of these pores associated with α formation is shown in
Figure 66. Evidence of crystal facets below the surface of the pore
suggests that it is in a β-Si_3N_4 matrix and that it may have developed
due to a break in the dense β-Si_3N_4 grain structure or other pore
mechanisms already discussed.

Figure

SEM Micrograph of Fracture
Formed from a Single

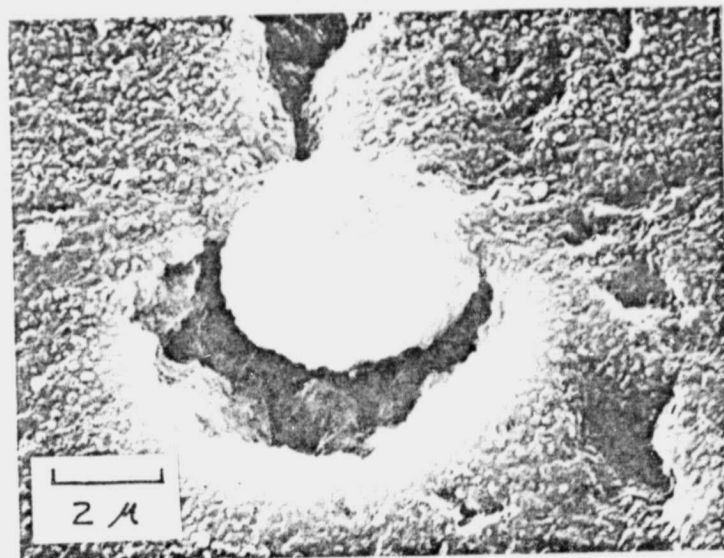
Figure

SEM Micrograph of as Ni
Formed on Single
α-Needles Formed in Regi

Figure 66

SEM Micrograph of a Pore Associated with the

α-Needles Formed on a Free Si_3N_4 Surface
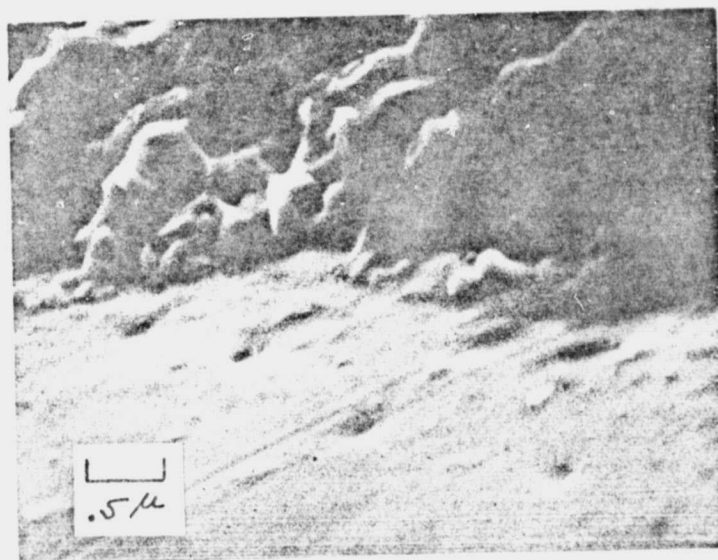
Figure 67

SEM Micrograph of the $Si-Si_3N_4$ Interface Showing

Small Pores Formed from Vacancy Condensation

The SEM micrographs shown in Figures 67 and 68 reveal the morphology in the vicinity of the Si-Si_3N_4 interface. This structure can account for some of the porosity in the nitride layer and, at the same time, verify the existence of a vacancy-condensation process ahead of the nitride growth front.

Just ahead of the α-matte growth front which is growing in the [111] direction with respect to the Si, there appear several small pores isolated in the bulk silicon crystal. According to Atkinson [3] and Danforth [7], the Si migrates out through this region to form subsequent Si_3N_4 on the exterior. This migration leaves vacancies in the bulk Si single crystal which condense to form nano-porosity ahead of the interface. The reaction of N_2 with Si vapor within the internal porosity causes infilling of the nano-pores to produce pico-pores in a fine grained α Si_3N_4. These particular pores observed in the single crystal were only associated with the α-matte formation and were small enough to be characterized as pico porosity.

Close examination of the Si-Si_3N_4 interface in the SEM micrograph shown in Figure 69 reveals the presence of randomly orientated, hexagonal prisms, characteristic of β-Si_3N_4. In addition, very small nuclei of β-Si_3N_4 appeared to be forming just ahead of the predominantly β-Si_3N_4 growth front. The hexagonal crystals at the growth front are not oriented in any given direction and they lose their prismatic character at the silicon surface. Since there is no expitaxial growth of Si_3N_4 from the silicon, there may be distortions of the crystal facets due to the nucleation and growth process. Away from the interface, these crystals became more regular.

Figure 68

SEM Micrograph of Pores Formed by Vacancy
Condensation Just Ahead of the α-Matte Growth Front

Figure 69

SEM Micrograph of Fracture Surface of Si_3N_4 Layer Showing
β-Si_3N_4 Growth Front and Small Prismatic Nuclei Forming
Just Ahead of it. Note Facets of the
Hexagonal Crystals in the Nitride Layer.

The SEM micrographs shown in Figures 67 and 68 reveal the morphology in the vicinity of the $Si-Si_3N_4$ interface. This structure can account for some of the porosity in the nitride layer and, at the same time, verify the existence of a vacancy-condensation process ahead of the nitride growth front.

Just ahead of the α-matte growth front which is growing in the [111] direction with respect to the Si, there appear several small pores isolated in the bulk silicon crystal. According to Atkinson [3] and Danforth [7], the Si migrates out through this region to form subsequent Si_3N_4 on the exterior. This migration leaves vacancies in the bulk Si single crystal which condense to form nano-porosity ahead of the interface. The reaction of N_2 with Si vapor within the internal porosity causes infilling of the nano-pores to produce pico-pores in a fine grained α Si_3N_4. These particular pores observed in the single crystal were only associated with the α-matte formation and were small enough to be characterized as pico porosity.

Close examination of the $Si-Si_3N_4$ interface in the SEM micrograph shown in Figure 69 reveals the presence of randomly orientated, hexagonal prisms, characteristic of $\beta-Si_3N_4$. In addition, very small nuclei of $\beta-Si_3N_4$ appeared to be forming just ahead of the predominantly $\beta-Si_3N_4$ growth front. The hexagonal crystals at the growth front are not oriented in any given direction and they lose their prismatic character at the silicon surface. Since there is no expitaxial growth of Si_3N_4 from the silicon, there may be distortions of the crystal facets due to the nucleation and growth process. Away from the interface, these crystals became more regular.
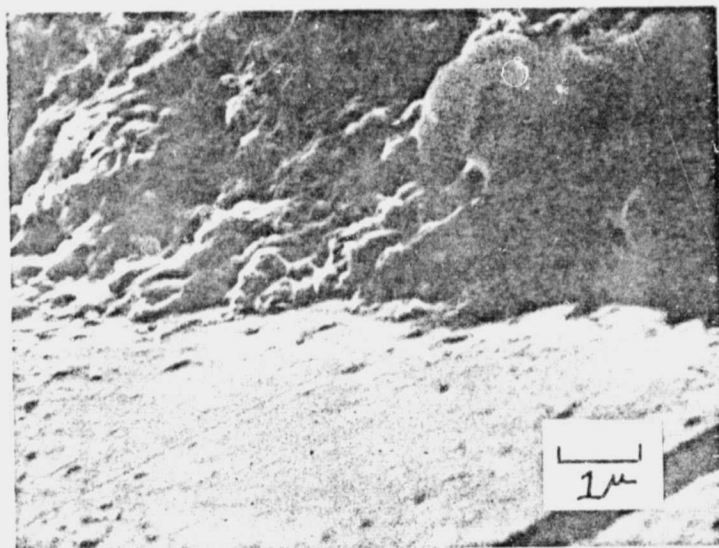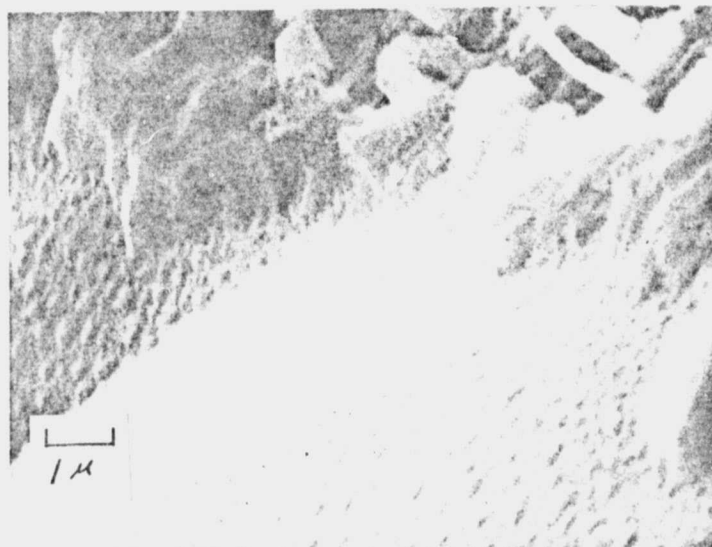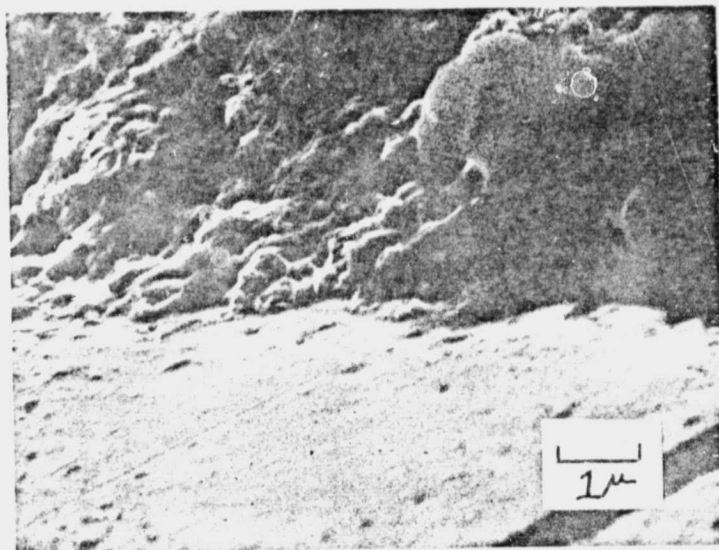
Figure 68

SEM Micrograph of Pores Formed by Vacancy
Condensation Just Ahead of the α-Matte Growth Front

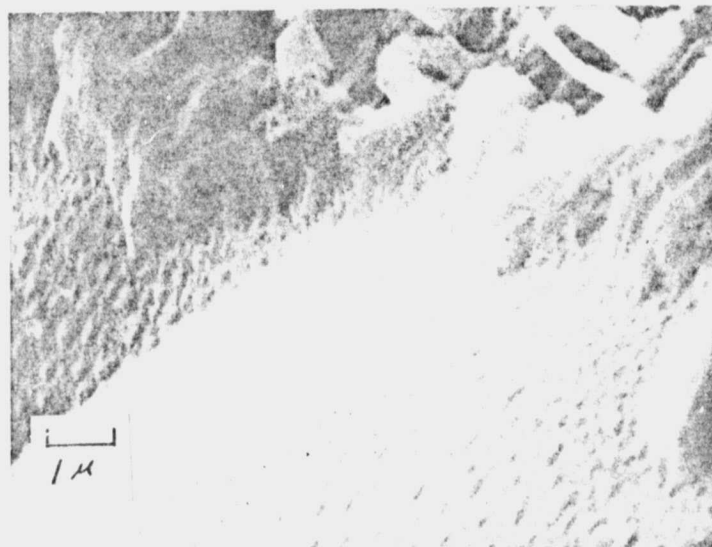Figure 69

SEM Micrograph of Fracture Surface of Si_3N_4 Layer Showing
β-Si_3N_4 Growth Front and Small Prismatic Nuclei Forming
Just Ahead of it. Note Facets of the
Hexagonal Crystals in the Nitride Layer.

The observation of such prismatic nuclei forming ahead of the β-Si_3N_4 growth front has not appeared in the literature to date. The mechanisms for β formation already discussed are mainly concerned with the growth of β spikes (β crystals) once they are formed. It appears from the single crystal nitridation experiments that a nucleation process involving the adsorption of nitrogen gas, the formation of β embryo and the stabilization of these β embryo of a critical size must be an integral part of the formation of β-Si_3N_4. Only those β nuclei of critical size will continue to grow by the mechanism already mentioned while those unstable nuclei will disappear. It has not been determined whether or not a favorable orientation of silicon will result in the stabilization of these β nuclei but it can be stated conclusively that β-silicon nitride forms by a nucleation and growth process and needs no Fe impurities in the silicon for its subsequent formation as mentioned in the literature [8].

A final experiment was designed to measure the effect of iron as an impurity on the microstructure and mechanical properties of reaction bonded silicon nitride. As previously noted, the E series silicon powder had an iron concentration of $\sim$0.03 wieght percent iron and the K series powder $\sim$1.0. These two powders were mixed together so that a range of composition from 0.03 to 1.0 weight percent iron in 0.097 increments was achieved. These eleven samples were nitrided and then characterized.

These EOI powder mixtures were combined in the appropriate ratios so that the final weight equaled 10 grams. The samples were labeled from EOI-1 to EOI-11 corresponding to the end points of 0.03 to 1.00 percent Fe respectively. The two powders were mixed together by hand using a mortar and pestle. Acetone was added to insure thorough mixing

and the mixing was continued until most of the acetone had evaporated (approximately 10 minutes) and the mixture was quite muddy, to minimize powder segregation. After drying the powder in an oven at $55^{o}C$, the mortar and pestle were used to break up the caked surface.

The powder was then pressed, with a little acetone, into 1 in. (2.54 cm) diameter cylinders in a split die under 6,000 psi using a standard laboratory press. Care was taken to insure the release of air from the compact by raising the pressure slowly and holding it for ten minutes at each 1,000 psi increment. This yielded a green density from 1.19 to 1.33. The variation of green density with iron content is shown in Figure 70.

After pressing, the powder compact was placed in vacuum to remove any residual acetone. All of the samples were nitrided using the 1% H_2 gas and in accordance with the nitridation schedule shown in Figure 4. (The $1360^{o}C$ hold was maintained for 24 hours.) As a direct result of the vapor interaction experienced during the GTG experiments, each EOI sample was nitrided separately. Weight gain was used to monitor the extent of the reaction and Figure 71 shows the variation in percent reacted as a function of iron concentration.

After nitridation, the color of the reaction bonded silicon nitride was examined. As anticipated from the earlier experimental results, a complete color spectrum from gold to gray (EOI-1 to EOI-11, respectively) silicon nitride resulted. The iron responsible for the change in color was not found to cause any observable change in the x-ray diffraction pattern.

The presence of Fe in silicon nitride can add more energy levels within the band gap of silicon nitride. In an effort to verify this
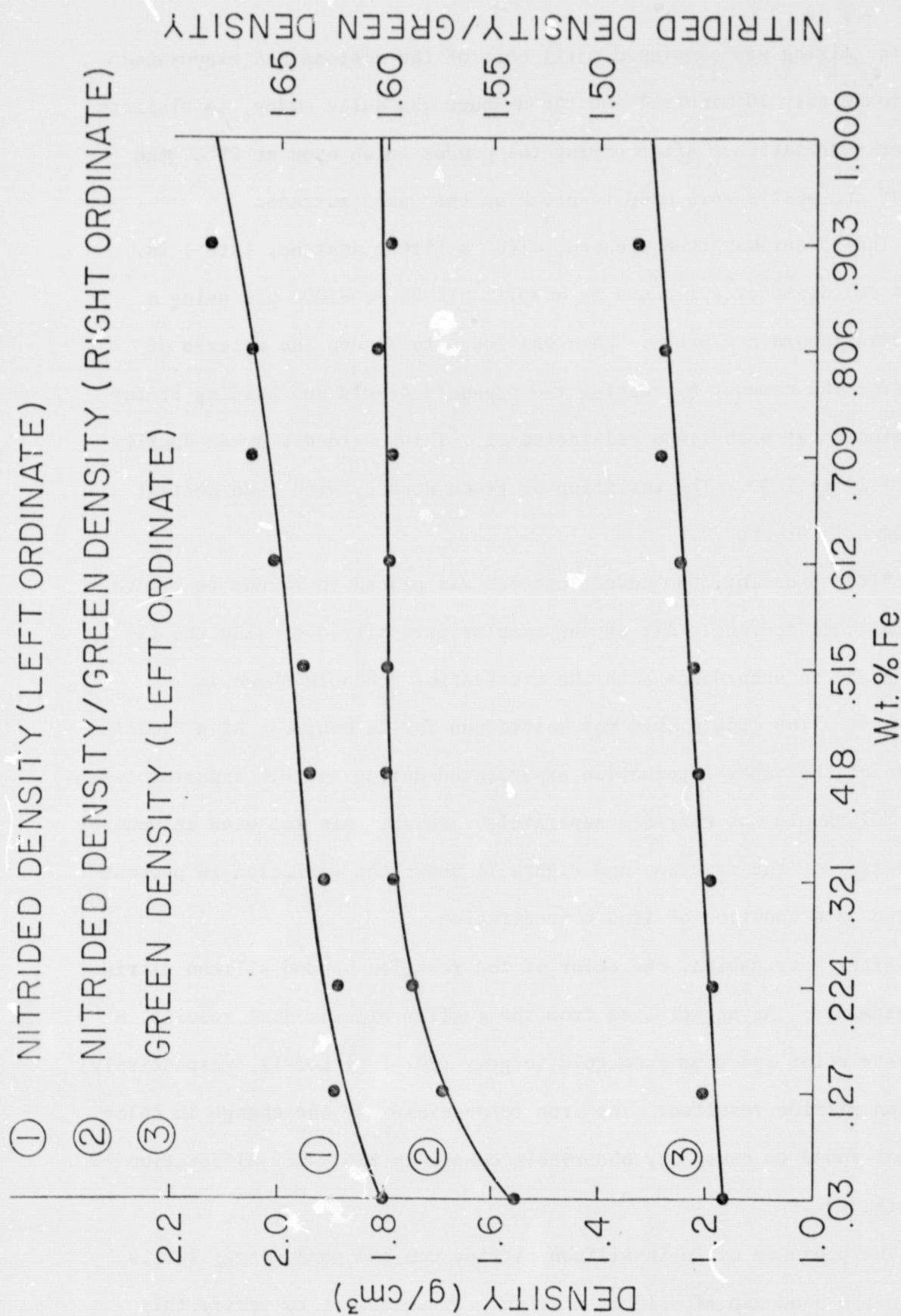
Figure 70

Plots of Green Density, Nitrided Density and
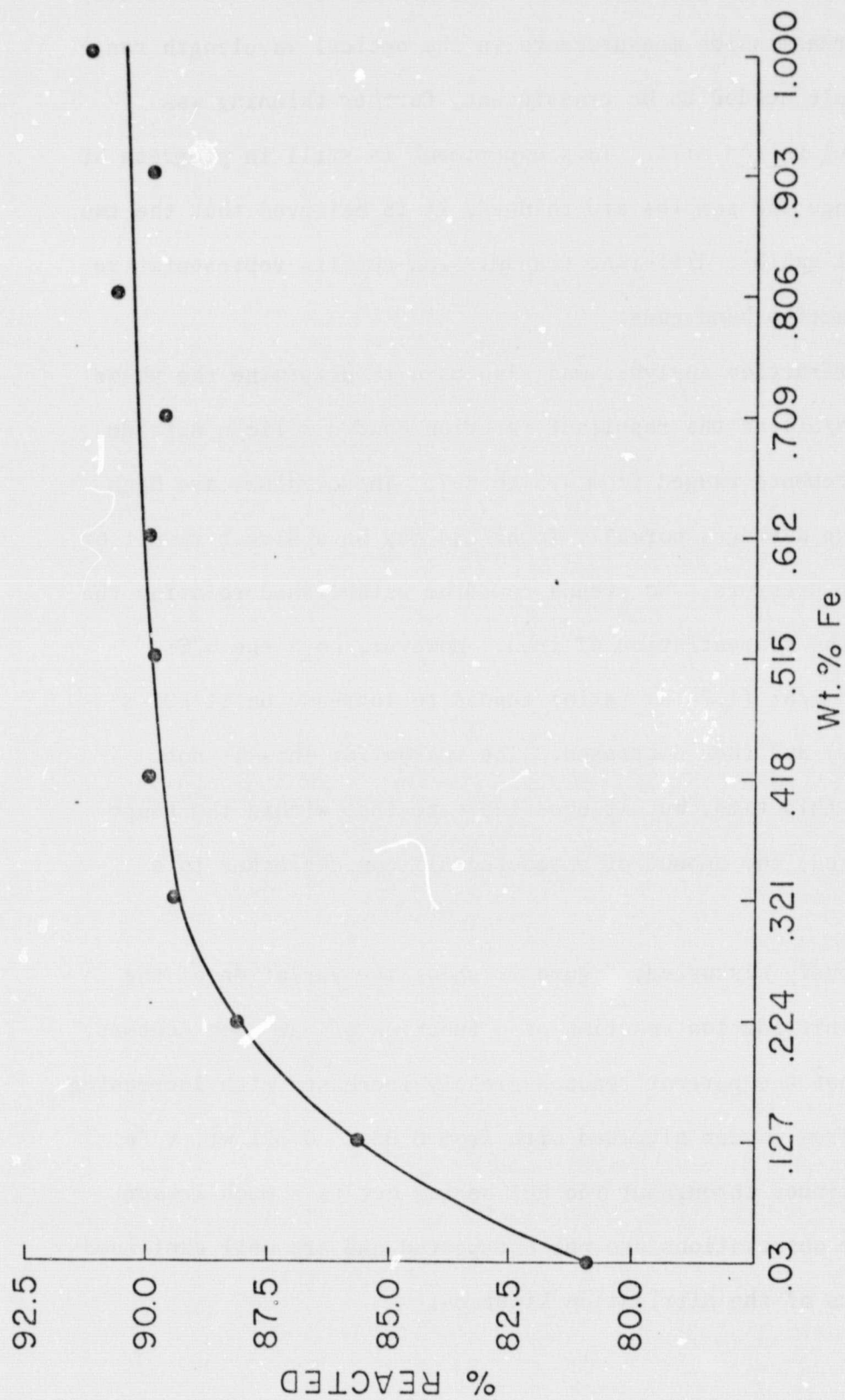Density Ratios as a Function of Fe Concentration

Figure 71

Percent Reacted Plotted as a Function of Iron Concentration

hypothesis, a gold and gray piece of silicon nitride was mechanically thinned for transmission measurements in the optical wavelength range. Since the sample needed to be translucent, further thinning was attempted using an ion mill. This experiment is still in progress at this date. Once the samples are thinned, it is believed that the two materials will exhibit different transmission cutoffs representative of their respective band gaps.

X-ray diffraction analysis was also used to determine the phase ratios (α/β, α/Si) of the resultant reaction bonded silicon nitride. The α/β measurements ranged from 4.5 to 8.7. These values are high compared to the averages normally found and may be a direct result of the compacting pressure. No trends could be established relating the α/β ratio to the concentration of iron. However, both the α/Si (7.9-64.6) and β/Si (1.7-15) ratios tended to increase until EOI-8 (0.709 wt % Fe) and then decreased. The reason for this is not understood at this time, but it does indicate that within the range being considered, the amount of unreacted silicon decreases to a minimum.

As previously discussed, Figure 71 shows the variation of the extent of the nitridation reaction as a function of the iron content. It is noted that the percent reacted greatly increases with increasing iron content from powder nitrided with from 0.03 to 0.321 wt. % Fe. The trend continues throughout the EOI series but to a much lesser degree. These observations are not unexpected and are well explained by the kinetics of the nitridation kinetics.

The nitrided density was found to increase with increased iron content. Figure 70 illustrates this and also shows the green density and the ratio of nitrided density to green density as a function of iron concentration. The increase in nitrided density is partially due to the observed increase in green density. However, since the ratio of the densities also increases with iron indicates that the green density is not the sole cause. It is consistent with present theories to note that the increasing density ratio curve closely resembles the percent reacted pattern.

Prior to presenting the mechanical properties of the reaction bonded silicon nitride products, the morphological observations made using the optical and scanning electron microscope will be presented.

All of the microstructures discussed were observed throughout the EOI samples. As indicated by the results cited above and suggested by the formation mechanisms presented, the occurrence of open micro-structures (isolated islands of material, pore channels, large pores) decreased with increasing iron content. Figures 72 through 75 show the densification and refinement of the reaction bonded silicon nitride with the addition of iron to the silicon powder.

A series of high magnification optical photomicrographs (Figures 76-78) clearly elucidate the nature of the disjointed microstructure previously discussed. As the series progresses (focusing further into the void), the underlying silicon nitride matrix is revealed. These void areas (more prevalent in the purer materials) may be the result of compaction macropores compounded by the diffusion of silicon to reaction sites and not filled in due to less formation by vapor-condensation mechanisms associated with the lack of iron.
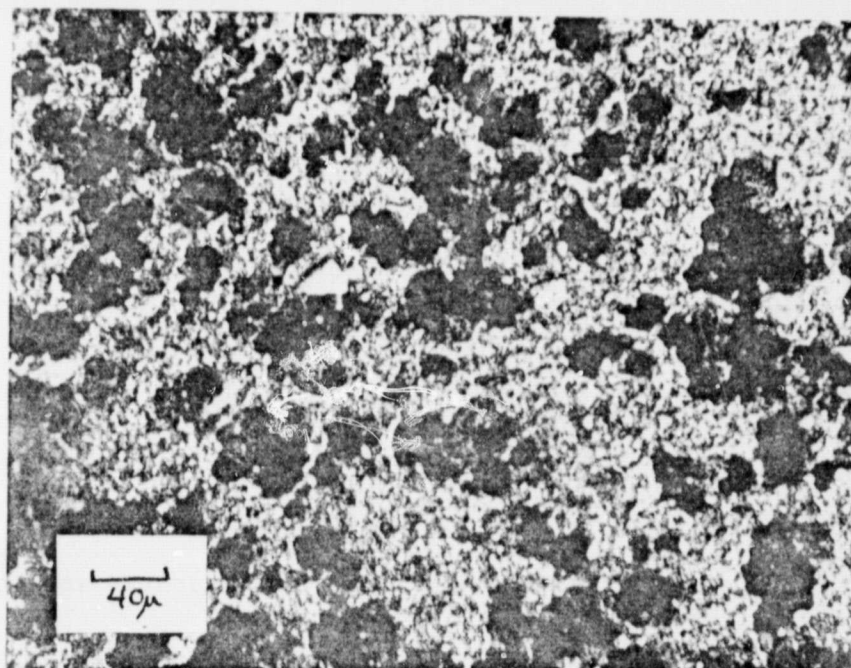
Figure 72

Photomicrograph of EOI-2 Microstructure wt. % Fe = 0.127 α/β = 8.7

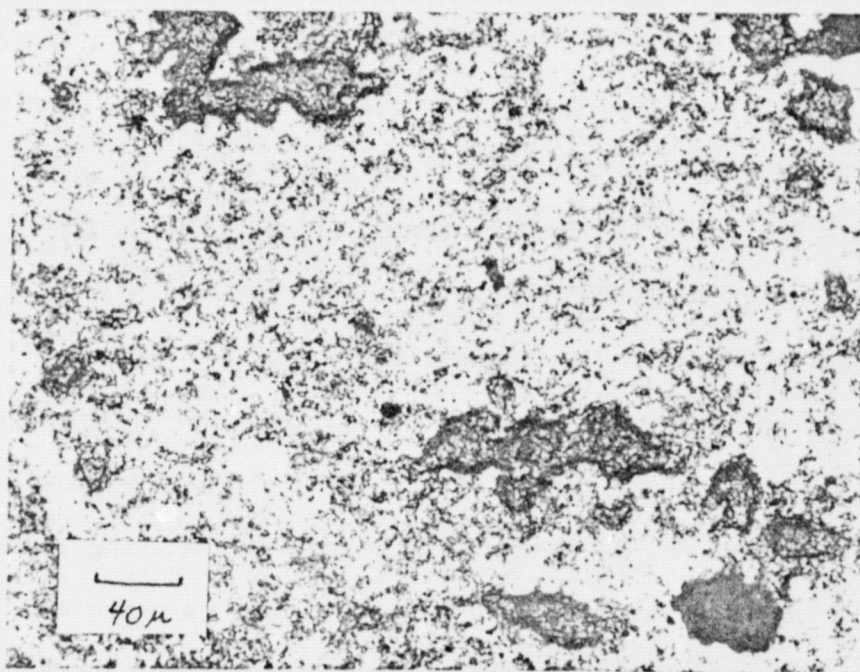Figure 73

Photomicrograph of EOI-5 Microstructure wt. % Fe = 0.418 α/β = 6.0
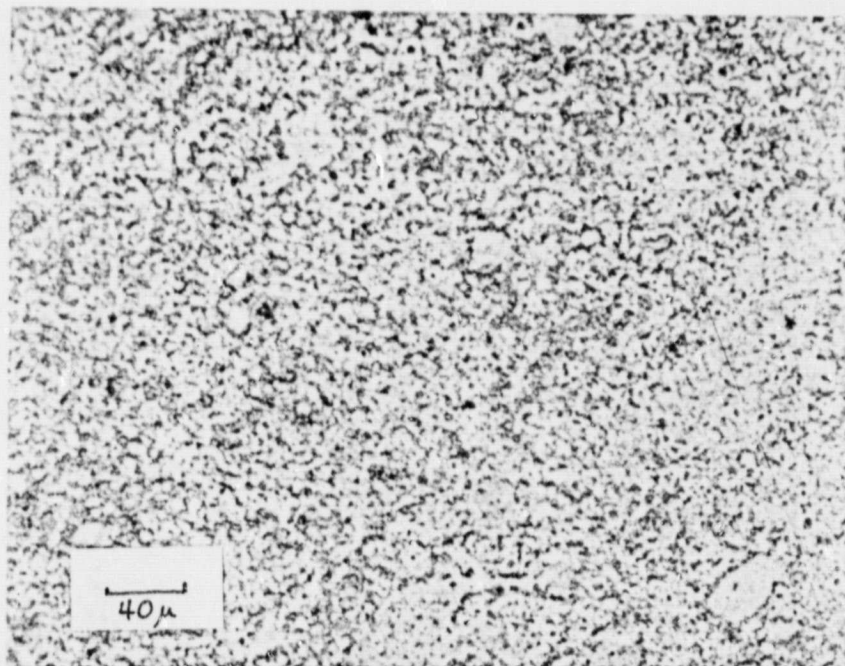
Figure 74

Photomicrograph of EOI-8 Microstructure wt. % Fe = 0.709 α/β = 5.7
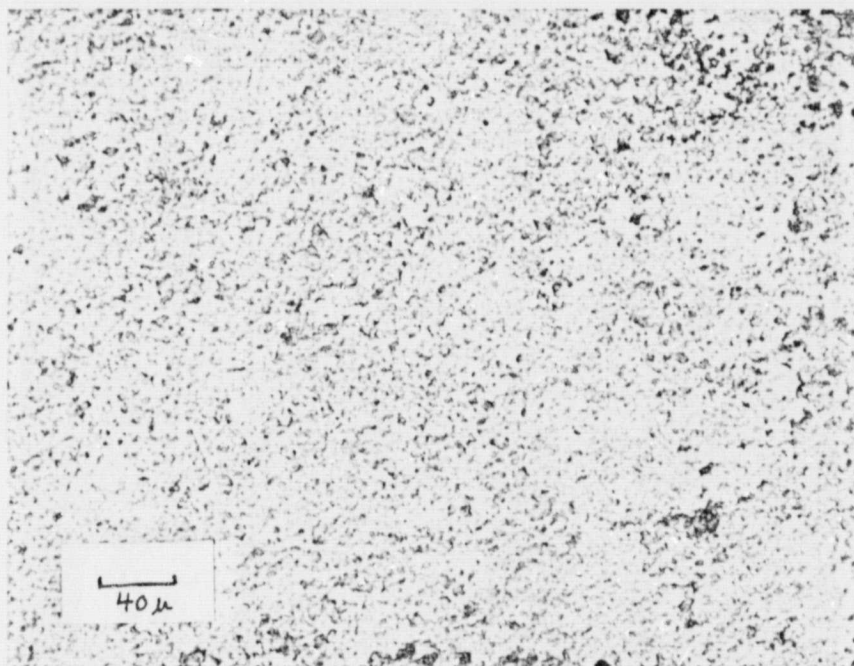
Figure 75

Photomicrograph of EOI-11 Microstructure wt. % Fe = 1.00 α/β = 6.46
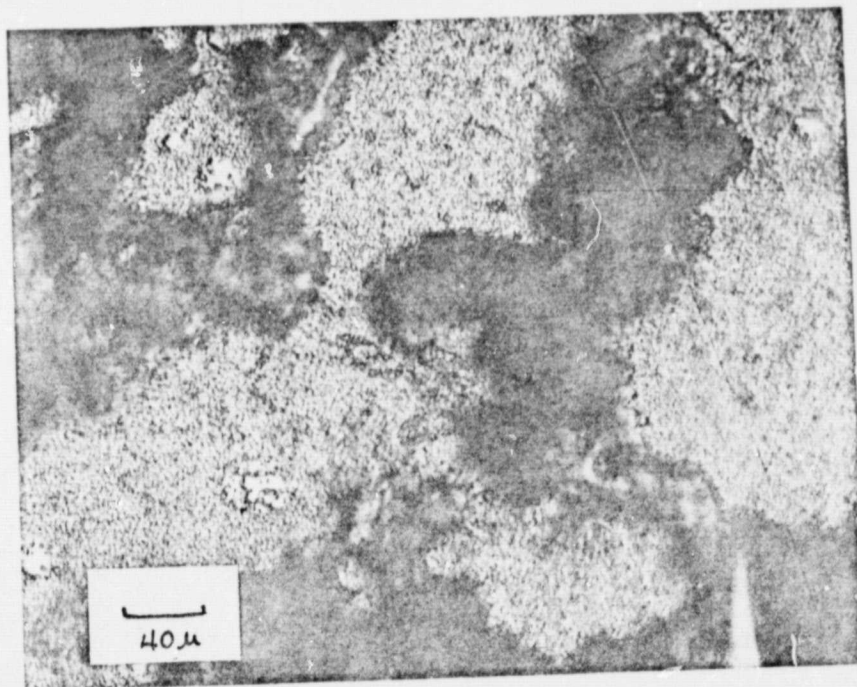
Figure 76

Focus on Top Surface of EOI-2 (0.127 st. % Fe)

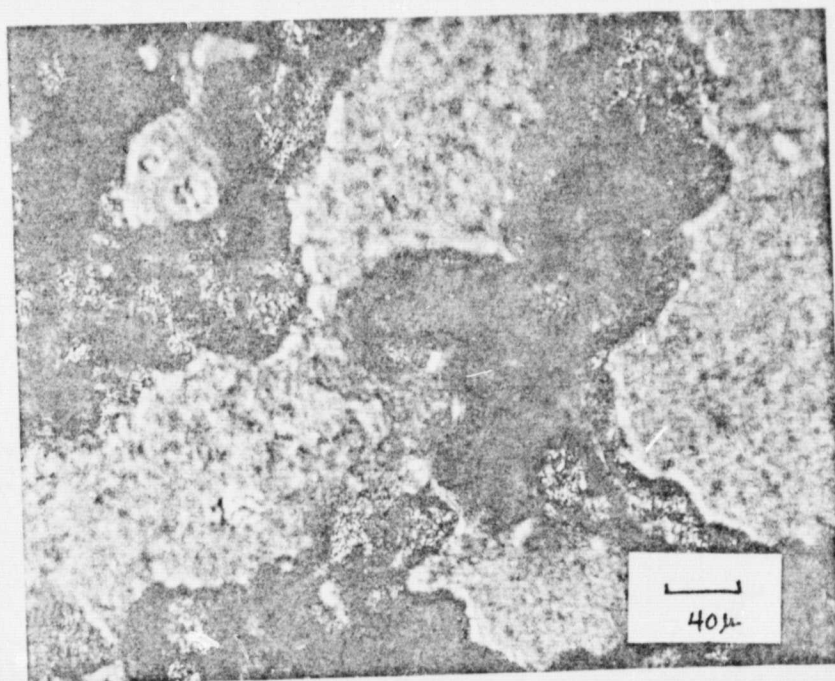Microstructure. Note Comparison with Figures 77 and 78

Figure 77

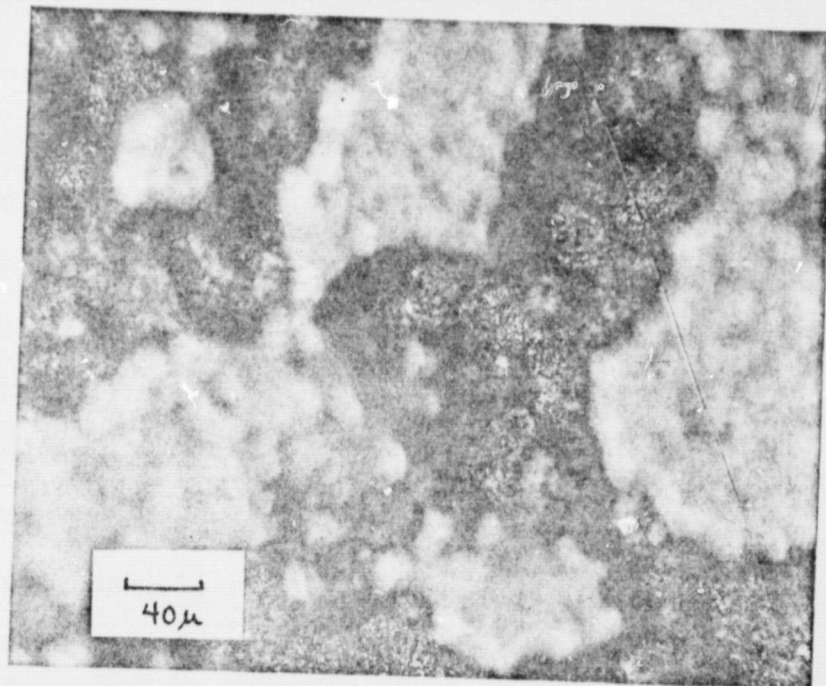Same Area as Figure 76 but Focusing Deeper into Microstructure

Figure 78

Same Area as in Figures 76 and 77

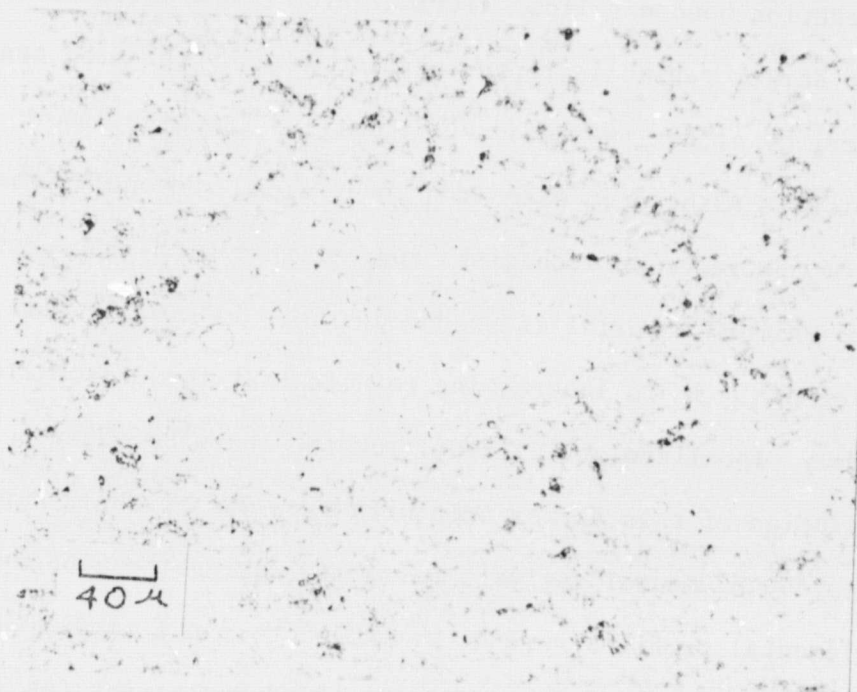Focus is on Bottom of Microstructure

Figure 79

EOI-4 (0.321 wt. % Fe) Microstructure Exhibiting

'Ghost' Grains (Lighter Regions)

Figures 79 and 80 show a microstructural component that is similar to that representing prior austenite grains seen in various steel alloys. These 'ghost' grains (or colonies) appear as the lighter phase in Figure 79. It is possible that these are partially reacted silicon grains, but close observation reveals smaller prismatic white regions within these ghosts that are more typical of unreacted silicon. Furthermore, the ghost in Figure 80 does not resemble unreacted silicon. It is possible that these areas are the result of powder agglomerates in the silicon compacts as well as subtle differences in the impurity content.

A more obvious effect of local impurity gradients is shown in Figure 81. This type of microstructure is present throughout the EOI series reaction bonded silicon nitride. From a microstructural viewpoint, the darker region is representative of a higher iron concentration. This is arrived at for two reasons. First, as has been shown, the darker color is associated with iron impurities. Secondly, the kinetics of the reaction mechanisms suggest that with iron present, a finer more uniform material is produced. This is clearly seen in the photomicrograph. It is interesting to note that the effect iron has is extremely localized as inferred from the sharp boundary observed. The association of this darker area with iron was strongly supported by the microprobe elemental analysis performed during the GTG experiments. As the elemental profiles were determined across the sample surface, readings were taken for neighboring light and dark areas (as seen through the microscope attached to the unit). The darker areas were
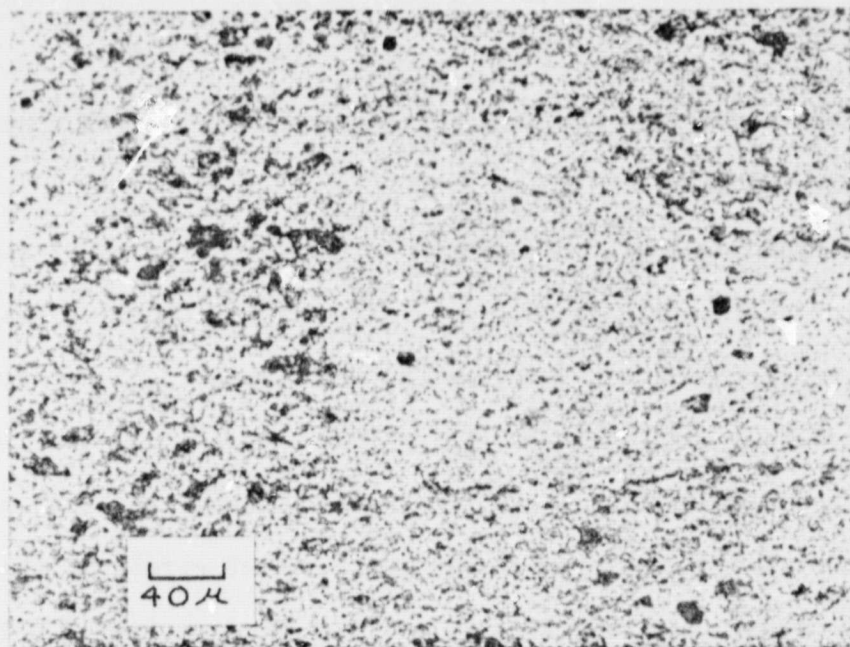
Figure 80

EOI-11 (1.00 wt. % Fe) Microstructure

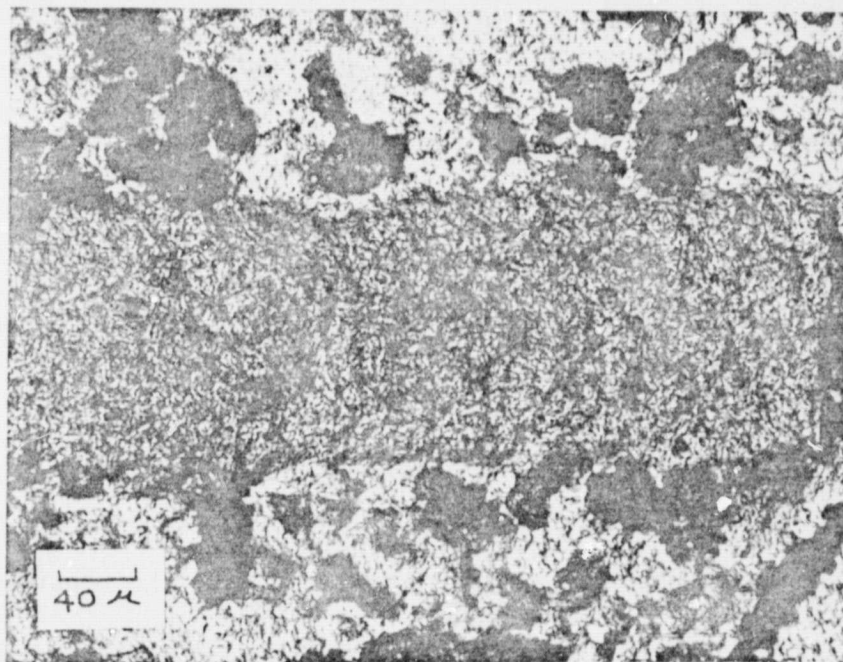Exhibiting a 'Ghost' Grain (Lower Center)

Figure 81

Photomicrograph of EOI-6 (0.515 wt. % Fe) Revealing

Microstructures Representative of High and Low Iron Levels

determined to contain more than twice the amount of iron contained in the lighter areas.

The scanning electron micrographs shown in Figures 82 and 83 were taken from neighboring areas. An EDAX (Energy Dispersive Analysis of X-Rays) profile of the two regions revealed iron to be present in one (Figure 83) but not the other (Figure 82). Again, the refining effect in the presence of iron can be seen. Furthermore, the high magnification of these pictures emphasizes the very localized effect of iron.

The mechanical properties of the EOI reaction bonded silicon nitride samples investigated include modulus of rupture, hardness and the fracture toughness parameter. These properties were related to the amount of iron present in the silicon compact and the material characteristics observed.

The hardness of the various samples was measured using a Wilson Hardness Tester with a Vickers Diamond Pyramid Indentor (136°) and a 20 Kg load. The Vickers Hardness Number, H, was calculated by measuring the diagonal lengths of several indentations. These lengths were often difficult to discern due to the inherent porosity of the material. Furthermore, the presence of this porosity leads to the crushing of the material and can alter the hardness measured. This effect was noted when the same material was tested under different loads and did not exhibit a constant hardness number. Nevertheless, the measurements made can be used for qualitative comparisons.

The results obtained for the EOI samples show that the hardness increases with increasing iron content. This increase becomes greater at the higher iron concentrations. This trend is understandable in light of the results and mechanisms previously discussed.

Figure 82

Scanning Electron Micrograph of EOI-2 (0.127 wt. % Fe)
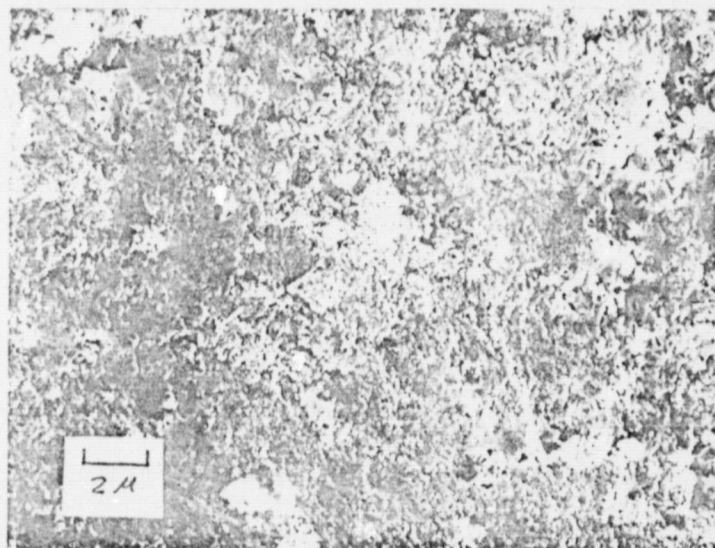
EDAX Analysis Showed No Iron

Figure 83

Region Directly Adjacent to That Shown in Figure 82.

EDAX Analysis Revealed the Presence of Iron

Due to the size limitations of the EOI reaction bonded silicon nitride cylinders, there were not enough bend bars to determine the fracture toughness according to the procedure previously outlined. Thus a method developed by Evans and Charles [9] to measure the effective fracture toughness of ceramic materials using indentation fracture was attempted. Once again, the pore structure of the silicon nitride precluded the measurement of the cracks emanating from the indented diamond corners needed, and the fracture toughness was not successfully measured.

The modulus of rupture of the EOI samples was determined in three point bending. The bend rig used was similar to that shown in Figure 37 but here the span between the lower pins was 0.625 in (15.9 mm). Any bend bars which were observed to contain pressing cracks were not included in the final calculations reported.

Figure 84 is a compilation of the modulus of rupture results for the EOI reaction bonded silicon nitride. The strongest material corresponded to EOI-11 (1.0 wt. % Fe) which had an average MOR of 24.2 Ksi (165 MN/m^2). This value is lower than expected for the K series silicon nitride and is a direct result of the compacting technique.

The EOI-5 (0.418 wt. % Fe) run was repeated using powder that was sieved to -325 mesh prior to compacting. The resultant increase in strength due to the processing is indicated in Figure 84. The effect of processing was to remove powder agglomerates to aid compaction and resulted in a 13.6% increase in nitrided density over the EOI-5 sample originally processed.
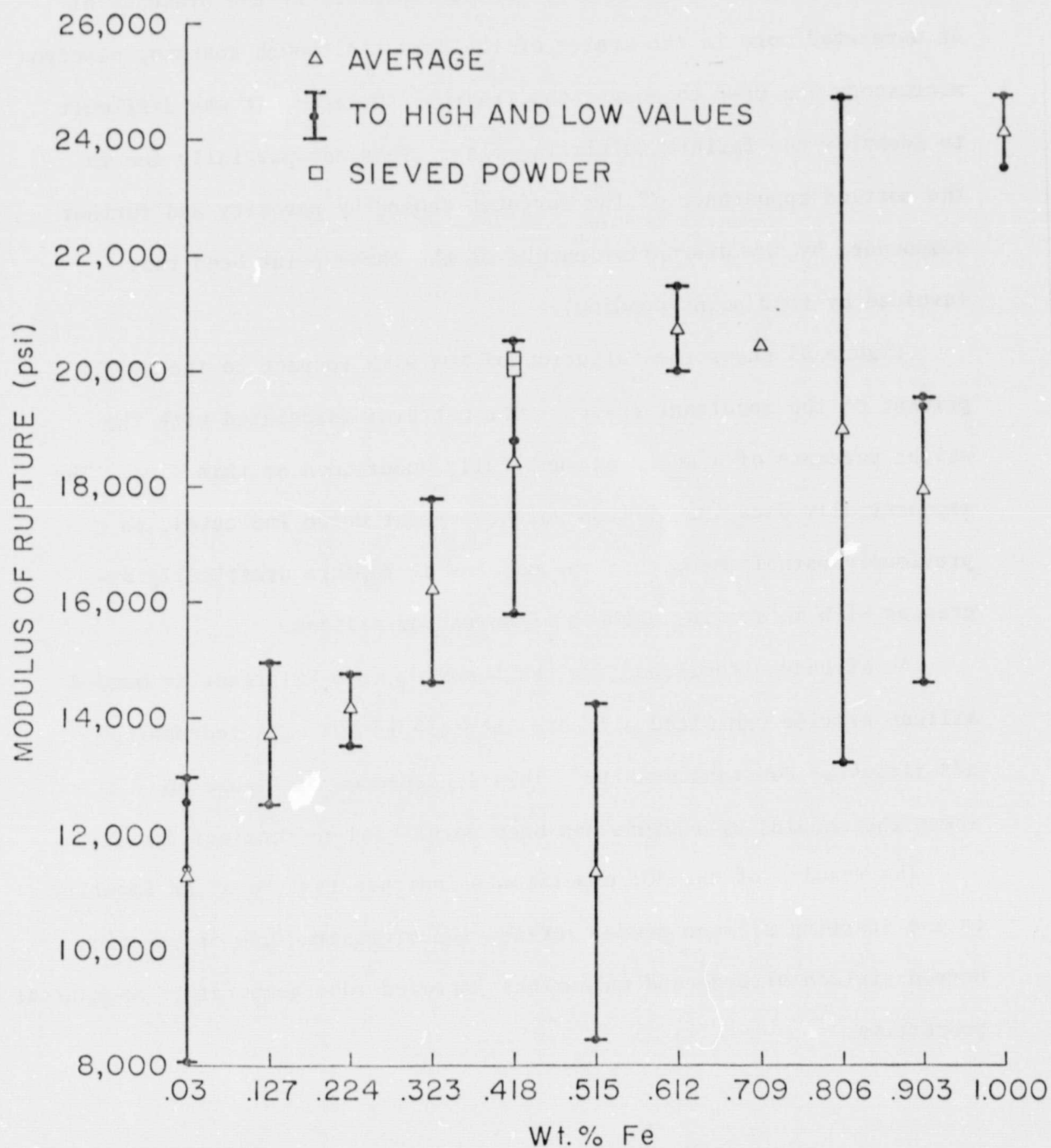
Figure 84

Modulus of Rupture as a Function of Fe

Content for the EOI Reaction Bonded Silicon Nitride Series

As expected, the strength of the reaction bonded material continually increased with increasing iron content. The low strength shown for 0.515 wt. % Fe (EOI-6) can be explained by the presence of an unreacted core in the center of the bars. Although scanning electron microscopy was used to survey the fracture surfaces, it was difficult to identify the failure initiating flaw. This was partially due to the mottled appearance of the surfaces caused by porosity and further compounded by the disruptive nature of the three point bend test (avoided by four point bending).

Figure 85 shows the variation of MOR with respect to the weight percent of the resultant phases. The patterns associated with the weight percents of α and β are not fully understood at this time. The exponentially decaying silicon weight percent curve indicates, as previously established, that the modulus of rupture drastically decreases with increasing amounts of unreacted silicon.

As already established for the N series, the EOI reaction bonded silicon nitride exhibited a linear increase in MOR with increasing α/β ratios at constant density. This is depicted in Figure 86 where the modulus of rupture has been normalized to constant density.

The results of the EOI experiments indicate that Fe as an impurity in the starting silicon powder refines the microstructure of reaction bonded silicon nitride and encourages improved room temperature mechanical properties.
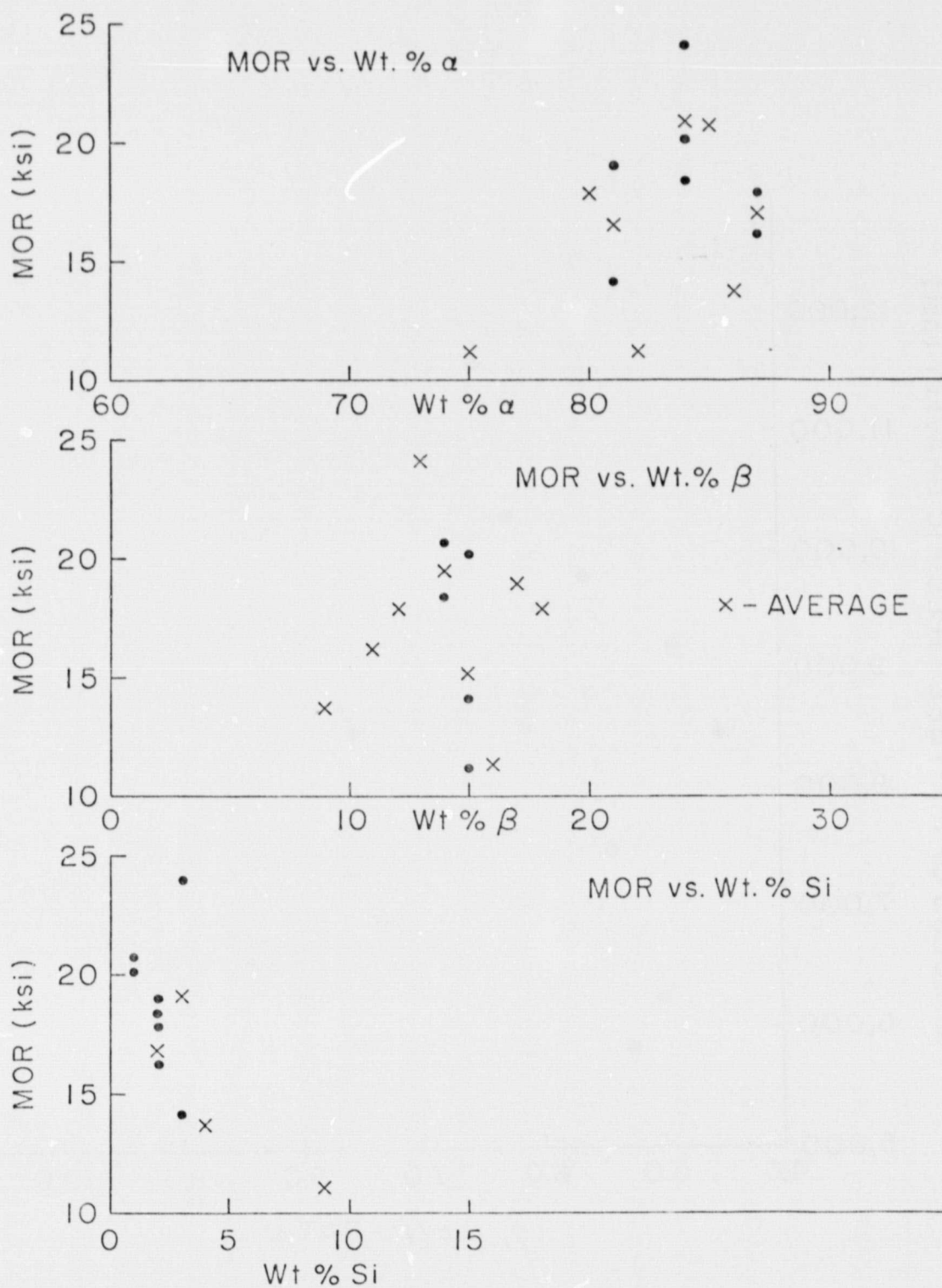
Figure 85

Modulus of Rupture vs. wt. % α; wt. % β;
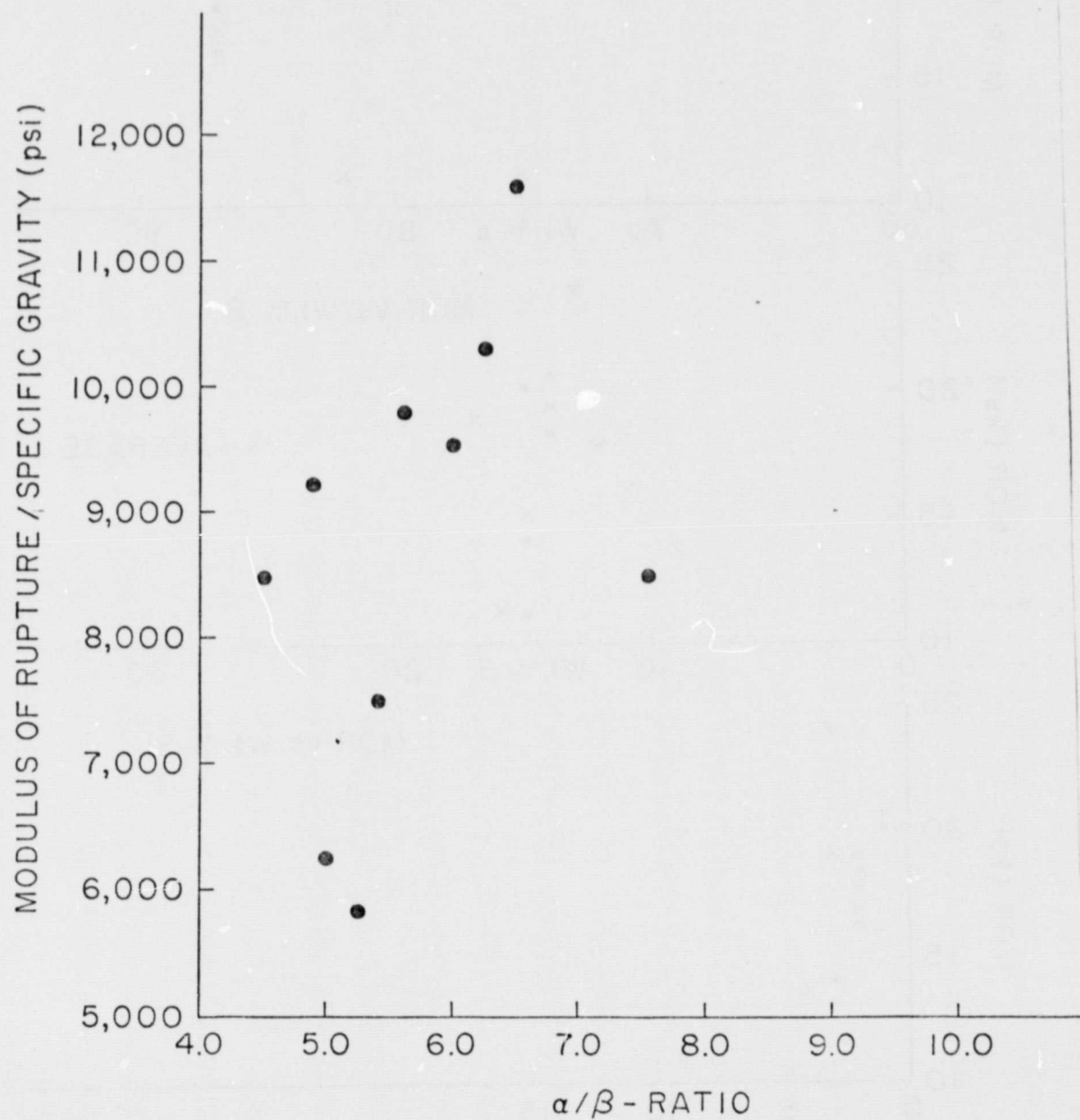
and wt. % Si for the EOI Reaction Bonded Silicon Nitride

Figure 86

MOR Data (Normalized to Nitrided Density) as a
Function of α/β-Ratio for the EOI Reaction
Bonded Si_3N_4 Series

CONCLUSIONS

The above investigation has revealed that through thorough control of the various processing parameters, improved understanding of the relationships between these variables and the reaction mechanisms involved in the growth of α and β-reaction bonded silicon nitride, one can successfully design and fabricate a reaction bonded Si_3N_4 material with improved microstructural features and increased MOR, K_{1c}, γ_i, and 2a (at room temperature).

It has been determined that the formation of β silicon nitride involves a nucleation and growth process and can occur in the absence of iron and without the melting of silicon.

Through a systematic evaluation of the effect of iron as an impurity in the starting silicon powder, it has been determined that improved microstructural and mechanical properties of reaction bonded silicon nitride are achieved with iron additions. The gold color of the reaction bonded silicon nitride was caused by the absence of iron.

References

1. H. E. White, S. F. Walton, Bull. Amer. Ceram. Soc., 10, No. 1, pps. 7-13, 1937.

2. R. W. Rice, J. Mater. Sci., 12 (1977) Letters 627-630.

3. A. Atkinson, A. J. Moulson and E. W. Roberts, J. Amer. Ceram. Soc. 59 (1976) 285.

4. N. J. Shaw and T. K. Glasgow, "Formation of Pourous Surface Layers in Reaction Bonded Silicon Nitride During Processing," NASA Technical Memorandum 81493.

5. W. Haidinger, "The Role of Surface Migration on the Epitaxial Growth of Al_2O_3 onto Si," Special Ceramics 5, Ed. P. Popper, The British Ceramic Research Association, England, March, 1972.

6. H. M. Jennings, J. O. Edwards and M. H. Richman, Inorg. Chim. Acta. 20 (1976) 167.

7. S. C. Danforth and M. H. Richman, J. Mater. Sci., 14 (1979) pps. 240-241.

8. S. M. Boyer, A. J. Moulson, J. Mater. Sci., 13 (1978) 1637-1646.

9. A. G. Evans, E. A. Charles, J. Amer. Ceram. 59 (1976) 371.

10. C. P. Gazzara, D. R. Messier, "Quantitative Determination of Phase Content of Silicon Nitride by X-Ray Diffraction Analysis," Army Materials and Mechanics Research Center, Watertown, Mass. Techn. Report No. AMMRC TR 75-4, Feb., 1975.

11 K. DWIGHT, PRIVATE COMMUNICATION

Personnel

The following personnel participated in this research project:-

Marc H. Richman	Professor of Engineering, Principal Investigator
Stephen C. Danforth	Research Assistant [*]
Otto J. Gregory	Research Assistant
Matthew B. Magida	Research Assistant
Joseph W. Fogarty, Jr.	Technical Assistant

[*] Currently at the Energy Laboratory, Massachusetts Institute of
Technology, Cambridge, Massachusetts.

Appendix A

Experimental Procedures

The furnace system used in the nitridation process (see Figs. A-C) was
capable of allowing various atmospheres, flow rates and heating schedules.
The furnace chamber was an open ended recrystallized Al_2O_3 tube, 3.125inID x
3.5 in OD x 48 in (7.9 x 8.9 x 122 cm). The ends of the tube were sealed using
rubber gaskets and stainless steel end cups modified for gas and viewing ports.
Alumina silicate $(Al_2O_3SiO_4)$ heat shields were placed into the tube in order
to achieve a large, constant hot zone by reducing radiant heat losses. The
heat shields also protected the Al_2O_3 tube by leveling the thermal gradient
along the length of the tube.

The central 20 inches of the Al_2O_3 tube was placed inside the stainless
steel shell of the furnace and surrounded by eight kanthal 33 molybdenum disilicide
resistance elements connected in series. These elements were surrounded by
fibrous aluminum silicate and zirconia insulation. The temperature of the
furnace was controlled using a R. I. Controls, silicon controlled rectifier
MPRY thermac controller. This unit compared the electrical signals from an
external programmer (representing the desired temperature) to those of a
type S (platinum-platnum/10% rhodium) thermocouple (representing actual
furnace temperature). The power for the system was supplied via a 6KVA stepdown
transformer.

The external programmer consisted of a motor box and potentiometer variac
geared to a heating rate of 50-75°C per hour. This heating rate was used in
order to protect the Al_2O_3 muffle tube from thermal shock and, as previously
pointed out, for better nitridation results. The temperature of the furnace
was monitored to within $\pm$ 4°C using the type S thermocouple and a Honeywell
2705 potentiometer. The temperature of the sample being nitrided was measured
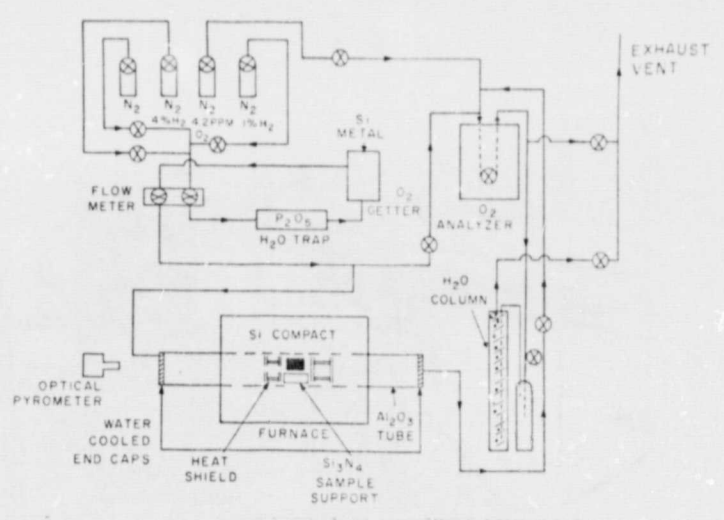
Figure A

Schematic of the furnace system used
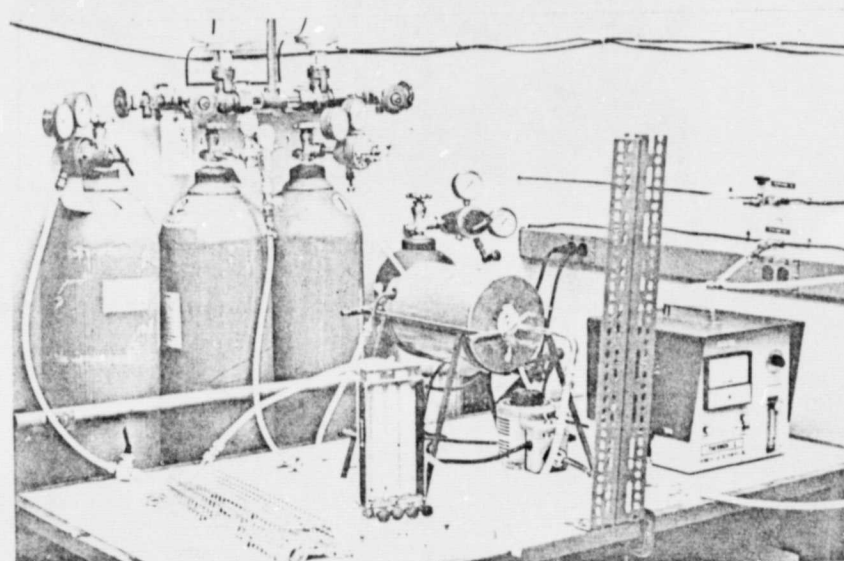during the K series experiments

Figure B

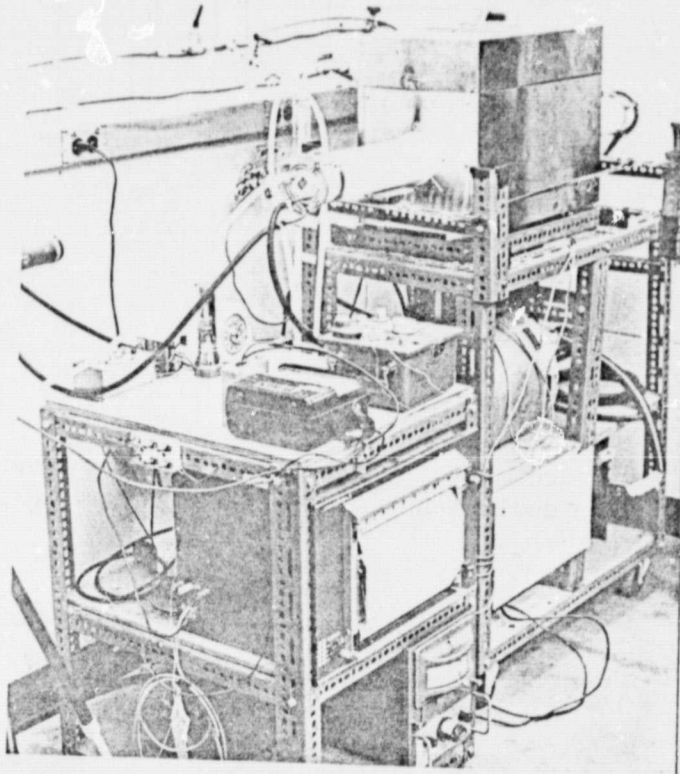A portion of the K series furnace system

Figure C

A portion of the K series furnace system used.

using the view port and a micro optical pyrometer measuring to $\pm 5°C$.

Three nitriding gases were used in the course of the investigation: N_2, 99% N_2 - 1% H_2 and 96% N_2 - 4% H_2. The system was also capable of supplying Ar gas for inert atmospheres. Prior to entering the reaction tube, the gases were first restricted by means of a Mathewson flow meter and valve and then passed over Si granules in a quartz tube maintained at 800°C by tube furnace. This acted as an oxygen getter with the partial pressure of O_2 over Si at 800°C being 1×10^{-33} atmospheres. Next, the gases were passed over P_2O_5 which acted as an H_2O getter and then through a controlling Mathewson flow meter. The gas flow could then be passed by the furnace entrance (a zero flow rate in the furnace) or directly through the reaction tube. Upon exiting the system, the gas bubbled through 21 inches (53 cm) of water to an exit through the roof. The columnof water was used to maintain a positive pressure throughout the system and to aid in leak detection.

Teflon tubing, .25 in (6.35 mm) in diameter was used throughout the system and connections madeusing .375 in (9.5 mm) brass swagelock fittings and valves.

Prior to nitriding, the green silicon bricks were weighed on a Christian Becker Chainomatic Scale to an accuracy of ± 1 mg. The brick is then put on top of a silicon nitride sample holder which is placed on an Al_2O_3 sleeve. This sleeve acts to protect the Al_2O_3 muffle tube in case the exothermic nitridation reaction causes the Si to melt. The brick, sample holder and sleeve were then inserted into the reaction tube centering in the hot zone. The $Al_2O_3SiO_4$ heat shields were then inserted and the end caps made secure. The system was then made leak tight and the run started.

Generally, argon was used to purge the system and was allowed to flow through the tube at a rate between 40 and 70 cc/min. After purging for approximately 5-7 hours, the programmer was activated and the temperature has increased. When the system approached 800-900°C, ($\sim$ 15 hours) the gas

was switched to one of the nitriding atmospheres which was allowed to flow

through the tube at a rate of 100 cc/min. When the temperature exceeded

1000°C, the flow was generally reduced to 60-85 cc/min and rerouted to pass

by the front of the reaction tube. This "easy exit" flow was used as an

approach to a zero flow rate in the tube. As the reaction calls for nitrogen,

it sucks it in from the infinite source. Otherwise, the gas does not see the

sample at all. Whenever the 96% N_2 - 4% H_2 gas was used, a small flow 30-70 cc/min

was maintained to avoid an explosive situation. During the reaction, N_2 is

consumed but the H_2 is passive and will build up. Thus, a slight flow needs

to be maintained. From this point, various time/temperature/atmosphere schedules

were used lasting from hours to days and temperatures up to 1370°C. After the

schedule was completed, the furnace was cooled via the programmer (again at

50-75°C per hour) until the temperature dropped below 200°C. The sample was

removed, weighed and prepared for further investigations.

After nitridation, various metallurgical techniques were used to enable

both qualitative and quantitative characterization of the material. This

included a weight determination of percent reacted, x-ray diffraction for the

relative amounts of phases present, optical and scanning electron microscopy

for morphology identification as well as energy dispersive analysis of x-rays

and electron microprobe analysis for elemental information. The mechanical

properties of the nitrided samples were determined by four point bend tests

for modulus, of rupture (MOR) and fractrue toughness (K_{1c}) characteristics.

The hardness of the reaction bonded material was also recorded. These methods

were conducted similarly for both the K and E series nitrided samples.

Immediately after nitridation, the weight of the sample was recorded and

compared to the previously recorded green weight. Assuming stoichiometric silicon

nitride formed, the percent reacted can be calculated according to the equation:

$$\% \text{ reacted} = \frac{\text{nitrided weight} - \text{green weight}}{(.667) \text{ green weight}} \times 100$$

It should be noted, that this method does not account for any material loss

during the reaction (vapor mechanisms). Hence, 100% reacted is never attained.

A piece of the nitrided sample was ground into a fine powder by hand

using an agate mortar and pestle. The mortar and pestle were only used for

the grinding of silicon nitride and were carefully cleaned with acetone before

and after each use. The resulting powder was then analyzed using a Phillips

x-ray diffractometer. A Cu target tube with a Ni filter produced Cu-K$_\alpha$

radiation with a wavelength of 1.54 A.

From the plot of angle (2θ) versus intensity, the interplanar spacings (d)

of the prominant peaks were determined according to Bragg's laws $\lambda = 2 d \sin\theta$

Consulting the tabulated values of d spacings for silicon nitride in the powder

diffraction files, specific intensity peaks were identified with the correlating

diffraction planes. This data was then normalized following the work by Gazzara

and Messier [10] to obtain the weight fraction fo the three phases (α, β, unreacted

Si). From these values, α/β and α/Si ratios were calculated.

The x-ray data compiled above was also used to determine the lattice

spacings of the phases present. A computer program developed by Dr. Kirby Dwight

[11] yielded a and c values for the hexagonal α and β phases from input

data consisting of the diffracting plane and the angle at which its peak was

found. This method was capable of offsetting the variances caused during the

set up and running of the diffraction apparatus.

Another piece of material was cut fromeach nitrided brick and mounted in

bakelite. This sample was then polished following standard metallographic

techniques on unlubricated 320, 600 and 600 soft grit silicon carbide papers

with intermediate ultrasonically cleaning in acetone. Final polishing was accomplished using a Buehler AB Vibromet polisher. The platen was covered wtih a Jarrett System Peilon pan-w polishing pad on which the samples were loaded under 666 grams of pressure. A slurry of 1-4 micron cerium oxide (CeO) powder and distilled water was used as the polishing medium. The use of CeO required increased polishing times of from 3 to 5 days. However, this method avoided pitting that resulted from the use of the more conventional alumina mixtures. Afterwards, the samples were again ultrasonically cleaned in acetone in preparation for microscopic examination at magnifications of up to 750 diameters. While this method does not allow the identification of α and β - $Si_3 N_4$ (the grain sizes being generally: α < .5 microns and β < 5 microns), it does reveal important morphological characteristics including pore size and structure and unreacted silicon.

An AMR $100\overset{o}{A}$ scanning electron microscope was used to achieve greater magnification and resolution of the various morphologies of the phases present in silicon nitride. Since silicon nitride is on the insulator side of semiconductors, a conductive coating of approximately 300 angstroms of gold was sputtered onto the silicon nitride prior to examination using a pS-2 sputtering unit.

The polished samples (now coated with gold) were examined and general morphologies photographed. Further, more detailed SEM observations were made on the fracture surfaces from the MOR and fracture toughness samples. Pores that were too small to see optically became visible using the SEM and α and β grains could be distinguished. Furthermore, by careful examination of the fracture surface, th failure initiation flaw could often be determined.

Frequently during optical or scanning electron microscopy, investigation of localized peculiar morphological areas was carried out using analytical elemental analysis. An EDAX (Energy Dispersive Analysis of X-rays) unit

attached to the scanning electron microscope allowed direct elemental identi-
fication of specific areas. Occasionally, another elemental determination
based on characteristic wavelengths was employed using an ARL EMX-SEM micro-
probe unit. The unusual morphologies were often associated with localized
impurities by these methods.

The density of the reaction bonded silicon nitride was obtained by simple
weight-to-volume ratios. The more accurat methods involving liquid displace-
ments and dry-to-wet weights were precluded due to the complicaticed pore
structure characteristic of this material. Green densities were often based
on nitrided volumes since in the green state, the bricks are extremely fragile.
This is considered valid in light of the small (< 1%) volume change upon nitridation.

Characterization of the mechanical properties of the reaction bonded silicon
nitride was accomplished using three and four point bend tests. The sample
configurations and the machine parameters have been described in the body of
this report (see page 58). From the load at failure; the modulus of rupture
(MOR) and the fracture toughness (K_{1c}) were calculated.

As noted elsewhere, the surface finish of the bend bar has a marked effect
on the failure strength. Throughout most of the later part of this investigation,
the bend bar preparation was performed in-house. Two grinding rigs were
designed and machined, one for the width (0.250 in. face) and the other for the
height (0.125 in. face). Final surface finish and sample dimensions were achieved
with a diamond embedded grinding wheel adapted onto a micromatic wafering
machine. The bars were then tested for MOR in the as-ground condition. K_{1c}
measurements were made on bend bars after the introduction of a machined notch.